Development, Characterization and *In Vivo* Evaluation of Biodegradable Nanospheres and Nanocapsules

Dissertation

zur Erlangung des akademischen Grades

doctor rerum naturalium (Dr. rer. nat.)

vorgelegt der

Naturwissenschaftlichen Fakultät I

Biowissenschaften

der Martin-Luther-Universität Halle-Wittenberg

von

Jun Li

geboren am 03. November 1982 in Jiangsu, China

Gutachter:

1. Prof. Dr. Karsten Mäder

2. Prof. Dr. Dagmar Fischer

3. Prof. Dr. Thomas Groth

Halle (Saale), 09.03.2012

"Knowledge is not equal to devotion.

Devotion is not equal to joy."

Confucius

TO ALL THE PEOPLE WHO HAVE SUPPORTED ME.

Table of Contents

List of abbreviations

NDDS	nano drug delivery system
NP	nanoparticles
NS	nanospheres
NC	nanocapsules
PEG	polyethylene glycol
PLGA	poly(D,L-lactic-co-glycolic acid)
PLGA-PEG	poly(lactide-co-glycolide)-poly(ethylene glycol)
PCL	poly(ε-caprolactone)
PCS	photon correlation spectroscopy
PDI	polydispersity index
DLS	dynamic light scattering
LD	laser diffraction
AF4	asymmetrical flow field-flow fractionation
CMC	critical micelle concentration
M.W.	molecular weight
OI	optical imaging
MRI	magnetic resonance imaging
CT	computed tomography
ESRI	electron spin resonance image
SPECT	single photon emission computed tomography
PET	positron emission tomography
MALLS	multi-angle laser light scattering
TEM	transmission electron microscopy
SANS	small angle neutron scattering
AFM	atomic force microscopy

NMR	nuclear magnetic resonance
ESR	electron spin resonance
EPR	electron paramagnetic resonance
CPA	cryoprotective agents
NIR	near-infrared
NR	nile red
DiR	1,1'-dioctadecyl-3,3,3',3'- tetramethylindotricarbocyanine iodide
DiI	1, 1'-dioctadecyl-3,3,3',3'- tetramethylindocarbocyanine perchlorate
HDPMI	2-Heptadecyl-2,3,4,5,5-pentamethylimidazolidine-1-oxyl
QD	quantum dots
HIV	human immunodeficiency virus
i.v.	intravenous
HPLC	high-performance liquid chromatography
CLSM	confocal laser scanning microscopy
ROI	region of interest
RES	reticuloendothelial system
MPS	mononuclear phagocytic system
BA	betulinic acid

1 Introduction

1.1 Nano Drug Delivery System

In the past few decades, the explosive growth of nanotechnology has brought rapid development in drug delivery, called nano drug delivery systems (NDDS) (Allen and Cullis, 2004; Couvreur and Vauthier, 2006; Mehnert and Mäder, 2001). The nano drug delivery systems are nanoparticles (NP) with diameters ranging from 1 nm to 1000 nm, and consist of various materials including polymers, lipids and inorganic materials. As shown in Fig. 1.1-1, the nano-drug delivery systems include a large range of nanocarries, such as micelles, nanospheres (NS), nanocapsules (NC), nanogels, polymersomes, liposomes, lipoplexes, solid lipid nanoparticles, dendrimers, carbon nanotubes, colloidal gold nanoparticles and silica nanoparticles (Bianco et al., 2005; Ghosh et al., 2008; Kabanov and Vinogradov, 2009; Müller et al., 2000; Sonke, 2009; Tan et al., 2004; Tros de Ilarduya et al., 2010).
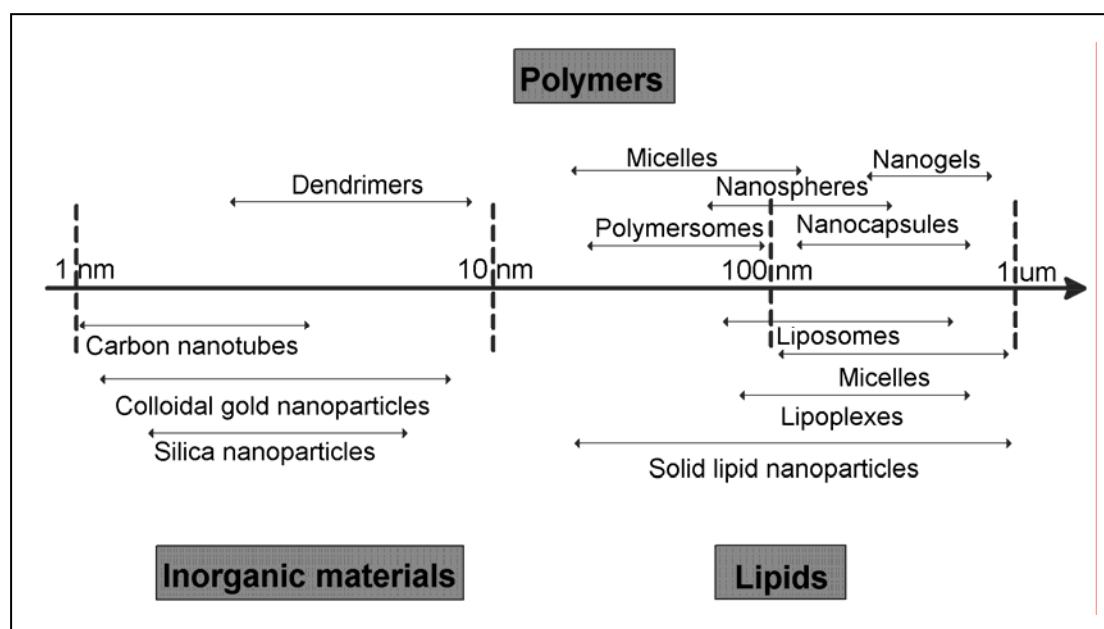
Fig. 1.1-1: Various types of nano-drug delivery system. The major components are composed of polymers, lipids or inorganic materials.

In general, several advantages may be achieved using NDDS (Farokhzad and Langer, 2009): (a) improving the delivery of water-insoluble drugs; (b) making the delivery of drugs in targeting manner; (c) protecting the drug from degradation; (d) co-delivery of two or more drugs for combination therapy; (e) real-time visualization of drug delivery with imaging modalities; and (f) modification of the biodistribution and pharmacokinetics of drugs.

1.2 Polymer Used to Design Nanoparticles

The need of polymeric drug delivery systems results in the development of several kinds of polymers (Kumari et al., 2010; Uhrich et al., 1999). However, only a limited number of polymers can be used as constituent of nanoparticles designed to deliver drugs *in vivo* (Qiu and Bae, 2006). All the polymers intended for drug delivery system *in vivo* should meet certain criteria and requirements. The minimum requirements include the following. Firstly, these polymers should be biodegradable and biocompatible; secondly, they must be non-toxic and non-immunogenic; thirdly, the properties of these polymers must be appropriate for the intended application.

The polymers designed for NDDS can be classified into natural polymers, synthetic homopolymers and copolymers. Table 1.2-1 gives a list for the most widely used polymers to design NDDS. Natural polymers are natural products of living organisms, relatively cheap, and multitude of chemical modifications. The natural polymers used for drug delivery system have focused on proteins (collagen, gelatin and albumin) and polysaccharides (chitosan, alginate, starch and dextran) (Dang and Leong, 2006).

Biodegradable synthetic polymers including homopolymers and block (diblock or triblock) copolymer have been widely investigated for pharmaceutical application (Adams et al., 2003; Chirila et al., 2002; Jeffrey A, 1998). Block copolymers are always defined as

polymers that have two or more blocks arranging in the main chain, and they can be classified according to their architecture as AB type diblock, ABA or BAB type triblock, star-shape block and multiblock, where A represents the soluble hydrophobic block and B designates the hydrophilic block (Kumar et al., 2001).

Table 1.2-1: The most widely used polymers for designing nanoparticles.

Material	Polymer	Reference
Natural polymers	Chitosan	(Prabaharan and Mano, 2004)
	Starch	(Le Corre et al., 2010)
	Alginate	(Tønnesen and Karlsen, 2002)
	Gelatin	(Coester et al., 2006)
	Albumin	(Kratz, 2008)
Synthetic homopolymers	PLA	(Lassalle and Ferreira, 2007; Leo et al., 2004)
	PLGA	(Kim and Martin, 2006; Sánchez et al., 2003)
	PCL	(Chawla and Amiji, 2002; Yang et al., 2006)
Copolymers	PLA-PEG	(Mosqueira et al., 2001)
	PLGA-PEG	(Li et al., 2001; McCarron et al., 2006)
	PCL-PEG	(Li et al., 2009; Pourcelle et al., 2007)
	PLGA-PEG-PLGA	(Chen et al., 2005)

Abbreviation: PLA, Poly(lactide); PLGA, Poly(lactide-co-glycolide); PCL, Poly(ε-caprolactone); PLA-PEG, Poly(lactide)-poly(ethylene glycol); PLGA-PEG, Poly(lactide-co-glycolide)-poly(ethylene glycol); PLGA-PEG-PLGA, Poly(lactide-co-glycolide)-poly(ethylene glycol)-poly(lactide-co-glycolide)

Due to the intrinsic affinity interactions of those blocks with the same physicochemical properties, block copolymers often show a tendency to form self-assemblies (Qiu and Bae, 2006). Among of block copolymer, linear amphiphilic block copolymers have attracted much attention due to their ability to simply form various types of nanoparticles, including nanosphere, nanocapsules, micelles and polymersomes (Fig. 1.2-1)
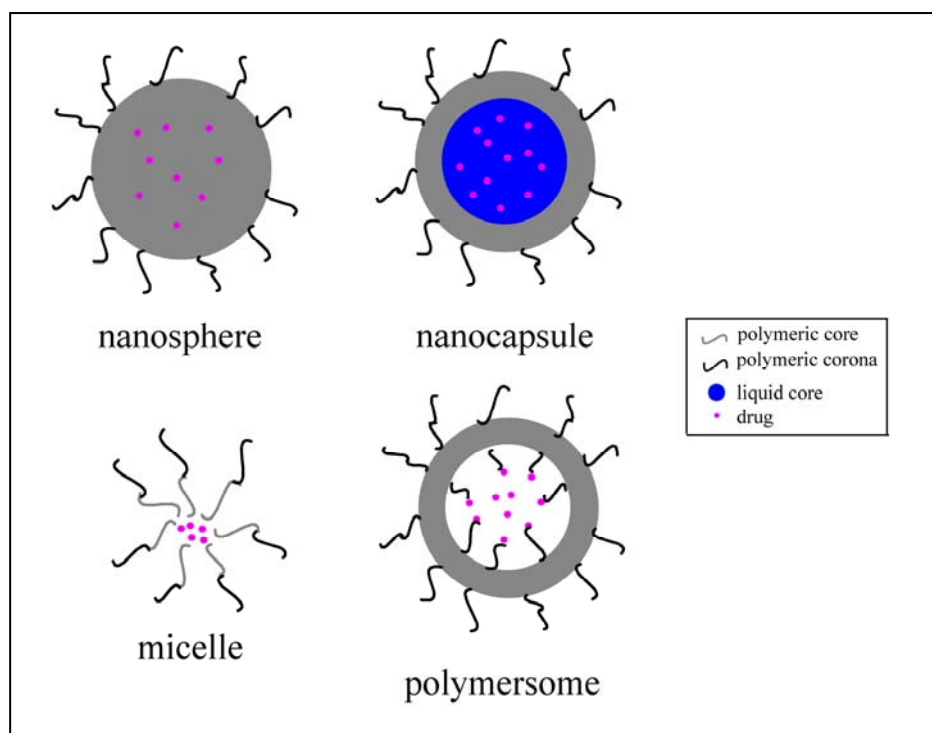
Fig. 1.2-1: Nano drug delivery systems (nanospheres, nanocapsules, micelles and polymersomes) formed by amphiphilic block copolymers.

Nanospheres are matrix particles with size ranging from several tenths of nanometers to a few hundred of nanometers (Peracchia et al., 1997). In contrast to matrix-structured nanospheres, nanocapsules consist of an external layer made of a biodegradable polymer and an inner liquid (oil or aqueous) compartment (Couvreur et al., 2002). In generally, nanocapsule formulations with the oily core allow a high payload of lipophilic drugs (Ren et al., 2007; Santos-Magalhães et al., 2000), while nanocapsules containing an aqueous core able to encapsulate water-soluble substances were also developed in the recent years (Anton et al., 2009; Lambert et al., 2000).

For polymersomes, the core of the vesicle is an aqueous phase and the surrounding coating is a polymer bilayer (Ahmed and Discher, 2004). These vesicles are able to make the encapsulation and delivery of water-soluble drugs which can be entrapped in their aqueous reservoir, but they are not the same as liposomes in that the external bilayer is composed of amphiphilic copolymers. Polymeric micelles are self-assembling nanoparticles with a hydrophobic block core and hydrophilic block shell (Torchilin, 2007). Polymeric micelles can improve the aqueous solubility of hydrophobic drugs, and modify

the biodistribution of drugs by passive or active targeting (Gaucher et al., 2005).

1.3 PLGA and Its Copolymer with PEG

Polyesters such as PLA, PLGA and PCL have been used for making NDDS because they are regarded as the synthetic biodegradable polymers with controllable biodegradability, excellent biocompatibility, and high safety (Breitenbach et al., 2000). Among of these polymers, the biodegradable, biocompatible and FDA-approved poly (D, L-lactic-co-glycolic acid) (PLGA) is a common choice since its safety and biofate has already been established in the clinic (Winzenburg et al., 2004).

PLGA made from L-poly lactide (L-PLA) and poly glycolide (PGA) is crystalline copolymers, while from D, L-PLA and PGA is amorphous in nature. Lactic acid (LA) is more hydrophobic than glycolic acid (GA), therefore, PLGA copolymers with high content of lactide are less hydrophilic. PLGA degrades by hydrolysis of its ester linkages in the presence of water. Random PLGA copolymers exhibit different degradation rates from weeks to months, depending on the different ratio of LA and GA. It is generally accepted that the PLGA with the higher content of lactide units has the lower degradation rate. An exception is that PLGA containing a ratio of LA and GA (50:50) exhibits the faster degradation. In addition, polymers that are end-capped with esters can demonstrate longer degradation half-lives.

PLGA-based nanoparticles are widely investigated for the delivery of drug, protein and gene (Mu and Feng, 2003; Patil and Panyam, 2009). And, the preparation of surface-modified polymeric nanoparticles with hydrophilic polymer such as polyethylene glycol (PEG) is the most common method to control the process of opsonization during passive targeting. Di-block PLGA-PEG and tri-block PLGA-PEG-PLGA copolymers are especially desirable because pegylated polymeric nanocarriers can significantly reduce

systemic clearance compared to PEG-free particles (Avgoustakis, 2004; Cheng et al., 2007). Thus, these block copolymers have been widely investigated for both fundamental research and product development.

1.4 Preparation Methods of Nanoparticles

Polymeric nanoparticles can be prepared by either preformed or monomers using a variety of methods (Pinto Reis et al., 2006). However, the most popular methods to prepare polymeric nanoparticles come from biodegradable performed polymers. Several methods can be used to perform nanoparticles, including solvent displacement, emulsification solvent evaporation, salting out and solvent diffusion (Vauthier and Bouchemal, 2009). Table 1.4-1 shows the summary of methods used for preparation of PLGA and PLGA-PEG nanoparticles.

The solvent displacement method (also called nanoprecipitation method) for nanoparticle preparation was first described by Fessi et al. (1989). In brief, polymer, oil (for nanocapsule formulation) and drug are dissolved in a water-miscible organic solvent (e.g. acetone). Then, the organic solution is drop-wise injected to an aqueous phase containing a surfactant (e.g. poloxamer 188) under mild stirring. A submicron o/w emulsion is spontaneously formed with the rapid diffusion of acetone into the aqueous phase. Following acetone diffusion, the nanospheres or nanocapsules are formed by aggregation of polymer, oil and drug. Finally, the organic solvent is removed by evaporation and the nanosphere suspension is concentrated under reduced pressure.

Table 1.4-1: Summary of methods used for preparation of PLGA and PLGA-PEG nanoparticles.

Method	Polymer	Drug	Size (nm)	Reference
Solvent displacement	PLGA	Procaine hydrochloride	210	(Govender et al., 1999)
	PLGA-PEG	Paclitaxel	112±4	(Danhier et al., 2009)
	PLGA-PEG	Docetaxel	70-250	(Cheng et al., 2007)
Solvent evaporation	PLGA	Vitamin E TPGS	240	(Win and Feng, 2006)
	PLGA-PEG	Vincristine sulfate	237±16	(Chen et al.)
Salting out	PLGA	Celecoxib	151	(McCarron et al., 2006)
Simple emulsion	PLGA-PEG	Paclitaxel	190±5	(Danhier et al., 2009)
Double emulsion	PLGA	IFN-alpha	280±12	(Sánchez et al., 2003)
	PLGA-PEG	Bovine serum albumin	198±11	(Li et al., 2001)
	PLGA-PEG	Cisplatin	134-158	(Avgoustakis et al., 2002)
Emulsion solvent diffusion	PLGA-PEG	imatinib mesylate: STI571	50	(Kimura et al., 2008)

The emulsification solvent evaporation method includes two alternatives depending on the nature of the drug to be entrapped within the nanospheres: the simple emulsion (w/o) and the double emulsion (w/o/w) techniques (Desgouilles et al., 2003). In the first method, which is used for the encapsulation of hydrophobic drugs, the polymer and the drug are dissolved in a volatile organic solvent immiscible with water, such as dichloromethane or ethyl acetate, and the organic phase is emulsified under intense shear using homogenization or probe sonication into an aqueous phase containing appropriate amounts of a surfactant (e.g. poloxamer 188). The organic solvent is allowed to evaporate (sometimes under reduced pressure). In the second method, which is used for the encapsulation of hydrophilic drugs and proteins, the drug is dissolved in a small volume of an aqueous phase and this is emulsified in an organic phase containing the polymer. The w/o emulsion formed is then dispersed in a larger volume of an aqueous

phase to form the double w/o/w emulsion. The remaining steps of the preparation are the same as in the simple emulsion method. So, the most advantage of emulsification solvent evaporation method is the possibility to encapsulate both hydrophobic and hydrophilic drugs (Hombreiro Pérez et al., 2000).

In the salting out method, the polymer and the drug are dissolved in a water-miscible solvent (e.g. acetone) and the solution is emulsified under vigorous mechanical stirring in an aqueous gel containing the salting out agent and a colloidal stabilizer (Soppimath et al., 2001). This o/w emulsion is diluted with a sufficient volume of water to enhance the diffusion of acetone into the aqueous phase, thus inducing the formation of nanospheres. The nanospheres are purified by cross-flow filtration. The advantages of this method are the possible incorporation of high amounts of polymer and drug, the excellent yields generally obtained and the easy scale-up of the process. However, the limitations of the method are that it is suitable for the encapsulation of only lipophilic drugs and that intensive purification of the nanospheres is required. And, another disadvantage of the method is that it uses salts that are not compatible with many bioactive compounds.

1.5 Characteristics of Nanoparticles

1.5.1   Particle Size

There is no doubt that particle size and size distribution are the most important characteristics of nanoparticle systems (Gaumet et al., 2008). They can determine the *in vivo* distribution, biological behavior and the targeting ability of drug delivery systems. In addition, they can also influence the drug loading, drug release and stability of nanoparticles. Many researches have demonstrated that nanoparticles with sub-micron size have a number of advantages over microparticles for drug delivery system (Hans and Lowman, 2002). Generally, nanoparticles have relatively higher intracellular uptake

compared to microparticles (Desai et al., 1997). It is also reported that nanoparticles are able to across the blood-brain barrier (Gao and Jiang, 2006; Lockman et al., 2002). Drug release is also affected by particle size and size distribution. Generally, smaller particles have larger surface area; therefore, most of the drug associated would be at or near the particle surface, leading to fast drug release. Whereas larger particles have large cores, which allow more drug to be encapsulated and slowly diffuses out. However, smaller particles also have greater risk of aggregation of particles during storage and transportation of nanoparticle dispersion. It is always a challenge to produce nanoparticles with the smallest size and possible maximum stability. Polymer degradation can also be affected by the particle size. For example, the rate of PLGA degradation increases with increasing particle size *in vitro* (Dunne et al., 2000).

1.5.2   Surface

When nanoparticles are intravenously (i.v.) administered, conventional nanoparticles are easily recognized by the mononuclear phagocytic system (MPS), also known as the reticuloendothelial system (RES). Thus, they are rapidly opsonized and massively cleared by the macrophages of MPS organs. Hence, to increase the likelihood of the success in drug targeting by nanoparticles, it is necessary to decrease the opsonization and to prolong the circulation of nanoparticles *in vivo* (Stolnik et al., 1995). There are two general approaches employed for this purpose. One is the use of surface coating of nanoparticles with hydrophilic polymers such as PEG or surfactants such as such as poloxamers or poloxamines (Stolnik et al., 1994; Veronese and Pasut, 2005). The second one is to use the nanoparticles with biodegradable copolymers with hydrophilic segments such as PLGA-PEG and PLA-PEG (Gref et al., 2000).

1.5.3   Colloidal Stability

There are several physical and chemical factors that play a major role in the instability of polymeric nanoparticles. The overall stability can be classified into physical and chemical stability (Abdelwahed et al., 2006b). The colloidal submicron particles in homogenous suspension do not sediment due to the continuous thermal motion of the particles known as Brownian motion. Random collision of suspended particles of various surface charge content and shape often lead to agglomeration and subsequent settling of the particles. In order to avoid this phenomenon, a suitable stabilizer such as poloxamer 188 is widely used. In addition, there are several factors affect the chemical instability of nanoparticles such as storage conditions including temperature and pH, chemical stability of entrapped drugs as well as the type and molecular weight of the polymer used. The stability of a nanoparticle formulation also depends on the chemical stability of the incorporated drugs. Therefore, to reduce drug degradation and improve the stability of the nanoparticle formulation for a long storage, freeze drying also known as lyophilization, is most commonly used (Chen and Wang, 2007).

1.5.4   Drug Loading and Release

Both drug loading and drug release of nanoparticles are important property for a drug delivery system (Soppimath et al., 2001). Several factors can affect drug loading and entrapment efficiency of nanoparticles such as drug solubility in the polymer matrix, molecular weight, drug polymer interaction and presence of end carboxylic groups. Ideally, a nanoparticle system should have high drug loading capacity. In addition, drug release can be affected by solubility of drug, desorption, drug diffusion, particle matrix degradation or erosion (Bittner et al., 1999). Generally, smaller particles have higher initial burst release caused by poorly entrapped drug or drug adsorbed onto the surface of the nanoparticles, while larger particles have longer sustained release with small initial burst release.

1.6 Biodistribution of Nanoparticles

Understanding the behavior of nanoparticles *in vivo* is a prerequisite for translating basic nanomedical research into clinical trials. For a drug delivery carrier, it is very important to stay in the bloodstream long enough to reach or recognize its therapeutic site of action (Moghimi et al., 2001). However, the opsonization or removal of nanocarriers from the body by MPS is a major obstacle to the realization of these goals. In generally, conventional nanoparticles are rapidly removed within a few minutes, while pegylated nanoparticles can reduce systemic clearance and increase blood circulation time (Gref et al., 1994). However, the clearance and final biodistribution of pegylated nanoparticles depend on many factors, such as composition, size, molecule and surface modification (Alexis et al., 2008; Owens Iii and Peppas, 2006). Thus, the visual information of nanoparticles in drug delivery system by a non-invasive manner is very important.

In recent years, several imaging and spectroscopic techniques have been widely developed for investigating the biodistribution of nanoparticles, including magnetic resonance imaging (MRI), X-ray computed tomography (CT), electron spin resonance image (ESRI), single photon emission computed tomography (SPECT), positron emission tomography (PET), and optical imaging (OI). Furthermore, the combination of two technique also be used to get a more detailed information or 3D images (Liang et al., 2010; Pisani et al., 2008). Table 1.6-1 shows the advantages and disadvantages of various imaging techniques used for investigating the biodistribution of nanoparticles.

Table 1.6-1: The advantages and disadvantages of imaging methods.

Technique	Type of probe	Advantages	Disadvantages	References
MRI	Paramagnetic metals (e.g. Gd and Mn) or superparamagnetic metals (e.g. iron oxide)	High resolution, no ionizing radiation, able to image physiological and anatomical details	High cost, can not be used in patients with metallic devices	(Khemtong et al., 2009)
Ultrasound	Gas filled microbubbles	Non-invasive, easy of produce, no radiation exposure, low cost	Low resolution	(Zhou et al., 2006)
OI	Fluorescent dyes, quantum dots, carbon nanotubes	High sensitivity, provide functional information, no radiation exposure,	Low resolution, Limited tissue penetration	(Rao et al., 2007)
Gamma scintigraphy (PET and SPECT)	Radionuclides (e.g. F-18, In-111, Cu-64, I-124)	Able to image biochemical process	Radiation, low resolution	(Janib et al., 2010)
CT	Heavy element (e.g. iodine)	High spatial resolution, able to differentiate between tissues, low radiation exposure	Radiation, require contrast agent for enhanced tissue contrast, high cost	(Popovtzer et al., 2008)
ESRI	paramagnetic species	Non-invasive, continuous measurement,	Long measurement times, insufficient signal intensity.	(Kempe et al., 2010)

1.7 Research Objective

The aim of the thesis was the development, characterization and *in vivo* evaluation of biodegradable nanospheres and oily core nanocapsules based on diblock copolymer PLGA-PEG and triblock copolymer PLGA-PEG-PLGA.

In this context, several aspects had to be addressed.

- To prepare stabilized polymeric nanospheres and oily core nanocapsules formulated with diblock PLGA-PEG and triblock PLGA-PEG-PLGA using nanoprecipitation method

- To evaluate the physical-co-chemical properties, such as particle size (PCS, LD and AF4), morphology (TEM, AFM), structure (NMR), dynamics (ESR), stability and freeze-drying study

- To study the *in vivo* and *ex vivo* distribution of nanospheres and nanocapsules by fluorescence imaging and confocal microscopy

- To investigate the development of nanospheres for betulinic acid delivery, also the characterization and cell culture study

2 Experimental

2.1 Materials

2.1.1   Polymer

Polymer (Resomer RGP d 5055, Resomer RGP d 50105, Resomer RGP d 50155 and Resomer RGP t 50106) used in this work were purchased from Boehringer Ingelheim, Germany. The explanation of the letters and number can be seen in Fig. 2.1-1, and the chemical structure of end-capping diblock PLGA-PEG and triblock PLGA-PEG-PLGA was shown in Fig. 2.1-2.
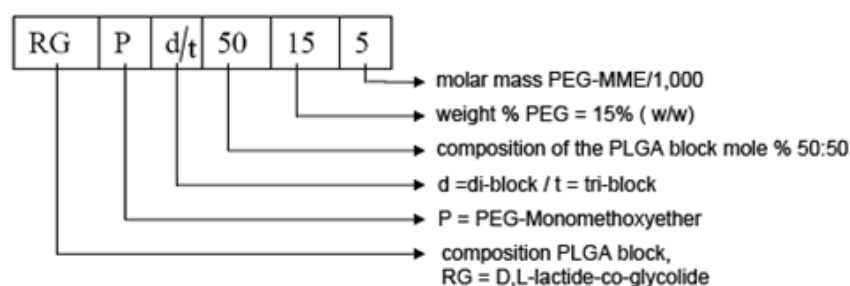
Fig. 2.1-1: Explanation of the letters and numbers of Resomer product used in this study.
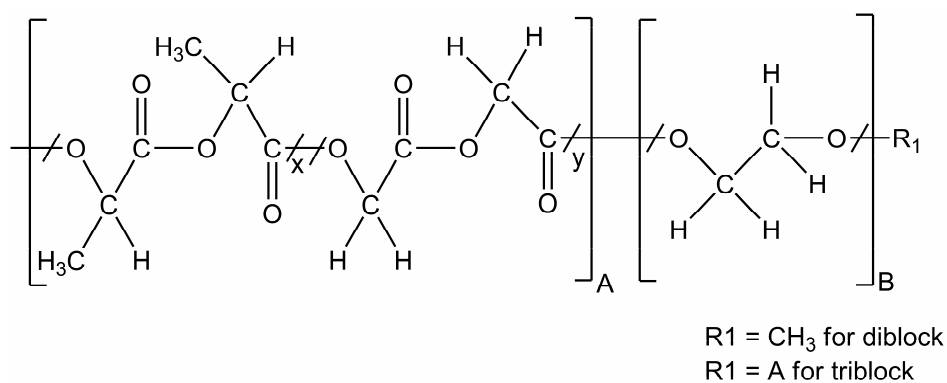
Fig. 2.1-2: Chemical structure of diblock and triblock copolymer.

Depending on their composition, PEG content and structure, the characteristics of diblock PLGA-PEG and triblock PLGA-PEG are listed in Table 2.1-1. And, the copolymers were named to 5AB, 10AB, 15AB and 10ABA, respectively.

Table 2.1-1: Brand name, composition, PEG content, structure and abbreviation of copolymer used for nanoparticle preparation.

Brand name	Copolymer	Mw in kDa	PEG % (w/w)[a]	Structure	Abb[b]
Resomer RGP d 5055	PLGA -PEG	95 kDa -5 kDa	5		5AB
Resomer RGP d 50105	PLGA -PEG	45 kDa -5 kDa	10		10AB
Resomer RGP d 50155	PLGA -PEG	28 kDa -5 kDa	15		15AB
Resomer RGP t 50106	PLGA -PEG -PLGA	27 kDa -6 kDa -27 kDa	10		10ABA

[a] w/w of total polymer concentration
[b] Abbreviations

2.1.2   Oil

Lipiodol (Lipiodol Ultra fluid), an iodized ethyl ester of fatty acids from poppy seed oil with 38% iodine by weight, was purchased from Guerbet GmbH (Sulzbach, Germany). It can be used as X-ray contrast agent for lymphography and hysterosalpingography (Guan et al., 2006).

Miglyol 812 (medium chain triglycerides; MCT) is a liquid lipid with low viscosity. Usually, the composition of fatty acids in MCT is dominated by C8 fatty acids (50 to 65 %), C10 (30 to 45 %), C12 (max. 5 %) and C6 (max. 2 %). MCT was purchased from Caelo, Hilden, Germany.

2.1.3   Drug

Betulinic acid (BA) is a triterpene of natural origin isolated from various plants, such as the bark of white birch. The substance was kindly supplied by BioSolutions Halle GmbH.

The fluorescent probe 1, 1'-dioctadecyl-3,3,3',3'- tetramethylindocarbocyanine perchlorate (DiI) and nile red (NR) were purchased from Sigma-Aldrich, Germany and 1,1'-dioctadecyl-3,3,3',3'- tetramethylindotricarbocyanine iodide (DiR) from Invitrogen, Germany.

The ESR spin probe 2-Heptadecyl-2,3,4,5,5-pentamethylimidazolidine-1-oxyl (HDPMI) was obtained by Prof. V.V. Khramtsov, Institute of Chemical Kinetics and Combustion, Novosibirsk, Russia.

2.1.4   Reagents

Deuterium oxide (D_2O) and chloroform-D1 were obtained from Sigma-Aldrich, Germany. Sucrose, trehalose and glucose were purchased from Fluka, Chemie AG (Buchs, Switzerland). All other chemicals were reagent grade.

2.2 Preparation of Nanospheres and Nanocapsules

Nanospheres and nanocapsules were prepared by the method based on interfacial polymer deposition after solvent displacement (Fessi et al., 1989). For nanocapsule preparation, polymer, drug and oil were dissolved in acetone and the acetone solution was drop-wise injected into bi-distilled water under mild stirring at room temperature. Afterwards, acetone and a part of water were evaporated under reduced pressure at 30°C (200 mbar slowly decreased to 30 mbar). Samples were centrifuged at 4000 rpm (MiniSpin, eppendorf) for 15 min to remove a potential fraction of larger particles in the µm-size range. The final volume of nanocapsule suspension was obtained as wanted.

Nanospheres were prepared only omitting the oil in the formulation. Fig. 2.2-1 shows the schematic representation of NS and NC formulated by nanoprecipitation method. For nanosphere preparation, polymer concentration in acetone changes from 5 mg/ml to 20 mg/ml, and the ratio of acetone to water varies from 1:1 to 1:10; For nanocapsule preparation, the oil/polymer ratio (5:1 or 5:2) was used.
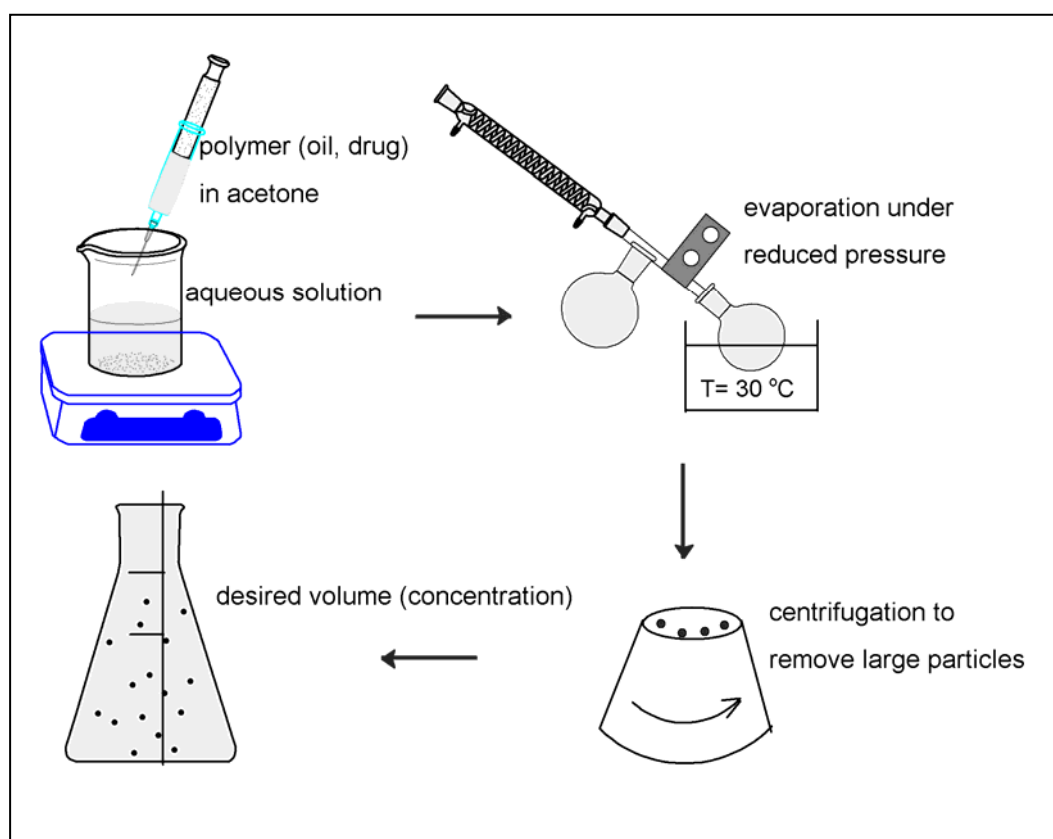
Fig. 2.2-1: Nanospheres and nanocapsules formulated by nanoprecipitation method.

2.3 Instrumentation and Characterization

2.3.1   Photon Correlation Spectroscopy

Photon correlation spectroscopy (PCS, HPPS, Malvern Instruments Ltd) was used for size determination of the nanospheres and nanocapsules. Results are given as mean particle diameters (Z-average) and the polydispersity index (PDI). The analysis was performed at 25°C and at a scattering angle of 173°. Samples were appropriately diluted

(1:50 for nanosphere, 1:20 for nanocapsule, v/v) with filtered (pore size 0.2 μm) water. Z-average diameter and the polydispersity index (PDI) were determined by the Dispersion Technology Software DTS 4.20 (Malvern Instruments Ltd., UK). Each sample was measured three times with 10 runs over 10 s.

2.3.2   Laser Diffraction

For the detection of potential fractions of particles in the μm-size range in addition to the nanoparticles, laser diffraction with adequate sub-micron instrumentation was used (Mastersizer 2000, Malvern Instruments Ltd.). For each measurement, 5 runs over 10 s were done and the results were then averaged. Data analysis was performed by means of the Mastersizer Software version 5.22 (Malvern Instruments Ltd., UK). The size distributions are characterized by the D10, D50, and D90.

2.3.3   Asymmetrical Flow Field-Flow Fractionation

The nanospheres suspensions were analyzed by an Eclipse A4F separation system and channel (Wyatt Technology Europe, Dernbach, Germany) connected to an isocratic pump and micro vacuum degasser (Agilent 1100 Series, Agilent Technologies, D-Boblingen). The channel was equipped with a trapezoidal-shaped spacer (height: 350 μm) and a membrane of regenerated cellulose (MWCO 5 kDa, Microdyn-Nadir, Wiesbaden, Germany) was used as accumulation wall. Bi-distilled and filtered (pore size 0.1 μm, VVLP, Millipore) water preserved with 0.02% w/v sodium azide was used as eluent and for sample dilution. After 1 min of cross flow adjustment and 1 min of focusing at 2 ml/min, 100 μl of the diluted nanosphere suspension (1:10 v/v) were injected into the channel during focusing (focus flow of 2 ml/min) with 0.2 ml/min over 2 min and the sample was focused further for 1 min after finishing injection. The elution mode started with the cross flow decreasing from 2 ml/min to 0.5 ml/min over 5 min and decreasing from 0.5 ml/min to 0 ml/min over 35 min. The detector flow rate was 1

ml/min during all the elution time. Size calculations were performed by the Astra software 4.90 (Wyatt) using the particle mode and assuming compact spheres.

2.3.4   Transmission Electron Microscopy

Negatively stained samples of TEM were prepared by spreading 3 μl of the nanoparticle dispersion onto a cupper grid (200 mesh) coated with a formvar film. After 1 min, excess liquid was blotted off with filter paper. The grid was then placed on a droplet of 1% (w/v) aqueous uranyl acetate solution and drained off after 1 min. The dried specimens were examined with a Zeiss EM 900 transmission electron microscope at an acceleration voltage of 80 kV. Electron micrographs were taken with a slow scan camera (Variospeed SSCCD camera SM-1k-120, TRS, Moorenweis, Germany).

2.3.5   Freeze-Fracture Electron Microscopy

Nanoparticles were frozen using a propane jet-freeze device JFD 030 (BAL-TEC, Balzers, Liechtenstein). Thereafter the samples were freeze-fractured at -150 °C without etching with a freeze fracture/freeze etching system BAF 060 (BAL-TEC, Balzers, Liechtenstein). The surfaces were shadowed with platinum to produce good topographic contrast (2 nm layer, shadowing angle 45°) and subsequently with carbon to stabilize the ultra-thin metal film (20 nm layer, shadowing angle 90°). The replicas were floated in sodium chloride (4% NaCl solution; Roth, Karlsruhe, Germany) for 30 min, rinsed in distilled water for 10 min, washed in 30% acetone (Roth, Karlsruhe, Germany) for 30 min and rinsed again in distilled water (10 min). The replicas were then mounted on copper grids coated with a formvar film and observed with a same transmission electron microscope, as described in 2.3.4.

2.3.6   Atomic Force Microscopy

Atomic force microscopy (Digital Instruments, Dimension 5000 SPM with X-Y stage, Tapping Mode) was employed to confirm the size of the nanoparticles and to determine the shape and surface morphology. 10 μl diluted samples (1:100 v/v) were deposited on a freshly cleaved silicon surface, spread and dried for 3 h at room temperature. Height and phase images and data evaluation (height profiles) were conducted with the software WSxM 3.1 software (Horcas et al., 2007).

2.3.7   Nuclear Magnetic Resonance

^{1}H-NMR spectra was acquired using a Varian Gemini 2000 400-MHz NMR spectrometer at 20°C (Varian, Inc., Grenoble, France). An aliquot of suspension was filled in a NMR-tube. Accurately weighted quantities of deuterium oxide (D_2O) (for all aqueous samples) or chloroform-D1 (for measurement of solid material) were added for field login and TMS was added as reference.

2.3.8   Electron Spin Resonance

An ESR spectrometer of 9.5 GHz (Miniscope MS 200; X-Band) from Magnettech (Berlin; Germany) was used (Fig. 2.3-1), where the probe is examined inside a glass capillary. Measurements were conducted at room temperature with the following typical parameters: B0 field: 335.4 mT; sweep: 10 mT; modulation frequency: 100 kHz; microwave power: 20 mW; scan time: 30 s; modulation amplitude: 0.1 mT.

Fig. 2.3-1: The ESR spectrometer Miniscope MS 200 (X-Band).

2.3.9 Freeze-drying

The nanosphere or nanocapsule dispersions were diluted (1:1) with the cryoprotectant solutions before freezing. The samples were frozen for at least 12 h at a temperature of -81 °C, and then kept at the room temperature for thawing. For freeze-drying, the NPs dispersions were diluted (1:1) with the cryoprotectant solutions before freezing. The samples were lyophilised using Christ Alpha-2-4 Laboratory Freeze Dryer (Martin Christ Gefriertrocknungsanlagen GmbH, Osterode am Harz, Germany) for 48 h at a temperature of -25 °C and a vacuum of 0.4 mbar. The freeze dried samples were then sealed to avoid moisture contamination and stored at 4 °C. The redispersibility of all the freeze-dried nanoparticles was tested by adding the same volume of water on top of the nanoparticle cakes and manually shaking the containers.

2.3.10 Animal Studies

All procedures of the *in vivo* experiments complied with the standards for use of animal subjects as stated in the guidelines from the animal care and use committee of

Saxony-Anhalt. The *in vivo* studies were performed in nude, female mice (SKH1-Hrhr, 25-30 g) from Charles River Lab. They were housed under controlled conditions (12 h light/dark schedule, 24 °C) in groups of three mice per cage and formulation. A 5.25% sorbitol stock solution was produced by adding sorbitol to water for injection and it was filtered through a 0.22 μm sterile filter. Then, 100 μl of the sorbitol solution was added to 900 μl of nanoparticle dispersion to get 1 ml isotonic solution. 100 μl of the isotonic nanoparticle dispersion was intravenously (i.v.) injected into the tail vein of each mouse in the group. Afterwards an inhalation narcotic system with a mixture of isofluorane/oxygen (initial flow of 4% isofluorane (3.0 L/min oxygen) and steady state flow of 1.8% isofluorane (1.5 L/min oxygen)) was used. During *in vivo* imaging the mice were placed on a 35 °C controlled heating plate to protect them for cooling out.

2.3.11 *In Vivo* Fluorescence Imaging

The measurements were carried out using the Maestro™ *in vivo* fluorescence imaging system (Cambridge Research & Instrumentation, Woburn, United States) an inhalation anesthesia system (Fig. 2.3-2). A Cermax®-type 300 Watt Xenon lamp with 5600 K, a NIR excitation filter (710 to 760 nm) and an 800 nm long pass emission filter were used to detect DiR. The software acquired multispectral image cubes in 10 nm steps in the spectral range between 780 and 950 nm. Exposure times of 15, 400, 800 and 1200 were used. A DiR reference spectrum was generated from accumulated nanoparticles in the liver and subsequent manual computing using background fluorescence spectra from an untreated mouse measured under the same conditions. Using these two spectra the Maestro™ software allows a manual computing of the *in vivo* DiR spectra. Based on these two spectra grayscale images and further RGB as well as intensity weighed images were generated. The *in vivo* fluorescence imaging was examined 15 min, 3 h, 6 h and 24 h after i.v. injection in mice. Detection of NR was carried out with the green filter set (503 to 555 nm excitation filter, 580 nm long pass emission filter, 550 nm to 800 nm acquisition setting) in 2 nm steps. Fluorescent imaging files were acquired during the first hour after

injection. All other parameters accorded to the DiR measurements.
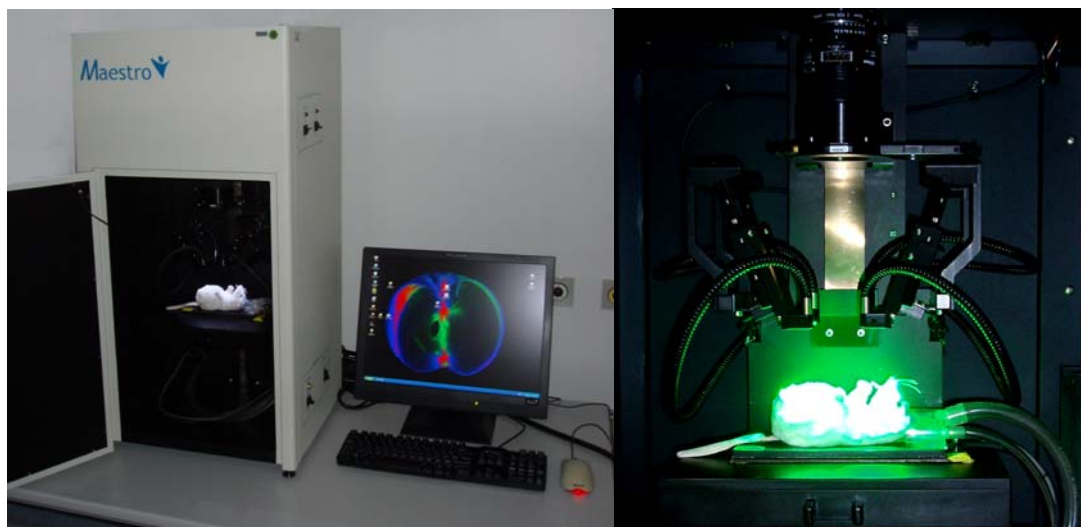
Fig. 2.3-2: The Maestro™ *in vivo* fluorescence imaging system.

2.3.12 *Ex Vivo* Fluorescence Imaging

For *ex vivo* experiments the mice were sacrificed and organs were placed into a 24 holes well-plate. For further calculation and evaluation, a region of interest (ROI) in the size of the holes of the well-plate was generated and the corresponding exposure-time weighted total and maximum fluorescence signals were calculated. To exclude the influence of different dye amounts due to different nanoparticle concentration, the *ex vivo* total intensity value was divided through the maximum intensity of the in *vitro* emission spectra of the nanoparticles. These *in vitro* spectra were measured prior to injection, and all in equal volumes and under same measurement conditions. Afterwards all values were normalized to 100% related to the highest fluorescence intensity. The measurements were carried out under same conditions like the *in vivo* measurements (NIR filter set, 10 nm steps, 400, 1200 ms).

2.3.13 Confocal Laser Scanning Microscopy

For confocal laser scanning microscopic measurements, a laser scanning microscope LSM 710 (Zeiss, Jena, Germany) was used. The microscope was equipped with 63x plan apochromat oil immersion objective. As DiI allow an excitation with the available 514 nm laser, it was incorporated to the nanocapsule instead of the DiR. Emission was detected in the range between 520 and 686 nm. Images were acquired in sequential scan mode using the ZEN software (Zeiss, Jena, Germany). The ovarian tissues of the mice were investigated 24 h after injection of the formulations. The tissue was excised, cut into a small panel (approximately 1 mm), slightly pressed between two cover glasses, and immediately viewed in the LSM. As a control, one droplet of the nanocapsule suspension put on a cover slip was also investigated.

2.3.14 UV-visible Spectroscopy

A UV-vis spektralphotometer (analytik Jena) SPEKOL 1500 was used to detect the dye amount in nanospheres and nanocapsules. The precipitated dye was dissolved in acetone and was used to quantify the level of non-encapsulated DiR/DiI/NR of nanoparticles by UV-visible spectroscopy at 750 nm/550 nm/535 nm.

2.3.15 High-Performance Liquid Chromatography

The BA entrapped in PLGA-PEG nanospheres was measured by High-Performance Liquid Chromatography (HPLC). A reverse phase column (Zorbax XDB C18; 3.5 μm, 4.6x150 mm with pre column) was used. 20 μl nanosphere dispersion was injected (mobile phase: 65/35 v/v acetonitril / 1.5% phosphoric acid in water, 1 ml/ min) at 30°C. The column effluent was detected at 210 nm with a UV/vis detector. The calibration curve for BA quantification was linear over the range of standard concentration between

0.0434 mg/ml and 0.273 mg/ml with a correlation coefficient of $R^2=0.9997$. The encapsulation efficiency (EE) was defined as the ratio of actual and original amount of BA encapsulated in nanospheres. Encapsulation efficiency (EE, %) was calculated by the following formula:

$$EE\ (\%) = (BA\ in\ nanospheres/total\ BA\ added) * 100\%$$

2.3.16   Cell Culture

The cytotoxic activities of all the compounds were evaluated using the sulforhodamine-B (SRB) (Sigma Aldrich) microculture colorimetric assay (Skehan et al., 1990). In short, exponentially growing A549 cells (2500 cell/well) were seeded into 96 well plates on day 0. After 24 h, the cells were treated with serial dilutions of the BA and nanospheres for 96 h. The percentages of surviving cells relative to untreated controls were determined 96 h after the beginning of drug exposure. After 96 h treatment, the supernatant medium from the 96 well plates was thrown away and the cells were fixed with 10% TCA. For a thorough fixation plates were allowed to stand at 4 °C for at least 2h. After fixation, the cells were washed in a strip washer. The washing step was done four times with water using alternate dispensing and aspiration procedures. The plates were then dyed with 100 μl of 0.4% SRB for 45 min. After dying, the plates were washed again to remove the dye with 1% acetic acid and allowed to air dry overnight. 100 μl of 10 mM Tris base solution was added to each well of the plate the next day and absorbance was measured at 570 nm using a 96 well plate reader (Tecan Spectra, Crailsheim, Germany). The IC_{50} value defined as the concentrations of the compound at which 50% cell inhibition was calculated from the semi-logarithmic dose-response curves.

3 Results and Discussion

3.1 Preparation of Nanospheres and Nanocapsules

3.1.1   Nanoprecipitation Method

Nanoprecipitation, also called solvent displacement of preformed polymer, is a popular technique to prepare nanoparticles. This technique has several advantages, in that it only involves one step process, rapid and easy to perform. It requires two solvents that are miscible. In brief, polymer, drug, oil (for nanocapsule preparation) and a lipophilic surfactant are dissolved in a water-miscible solvent such as acetone, and the solution is injected in to an aqueous solution containing a hydrophilic surfactant such as poloxamer 188. The nanoparticles are formed by rapid diffusion of the acetone into the aqueous phase.

The process of nanoprecipitation method can produce nanoparticles with small size of 100-300 nm and a narrow distribution (Chorny et al., 2002). This method does not require shear stirring rate, high temperature and sonication. The process use low-toxicity of solvent (such as acetone), which is more suitable for intravenous (i.v) injection. However, the most limitation of this method is more time-consuming.

In this study, the diblock copolymer PLGA-PEG and tri-block copolymer PLGA-PEG-PLGA as polymer shell materials were used to produce nanospheres and nanocapsules. Fig. 3.1-1 shows the schematic representation of PLGA-PEG nanosphere and oily core nanocapsules. Due to their amphiphilic property with hydrophobic PLGA block and hydrophilic PEG block, the hydrophilic surfactant for nanoparticle formulation can be avoided. In most cases, lecithin was used as a lipophilic surfactant for

nanocapsule preparation, however, liposomes were detected in the nanocapsules samples by freeze-fractured electron microscopy (Couvreur et al., 2002). So, it is the best way to produce nanocapsules without lecithin to avoid this problem.
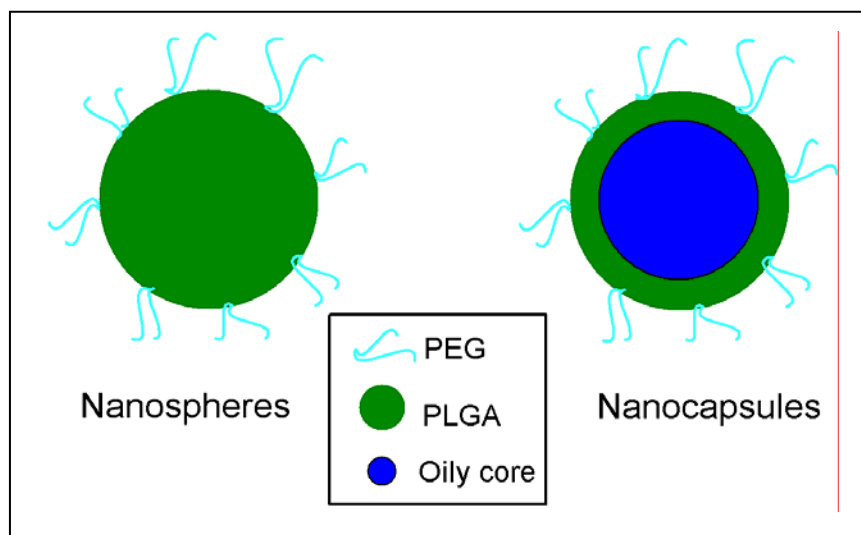
Fig. 3.1-1: Schematic representation of the PLGA-PEG nanosphere and oily core nanocapsule.

3.1.2   Mechanism of Nanoparticle Formulation

Nanoparticles formulated by nanoprecipitation can be explained by two theories. The common one is the Marangoni effect presented in many literatures (Bilati et al., 2005). The formulation of nanoparticles is formed by spontaneous emulsification, where movement in an interface is caused by longitudinal variations of interfacial tension. The emulsification step occurs because severe fluctuations in surface tension cause the movement of the organic phase into the aqueous phase and the subsequent formation of nanoparticles. Recently, the Katz research group (Ganachaud and Katz, 2005; Vitale and Katz, 2003) provides a new insight into the formulation of nanospheres and nanocapsules by Ouzo effect, which is well-known as aperitifs (ethanol extracts of anis seeds). Upon dilution with water, such extracts become cloudy and remain for a long

time. This phenomenon is very general that it can occur upon mixing large amounts of water with almost any solution consisting of a small concentration of oil in a hydrophilic solvent. Fig. 3.1-2 shows the schematic representation of the liquid-liquid nucleation process or Ouzo effect.
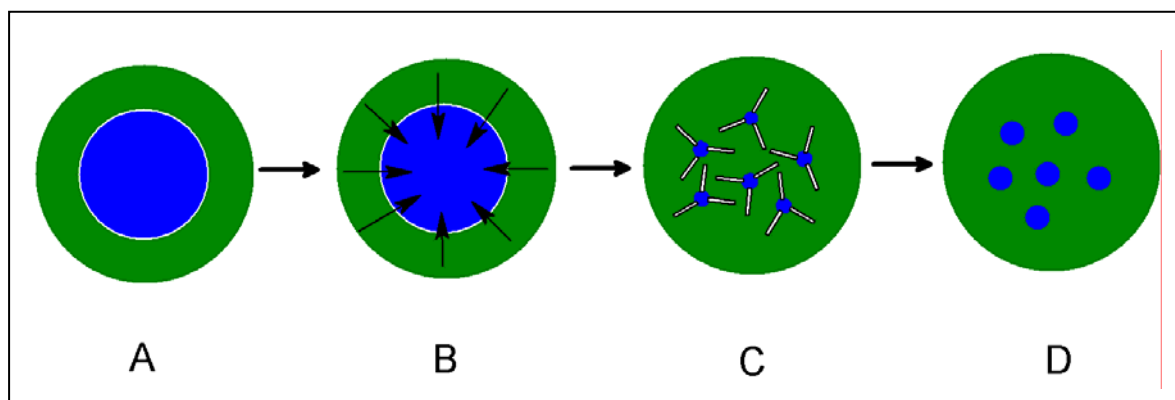
Fig. 3.1-2: Schematic representation of the liquid-liquid nucleation process or Ouzo effect, A: region of oil in solvent mixture surrounded by water; B: water diffusion into the droplet containing the oil; C: supersaturation of the oil causing homogeneous ~ 1nm size droplets and diffusion of oil into nearby droplets; D: final metastable emulsion (modified from Ganachaud and Katz, 2005).

3.1.3   Oil Choice for Nanocapsule Preparation

Nanocapsules have more complex structure than nanospheres. The special characterization is their liquid phase, mainly oily phase suitable for water-insoluble substance. The requirements of oil selection for nanocapsule preparation include the absence of toxicity, risk of degradable, no dissolution of the polymer and high drug encapsulation. A wide range of oils can be suitable for nanocapsule preparation, including vegetable oils, mineral oils, triglycerides, large-sized alcohols, pure compounds such as ethyl oleate (Mora-Huertas et al., 2010). And, nanocapsules have several advantages, including low toxicity of polymer and surfactant components, low wall thickness, high drug encapsulation (if oil is a good solvent for the drug), long half life

time, and good protection from degradation. However, until now only few limited oils can be successfully applied for nanocapsule preparation in literatures.

The most common oils for nanocapsule studies are medium-chain triglycerides (MCT) and long-chain triacylglycerols (LCT), which can be commercially available such as Miglyol® or Myritol®. In this study, lipiodol (Fig. 3.1-3) was used to develop the oily-core PLGA-PEG and PLGA-PEG-PLGA nanocapsules. The lipiodol oil is commercially available for several purposes, including the use as X-ray contrast agent for lymphography and chemoembolization.
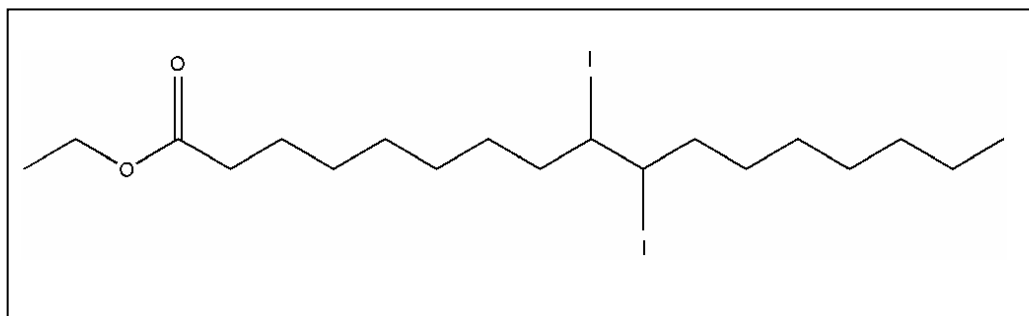
Fig. 3.1-3: Chemical structure of lipiodol oil.

3.2 Size Determination

Particle size and size distribution are most important for pharmaceutical applications. In this study, three different techniques were used to characterize the particle size. Photon correlation spectroscopy (PCS) was used to determine the particle size and size distribution. Laser diffraction (LD) with sub-micron instrumentation was used to detect the potential fractions of particles in the μm-size range. Asymmetrical flow field-flow fractionation (AF4) can provide the possibility to get more detailed information about particle size.

3.2.1   PCS and LD

PCS is a dynamic light scattering (DLS) method where the fluctuations of the intensity of scattered light due to the Brownian motion of particles are measured in dependence on time. The particle size that can be reliable measured by PCS ranges from about 5 nm up to 1-5 μm, depending on the sensitivity of the instrument. A hydrodynamic mean diameter (Z-average) and the polydispersity index (PDI) as an indication for the width of the particle size distribution can be obtained. The Z-average diameter presents a robust value but only represents a reliable mean size of the sample when the size distribution is sufficiently narrow. However, it is not sensitive to detect the particles in the μm-size range using PCS, even micro-particles remains in the samples sometimes. As for samples with broad size distribution and sizes in the mid and upper nm-range, laser diffraction appears more applicable. So, it is necessary to use the combination of PCS and LD to get accurate information on particle size and size distribution of nanoparticles (Gaumet et al., 2008). Fig. 3.2-1 shows the size distribution results of a nanosphere suspension before centrifugation and after centrifugation by LD and PCS. Particles in the micro-range were detected in the nanoparticle sample before centrifugation (Fig. 3.2-1B). For the same sample before centrifugation, no μm-size particles were found from PCS results (Fig. 3.2-1A).
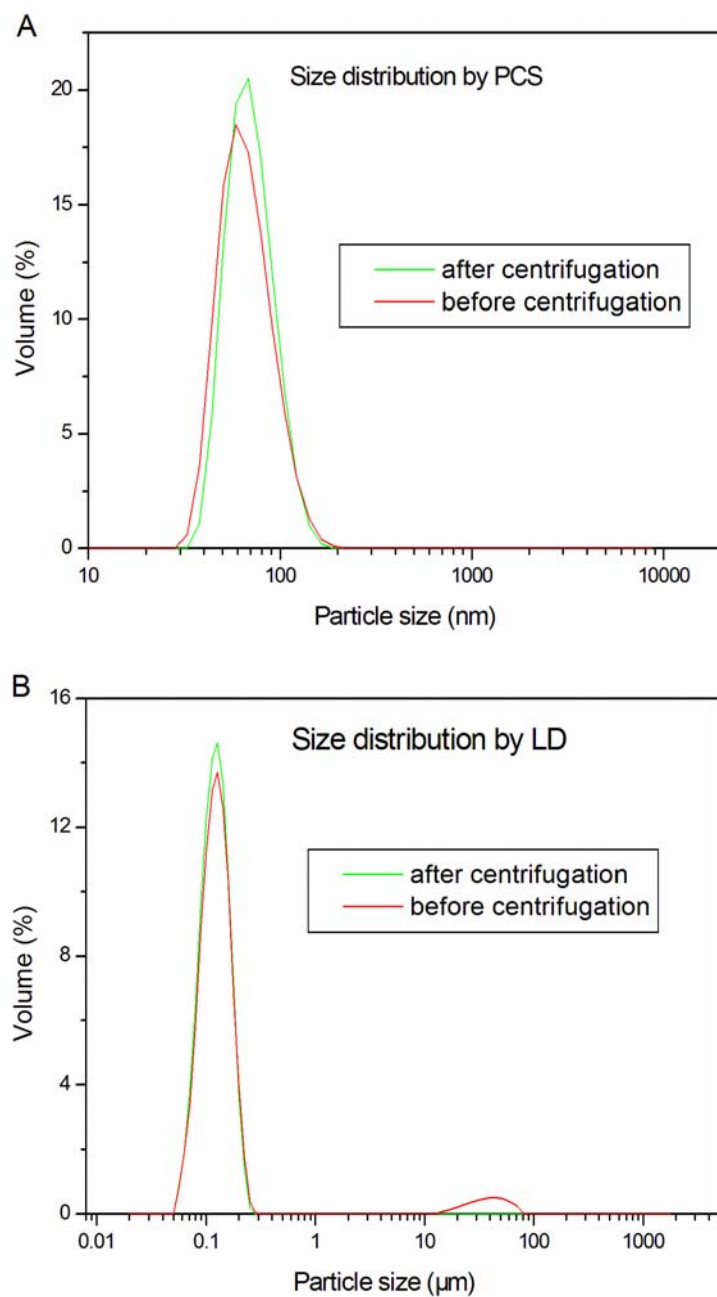
Fig. 3.2-1: Size distribution result of a nanosphere suspension before centrifugation and after centrifugation by PCS (A) and LD (B).

3.2.2   AF4

Asymmetrical flow field-flow fractionation (AF4) combined with multi-angle laser light scattering (MALLS) is a promising method to characterize the colloidal nanoparticle

formulations depending on its versatility, broad separation range (20 nm-1 μm) and the possibility to obtain homogeneous sample fractions (Augsten et al., 2008). Compared with PCS and LD, AF4 can obtain more information about particle size of nanoparticle, but it is difficult to handle, and optimization needed for each kind of particles (Fraunhofer and Winter, 2004). Fig. 3.2-2 shows the schematic presentation of the channel dimensions and flow conditions principle in this study. With AF4, particles are separated depending on their sizes by the cross flow. Large particles are remained, while smaller ones can easily diffuse back into the centre of the main stream.
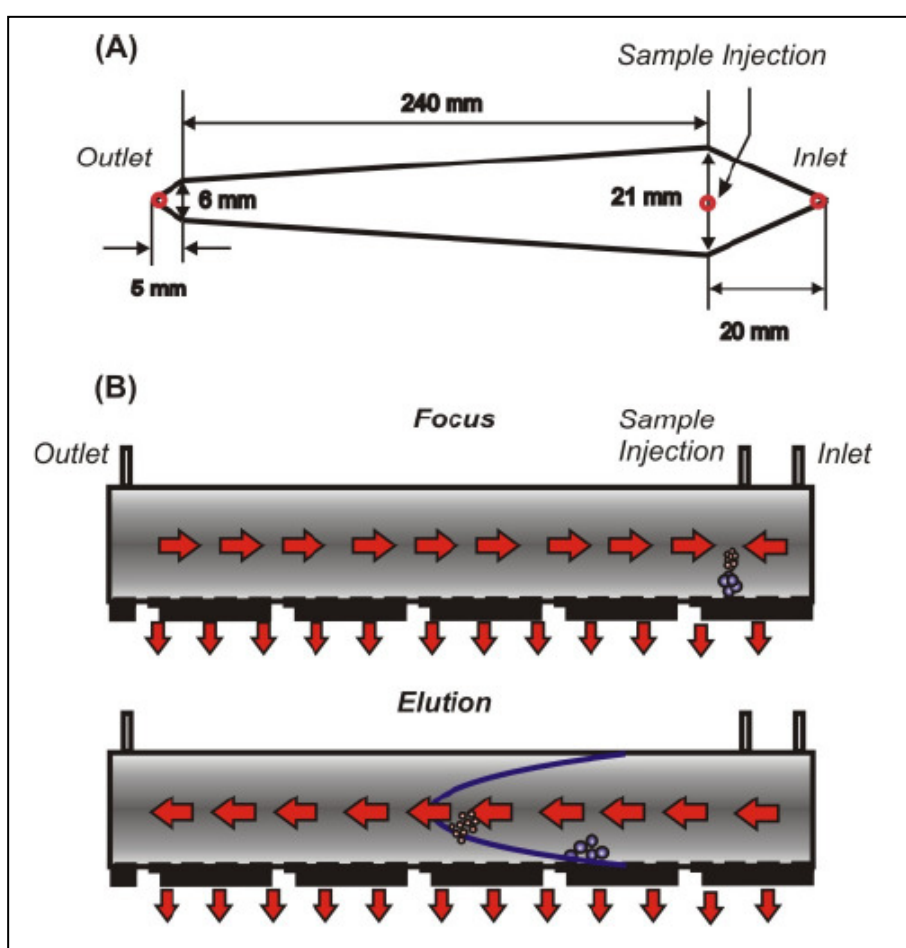
Fig. 3.2-2: Schematic presentation of the channel dimensions (A) and flow conditions principle (B). (Kuntsche et al., 2009).

AF4 combined with MALLS allows accurate size evaluation for sample separation prior to size determination. Table 3.2-1 shows the D10, D50, D90 and Mean diameter determined by AF4/MALLS and hydrodynamic size determined by PCS. The mean

diameter of 5AB (109.1 nm), 10AB (67.9 nm) and 15AB (69.7 nm) from AF4 was in a good agreement with the hydrodynamic size of 5AB (103.3 nm), 10AB (71.0 nm) and 15AB (76.7 nm) from PCS. The smaller size difference determined from PCS and AF4 can be explained by the result of the water binding between the PEG chains on the nanosphere surfaces. This influences the movement of the nanospheres during the PCS measurements and thereby the detected nanosphere size. Due to principle of MALLS measurements, which is applied to retrieve geometrical mass weighted particle sizes (RMS radius), the influence of the water shell is reduced.

Table 3.2-1: D10, D50, D90 and Mean diameter determined by AF4/MALLS and hydrodynamic size determined by PCS.

Sample	D10 (nm)	D50 (nm)	D90 (nm)	Dz (nm)	Z-Ave (nm)
5AB NS	52.9±0.8	75.0±1.5	112.8±0.3	109.1±0.2	103.3±0.6
10AB NS	34.5±1.2	48.8±0.7	70.8±0.8	67.9±1.9	71.0± 0.6
15AB NS	38.9±1.5	53.8±0.5	76.0±0.1	69.7±0.4	76.7±0.3

Their FlFFF/MALS fractograms of PLGA-PEG nanospheres are given in Fig. 3.2-3. Depending on the polymer type (PEG content of copolymer from 5% to 15%), peaks with different elution time and width were received. Compared with 5AB NS (103.3 nm hydrodynamic size) and 15AB NS (76.7 nm hydrodynamic size), 10AB NS with small PCS hydrodynamic size (71.0 nm) represented shorter elution time at maximum light scattering signal. This result suggests that the smaller particles elute first while larger particles elute last, which is in a good agreement with AF4 theory.
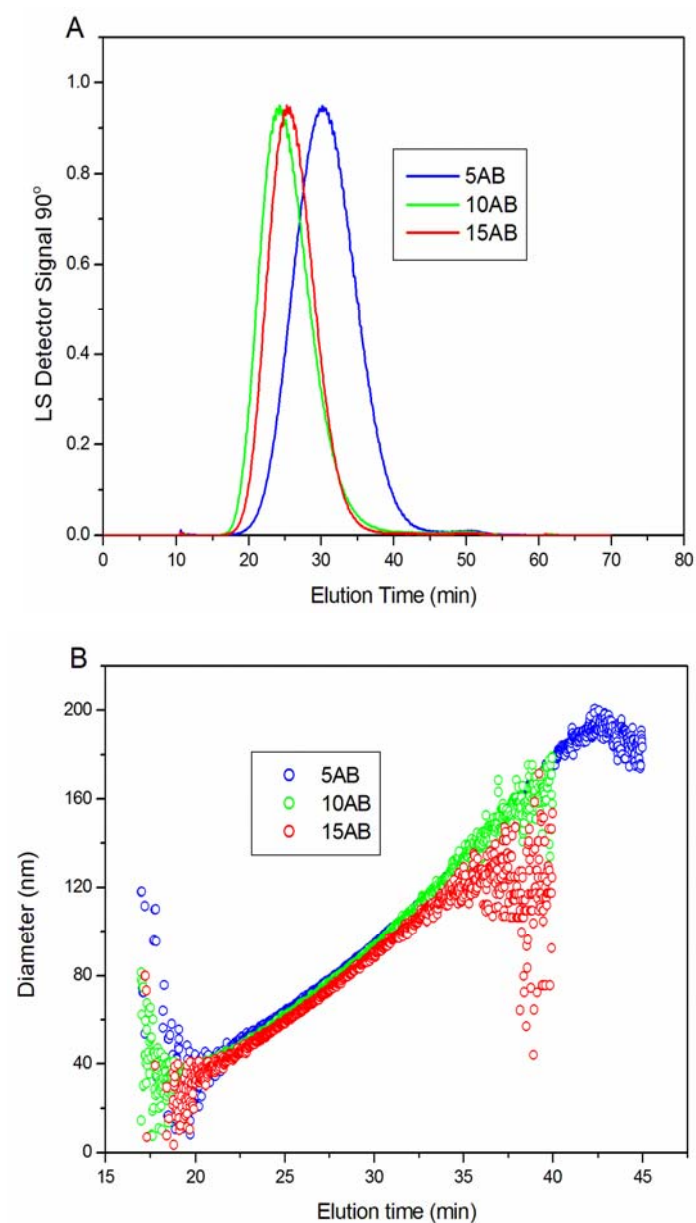
Fig. 3.2-3: The LS Detector Signal at 90° (A) of AF4 elution profiles of nanospheres formulated with different polymer 5AB, 10AB and 15AB and the corresponding diameters with elution time (B).

Fig. 3.2-4 shows the cumulative number and mass weighted size distributions from AF4/MALS data. Compared to PCS, the results represent size distributions of higher quality. Most particles corresponded to a single size result in much sharper peaks. This can be explained by the AF4 separation step prior to size detection.
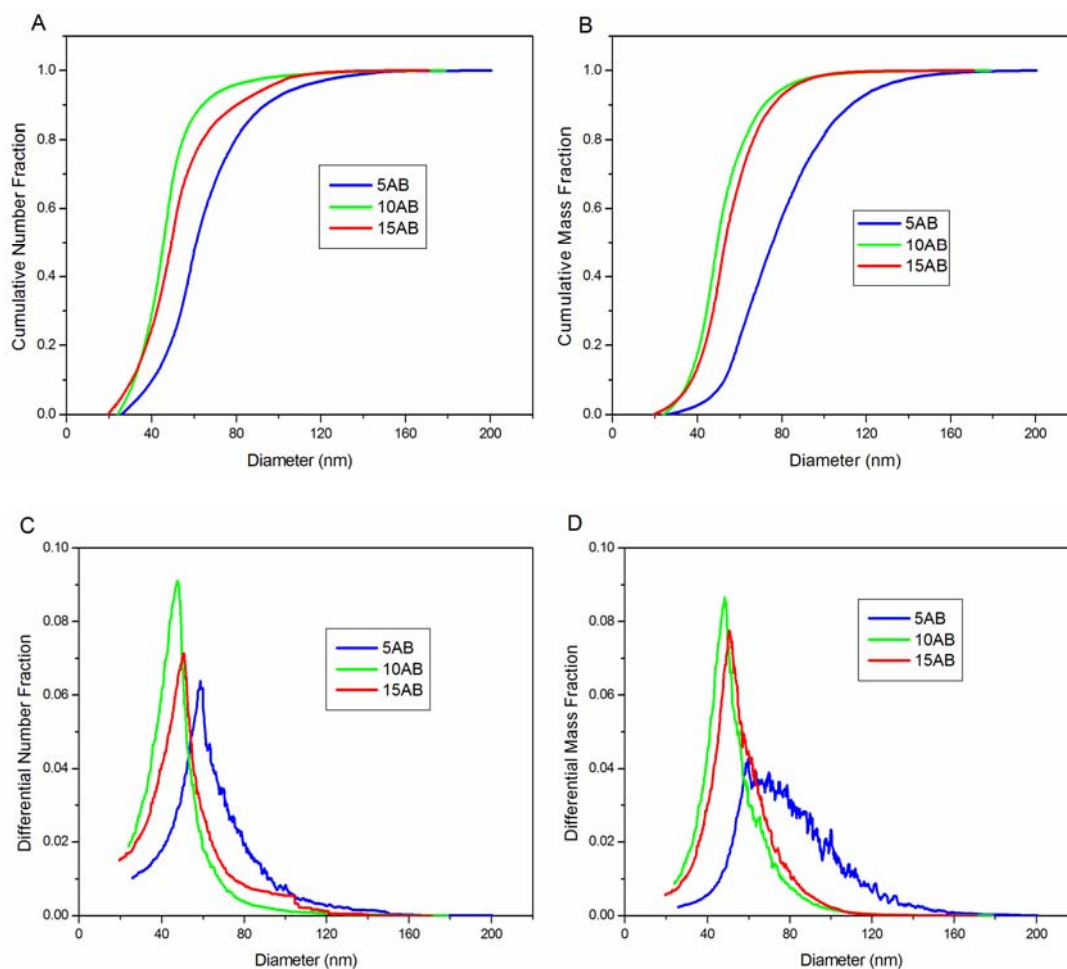
Fig. 3.2-4: Cumulative (A, B) and differential (C, D) number and mass weighted size distribution of 5AB, 10AB and 15AB nanospheres.

3.2.3   Nanosphere Size

The size of PLGA-PEG nanospheres can be influenced by several formulation variables with polymer concentration in solvent, volume ratio of solvent and water, molecular weight of PLGA block and PEG content of polymer (Avgoustakis, 2004; Chorny et al., 2002). Table 3.2-2 shows the particle size of nanospheres formulated with different polymer depending on the polymer concentration. When the polymer concentration in acetone increased, the particle size increased. For 5AB, 10AB, 15AB and 10ABA, the particle size increased from 81.2 nm, 55.2 nm, 75.7 nm and 73.2 nm to 134 nm, 92.3 nm,

88.8 nm and 145 nm when the polymer concentration increased from 5 mg/ml to 20 mg/ml, respectively. The effect of the polymer concentration on the nanosphere size appears mainly to be attributed to the higher resultant organic phase viscosity, which can result in large nanodroplet formation (Chorny et al., 2002).

Table 3.2-2: Size VS polymer concentration of nanospheres formulated by different polymers.

Sample	Concentration (mg/ml)	Z-Ave (nm)	PDI
5AB NS	5	81.2±5.45	0.095±0.016
5AB NS	10	103±2.52	0.094±0.003
5AB NS	15	118±4.51	0.090±0.010
5AB NS	20	134±3.21	0.085±0.015
10AB NS	5	55.2±1.99	0.095±0.016
10AB NS	10	68.8±1.91	0.104±0.006
10AB NS	15	76.6±2.33	0.110±0.005
10AB NS	20	92.3±1.81	0.113±0.014
15AB NS	5	75.7±1.23	0.092±0.016
15AB NS	10	77.8±2.54	0.098±0.015
15AB NS	15	83.4±1.19	0.098±0.012
15AB NS	20	88.8±1.50	0.095±0.012
10ABA NS	5	73.2±2.49	0.133±0.005
10ABA NS	10	99.5±2.40	0.144±0.012
10ABA NS	15	122±7.09	0.137±0.006
10ABA NS	20	145±1.53	0.186±0.008

Values express the mean±SD values of three batches.

Most interestingly, the data in terms of changes in nanosphere size showed linear agreement between particle size and polymer concentration. The R^2 values for the plot of mean nanosphere size and polymer concentration (Fig. 3.2-5) were 0.978, 0.956, 0.904 and 0.996 for 5AB, 10AB, 15AB and 10ABA, respectively. In the polymeric nanosphere system, using the linear correlation of the nanosphere size and polymer concentration can allow for formulation of nanosphere with predefined and desirable sizes.
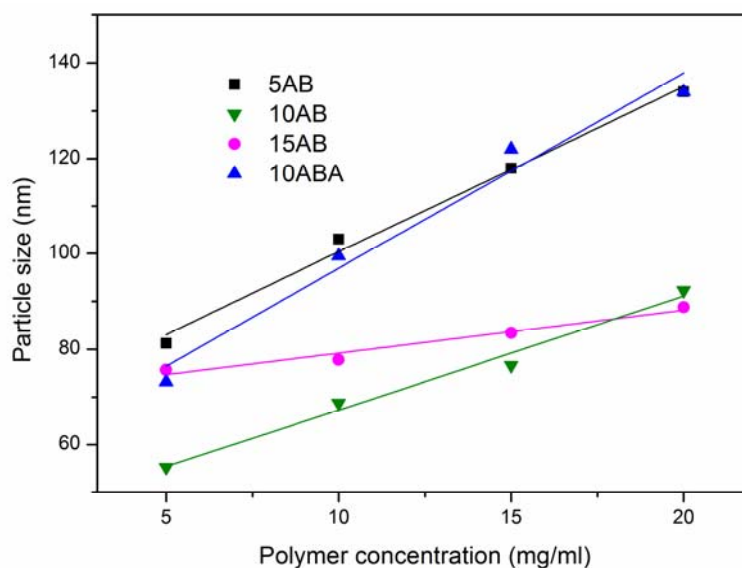
Fig. 3.2-5: Plot of the nanosphere size and polymer concentration for different polymer. The equation and R^2 values of the plot for different polymers: 5AB (Y=65.7+3.468X, R^2= 0.978), 10AB (Y=43.45+2.382X, R^2= 0.956), 15AB (Y=70.2+0.898X, R^2= 0.904) and 10ABA (Y=50.45+4.758X, R^2= 0.996).

Table 3.2-3: Size VS ratio of acetone to water of nanospheres formulated by different polymers (polymer concentration: 10 mg/ml).

Sample	Ratio (acetone/H20)	Z-Ave (nm)	PDI
5AB NS	1:1	109±2.08	0.097±0.004
5AB NS	1:2	103±2.52	0.094±0.003
5AB NS	1:5	107±2.08	0.099±0.009
5AB NS	1:10	105±1.53	0.097±0.005
10AB NS	1:1	67.5±2.06	0.109±0.007
10AB NS	1:2	68.8±1.91	0.104±0.006
10AB NS	1:5	66.8±1.60	0.122±0.003
10AB NS	1:10	66.2±1.54	0.128±0.004
15AB NS	1:1	85.6±2.80	0.091±0.006
15AB NS	1:2	77.8±2.54	0.098±0.015
15AB NS	1:5	78.4±1.83	0.130±0.008
15AB NS	1:10	75.8±2.04	0.103±0.010
10ABA NS	1:1	102±3.11	0.143±0.011
10ABA NS	1:2	99.5±2.40	0.144±0.012
10ABA NS	1:5	85.4±3.58	0.125±0.007
10ABA NS	1:10	82.3±1.86	0.118±0.004

Values express the mean±SD values of three batches

Table 3.2-3 shows the particle size of nanospheres formulated with different polymer

depending on the ratio of acetone to water. The results show no apparent difference when the ratio varied. Only a very slight decrease on particle size of 10 AB and 10ABA nanosphere happened when the ratio of acetone and water increased from 1:1 to 1:10.

Table 3.2-4 shows the particle size of nanospheres formulated with different polymer depending on the PEG content of polymer. When PEG content of polymer increased from 5% to 13%, the particle size decreased from 103 nm to 66.6 nm. However, the particle size increased when the PEG content increased to 15%. Avgoustakis (2003) investigated the PLGA-PEG nanospheres with different PEG content using a solvent evaporation technique, and the result show that particle size decreased from 114.8 nm (PDI: 0.245) to 57.5 nm (PDI: 0.347) when PEG content increased from 0.2% to 3%.

Table 3.2-4: Size VS PEG content of PLGA-PEG nanospheres (polymer concentration: 10 mg/ml.

Composition	PEG% (w/w)	Z-Ave (nm)	PDI
5AB	5	103±2.52	0.094±0.003
5AB/10AB (1:1)	8	85.6±1.21	0.111±0.007
10AB	10	68.8±1.91	0.104±0.006
10AB/15AB (1:1)	13	66.6±1.37	0.096±0.007
15AB	15	77.8±2.54	0.098±0.015

Values express the mean±SD values of three batches

PLGA-PEG nanospheres have been widely investigated for pharmaceutical applications by many research groups (Avgoustakis et al., 2002; Danhier et al., 2009; Li et al., 2001). Beside polymer concentration, ratio of solvent to water and PEG content, particle size of PLGA-PEG nanospheres can also be influenced by other parameters. Cheng (2007) investigated the effect of the water miscibility of solvent with tetrahydrofuran (THF), acetonitrile, acetone and N,N-dimethylformamide (DMF) on the particle size. Nanospheres formulated with DMF (the most water miscible solvent) had the smallest particles, which can be explained by more efficient diffusion of the solvent into water phase. The most important thing on the size determination of nanospheres is to get good nanosized particles (low than 200 nm) with narrow size distribution (a PDI value

low than 0.2), and no potential µm-size range particles should be detected for the further *in vivo* investigation.

3.2.4   Nanocapsule Size

Nanocapsules have complex structure than nanospheres, and particle size can be influenced by many factors, such as type of oil, oil concentration, oil viscosity and polymer concentration (Mora-Huertas et al., 2010). In this work, different polymer 5AB, 10AB, 15AB and 10ABA were used as the polymer shell, and lipiodol and MCT used as oily phase for nanocapsule preparation. When nanocapsules prepared only with the MCT oil, µm-range particles can be detected by LD, while nanocapsules with lipiodol oil reduced the particle size, and had no µm-range particles.

Table 3.2-5 shows the particle size and size distribution of lipiodol oily core nanocapsules formulated by different ratio of polymer to oil. When the ratio of polymer to oil was 1:5, nanocapsules prepared with different polymer had similar particle size around 147 nm to 158 nm with PDI from 0.165 to 0.224. And, when the ratio of polymer to oil was 2:5, nanocapsules prepared with different polymer had similar particle size around 131 nm to 139 nm with PDI from 0.119 to 0.225. The similar particle size of nanocapsules prepared with the different polymers (5AB, 10AB, 15AB and 10ABA) can be attributed to the same oily phase.

Table 3.2-5: Particle size and size distribution of lipiodol oily core nanocapsules formulated by different polymer. Data express the mean±SD values of three batches.

Sample	Polymer/ lipiodol (mg/µl)	Z-Ave (nm)	PDI
5AB NC	1 : 5	147±9.87	0.165±0.031
10AB NC	1 : 5	152±12.2	0.198±0.033
15AB NC	1 : 5	158±8.54	0.189±0.018
10ABA NC	1 : 5	153±14.2	0.224±0.028
5AB NC	2 : 5	135±2.90	0.119±0.013
10AB NC	2 : 5	131±5.69	0.225±0.023
15AB NC	2 : 5	139±14.1	0.215±0.049
10ABA NC	2 : 5	132±6.16	0.194±0.012

The combination of two oils (lipiodol and MCT) was used to investigate the particle size of nanocapsules. Fig. 3.2-6 shows the particle size of 15AB oily core nanocapsules prepared the mixture of lipiodol and MCT. Nanocapsules prepared with the lipiodol/MCT (1:1) had a smaller size around 164 nm with a PDI value of 0.098. Compared with the nanocapsules prepared only with the lipiodol oil (Table 3.2-5), the combination of lipiodol oil and MCT oil to prepare nanocapsules can increase particle size and decrease the PDI depending on the ratio of the two oil.
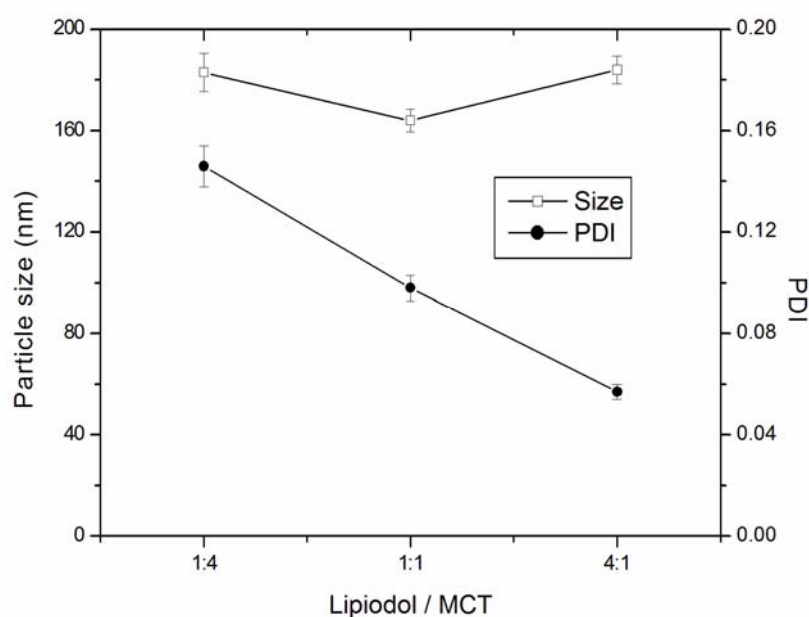
Fig. 3.2-6: Particle size and size distribution of 15AB lipiodol-MCT oily core nanocapsules (polymer/oil=1:5).

3.3 Morphology and Structure

3.3.1 TEM

Electron microscopy such as transmission electron microscopy (TEM) is a common technique to study the structure and the morphology of polymeric nanoparticles. In addition, methods of PCS, LD and AF4 in Chapter 3.2 are not measuring the real size of nanoparticles (only detect light scattering or elution effects which can be used to

calculate particle sizes), TEM as an additional and useful technique can thus provide direct information on the particle size of nanospheres and nanocapsules (Gaumet et al., 2008).

TEM structural and morphological study of polymeric NS and NC can be made using the classic negative stained method. Fig. 3.3-1 shows the TEM images of nanospheres formulated with different polymer 5AB, 10AB, 15AB and ABA. The results reveal spherical nanospheres with a narrow size distribution. 10AB nanospheres had a smaller size than other polymer, which is a good agreement with the size from PCS in Table 3.2-3. However, the particle size of nanospheres from TEM was smaller than that determined by PCS. It was due to the collapse of particles during the sample preparation of TEM.

(A)   (B)

(C)   (D)
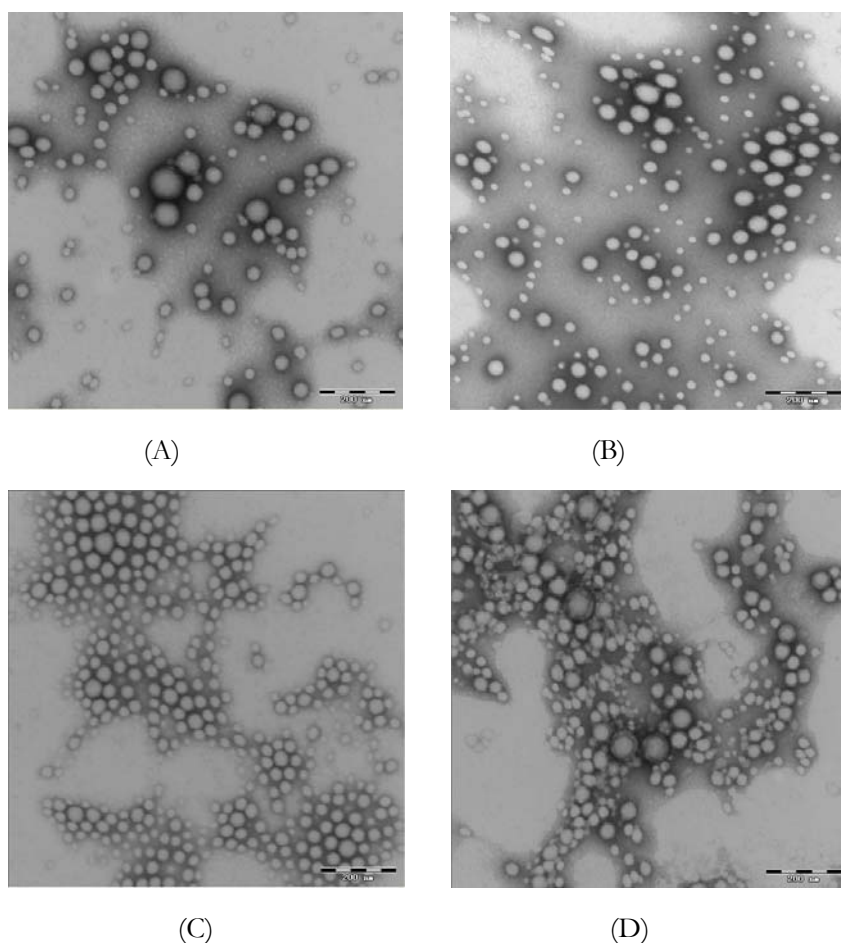
Fig. 3.3-1: TEM images of (A) 5AB, (B) 10AB, (C) 15AB and (D) ABA nanospheres (Scale bars: 200 nm). Polymer concentration= 10 mg/ml.

Fig. 3.3-2 shows the TEM images of nanocapsules formulated with different polymer 5AB, 10AB, 15AB and ABA. The results reveal spherical nanocapsules. Compared to nanospheres (Fig. 3.3-1) formulated with the same polymer, nanocapsules had a bigger size and broader size distribution, where the particle size from PCS had a larger mean size and large PDI.

(A)   (B)

(C)   (D)
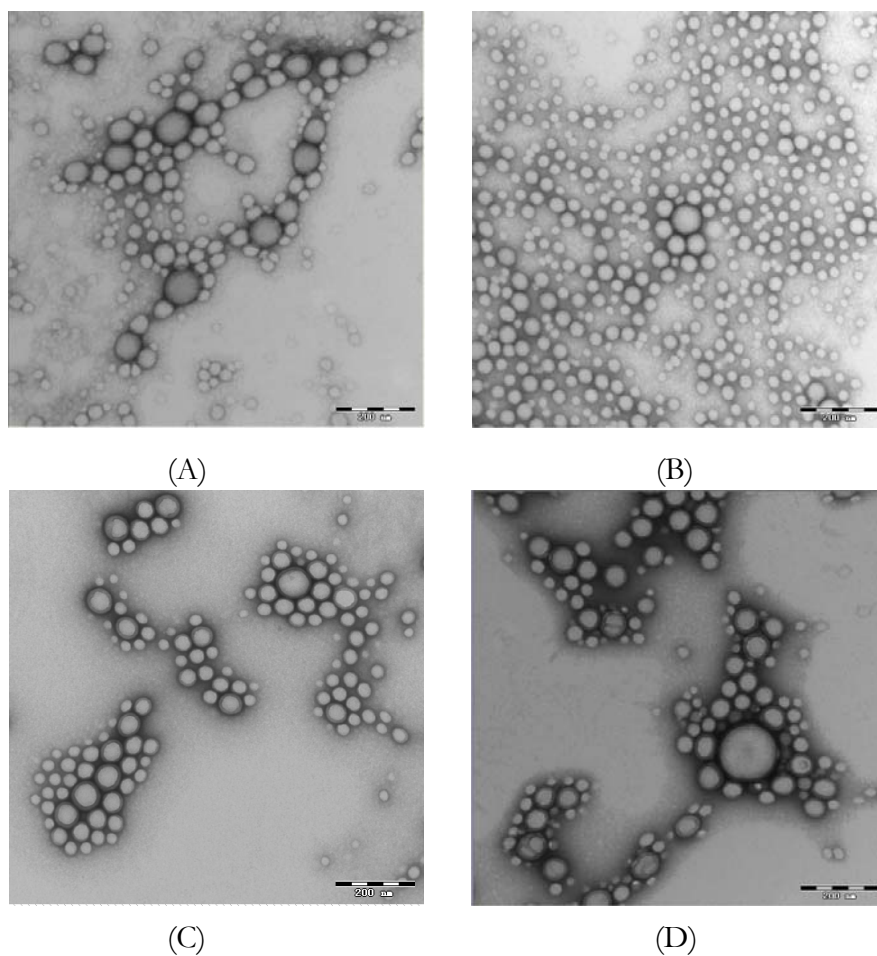
Fig. 3.3-2: TEM images of (A) 5AB, (B) 10AB, (C) 15AB and (D) ABA nanocapsules (Scale bars: 200 nm). Polymer concentration= 10 mg/ml. Polymer: oil= 1:5.

3.3.2   Freeze-Fractured TEM

Beside the classic negative staining method, the direct deposition of the nanoparticles on the TEM grids provides the information about all the components of the nanospheres

and nanocapsules. Freeze fracture is unique among electron microscopic techniques in providing the inner structure of nanospheres and nanocapsules. Freeze-fracture technique has four key steps, including rapid freezing, fracturing, replication and replica cleaning (Severs, 2007). Fig. 3.3-3 shows the freeze-fractured TEM images of lipiodol nanocapsules. The fractured nanocapsules exhibited a typical core-shell structure with homogeneous shells.

It is well known that the polymeric shell plays an important role in protecting the active substances incorporated in oil phase of NC. In the freeze-fractured image (Fig. 3.3-3), the wall thickness was estimated to be about 10 nm, in reasonable agreement with earlier work using the small angle neutron scattering (SANS) method (Rübe et al., 2005). However, for a reliable determination of shell thickness by TEM, a large number of particles had to be studied. Cauchetier et al (2003) made a theoretical approach to calculate the shell thickness of poly-o-caprolactone (PECL), poly(lactic acid) (PLA) and poly(lactic-co-glycolic acid) (PLAGA) nanocapsules about 20 nm.
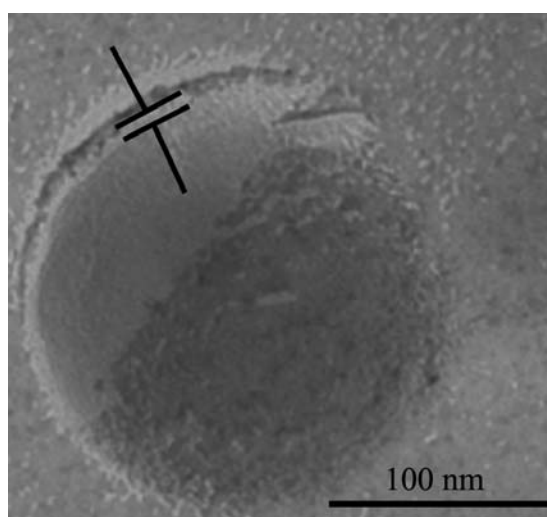
Fig. 3.3-3: Freeze-fractured TEM images of lipiodol nanocapsules. (Scale bar: 100 nm).

Fig. 3.3-4 shows the freeze-fractured TEM images of nanocapsules composed of the lipiodol oil and MCT oil. The fractured nanocapsules also exhibited a core-shell structure with homogeneous shells. And, the wall thickness was estimated to be about 10 nm, as

the same as the lipiodol nanocapsules. The composition of oil phase may not impact in the wall thickness of nanocapsules prepared with the same polymer and same nanoprecipitation method. Research has reported that nanocapsules prepared by different method such as emulsion-diffusion method had shell thickness values about 30 nm (Moinard-Chécot et al., 2008). However, until now, there is not enough explanation about the big difference on shell thicknesses between the nanoprecipitation and emulsion-diffusion methods.

However, everyone should keep in mind, for reliable determination of shell thickness using freeze-fractured TEM technique, a large number of particles had to be studied. And, the particles may not be necessarily representative because fracture occurs not only in the particle center and only small number of particles has been broken.
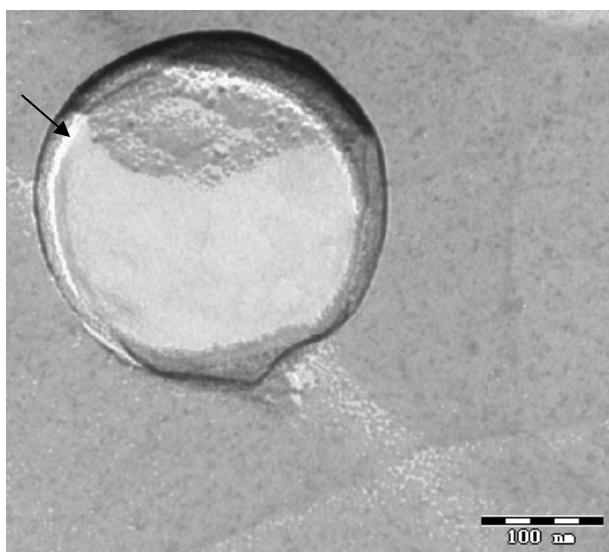
Fig. 3.3-4: Freeze-fractured TEM images of lipiodol-MCT nanocapsules. (Scale bar: 100 nm).

In order to know the structure difference between the nanospheres and nanocapsules, the freeze-fractured TEM images of nanospheres was also investigated, as seen in Fig. 3.3-5. Compared with nanocapsules, no apparent polymer shells in nanospheres can be visible. Thus, the freeze-fractured TEM results of nanospheres and nanocapsules also

indicate that nanospheres are matrix, while nanocapsules are vesicular system with a polymer shell around the oily core.
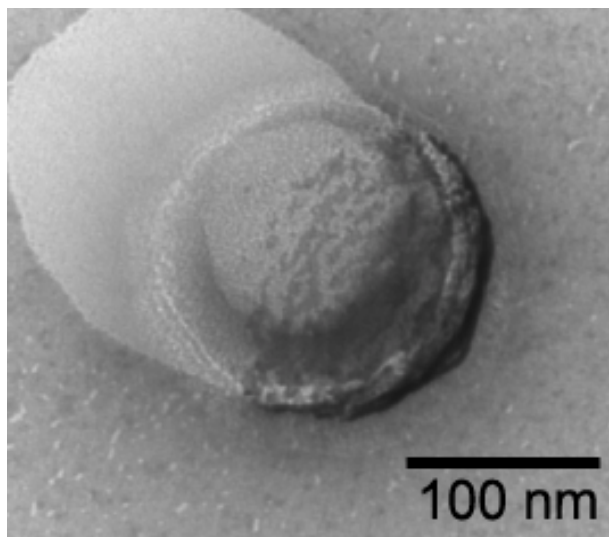
Fig. 3.3-5: Freeze-fractured TEM images of nanospheres (Scale bars: 100 nm).

3.3.3   AFM

Atomic force microscope (AFM) is a surface analytical method that can generate nano-scale topographic images, and also provides the possibility for visualizing the particle shape and surface structure in a natural environment. It offers the capability of 3D visualization and both qualitative and quantitative information on many physical properties of nanoparticles including size, morphology, surface texture and roughness (Pereira et al., 2008).

Tapping mode of AFM, the most commonly used AFM modes used in this study has three main advantages, including almost eliminated lateral forces, higher lateral resolution on most samples and lower forces and less damage to soft samples. Tapping mode atomic force microscopy (TM-AFM), is a versatile technique, which allows probing soft samples such as biological and polymeric materials. Compared with TEM, AFM has

several advantages for characterizing nanoparticles. Images from an AFM can represent data in three dimensions, so that it is possible to measure the height of the nanoparticles quantitatively, while the TEM images are only two-dimensional.

(a)   (b)
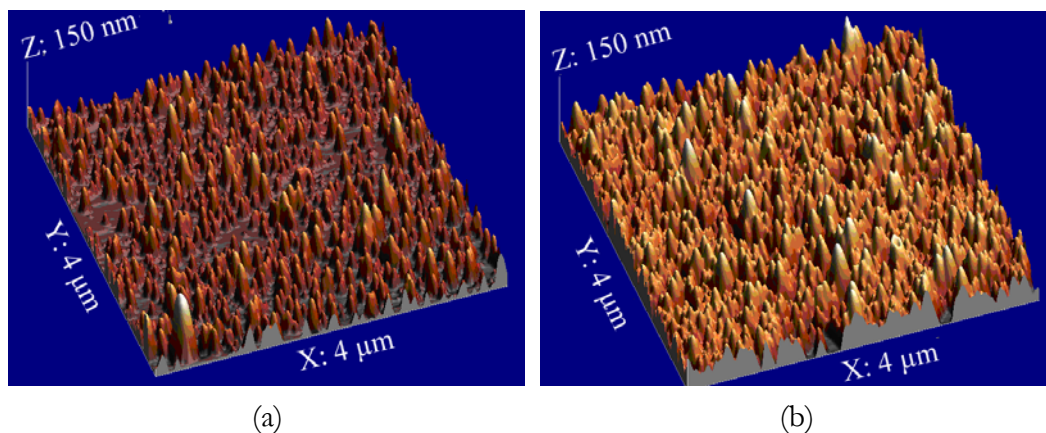
Fig. 3.3-6: AFM image: three-dimensional view of PLGA-PEG nanospheres (a) and nanocapsules (b), X: 4.0 μm, Y: 4.0 μm.

Fig. 3.3-6 shows the three-dimensional view of PLGA-PEG nanospheres and nanocapsules. In addition, the AFM scans more slowly than a TEM. However, a complete measurement session that includes sample preparation, acquiring an image, and then analyzing the image takes much less time with an AFM. In fact, typically it takes less time to get data from an AFM than with a TEM.

Fig. 3.3-7 shows the AFM tapping mode height images and phase images of 5AB nanocapsules. The TM-AFM images revealed that nanocapsules (Fig. 3.3-7a, c) were homogeneous particles with spherical shape. The nanocapsules had particle size in the range of 60 nm to 180 nm. Phase image analysis (Fig. 3.3-7b, d) using the same TM-AFM was done on samples to check the different composition of nanocapsules depending on their material composition.

Height image   Phase image

(a)   (b)

(c)   (d)
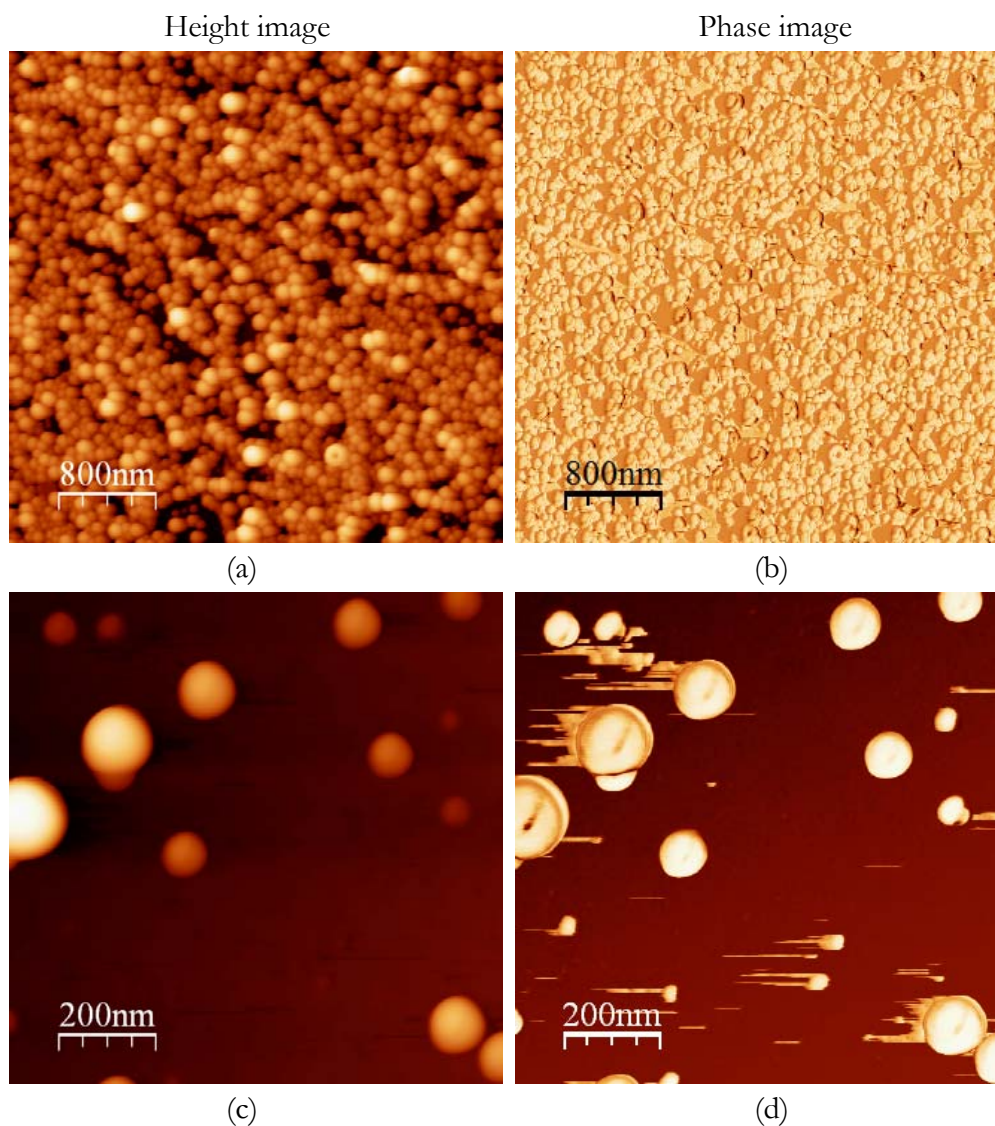
Fig. 3.3-7: AFM tapping mode height images (left side) and phase images (right side) of 5AB lipiodol nanocapsules.

Fig. 3.3-8 shows the AFM tapping mode height images (Fig. 3.3-8a, c) and phase images (Fig. 3.3-8b, d) of 5AB nanospheres. The images revealed that nanospheres were homogeneous particles with spherical shape. Compared with AFM images of nanocapsules in Fig. 3.3-8, nanospheres had a smaller size in the range of 40 nm and 100 nm, which also confirmed the size data obtained by PCS.

Height image   Phase image

(a)   (b)

(c)   (d)
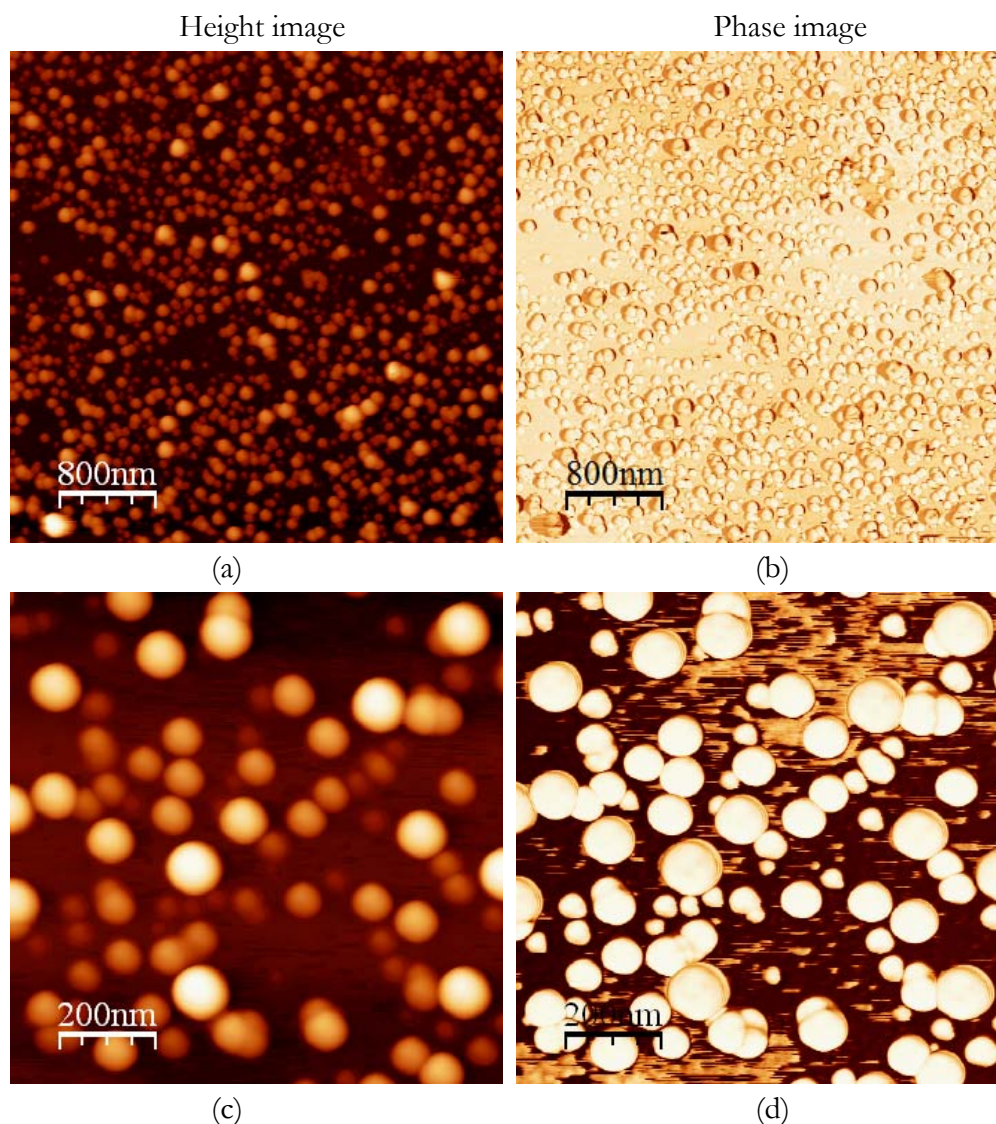
Fig. 3.3-8: AFM tapping mode height images (left side) and phase images (right side) of 5AB nanospheres.

Fig. 3.3-9 and Fig. 3.3-10 show the AFM tapping mode height images and phase images of 15AB nanocapsules and nanospheres, respectively. Like the 5AB nanocapsules and nanocapsules, 15AB nanospheres and nanocapsules were spherical and homogeneous particles. The nanocapsules (Fig. 3.3-9c) had larger size distribution than nanospheres (Fig. 3.3-10c), which was in good agreement of PCS results with PDI value of 0.215 for nanocapsules and 0.098 for nanospheres.

In this study, phase image analysis using TM-AFM can be used to investigate nanocapsules and nanospheres samples to examine the PEG chains at the surface of

pegylated nanoparticles. It is well known that phase images are based on the use of changes in the phase angle of cantilever probe. The images show more contrast than the height ones as well as more sensitivity to material surface properties such as roughness, stiffness, and chemical composition. It could be seen in Fig. 3.3-9 and Fig. 3.3-10 that the 15AB nanocapsule and nanosphere surface were smooth in comparison with that of 5AB nanocapsules (Fig. 3.3-7 and Fig. 3.3-8). The increased surface roughness may be attributed to the high PEG content of the copolymer (Jain and Kumar, 2010).

Height image   Phase image
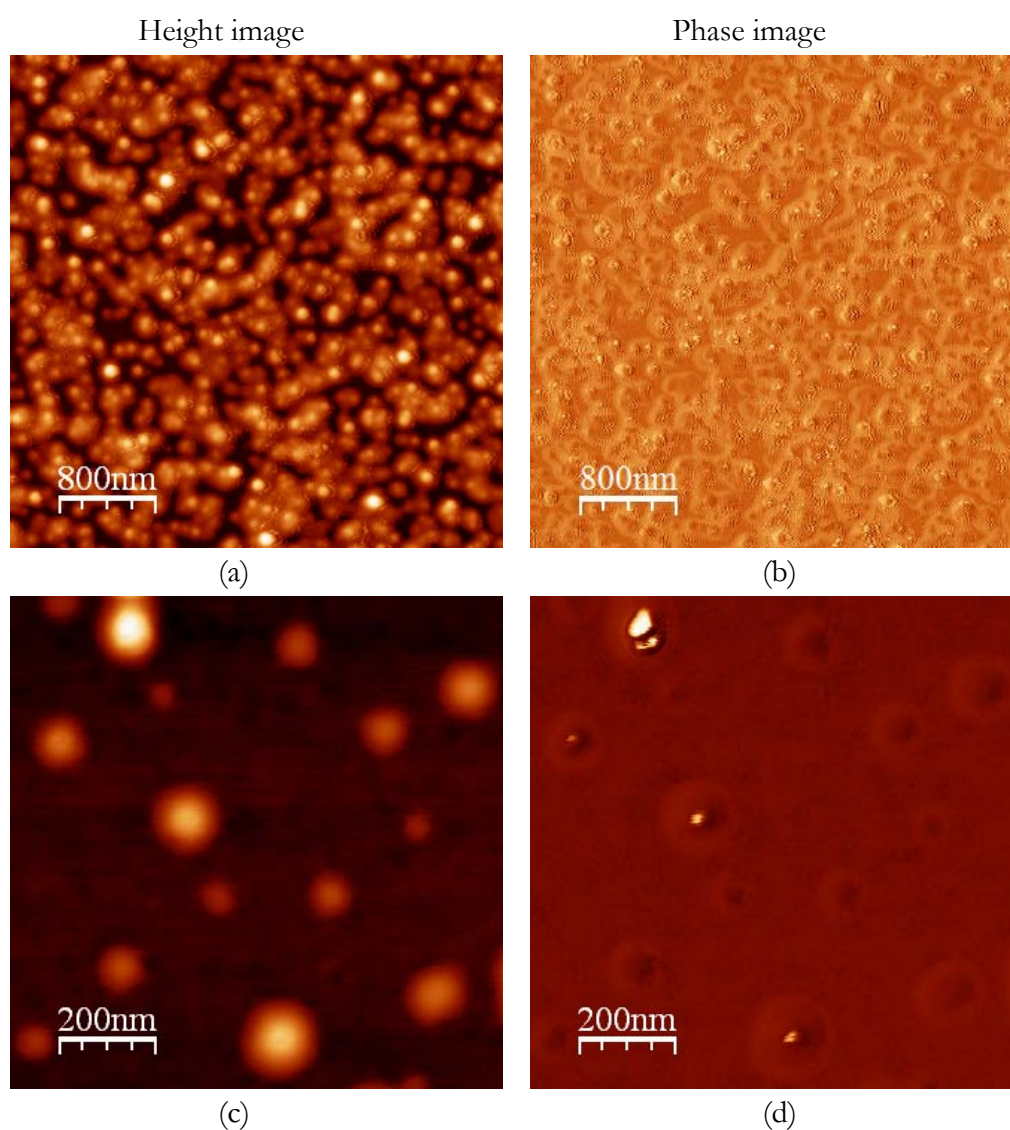
Fig. 3.3-9: AFM tapping mode height images (left side) and phase images (right side) of 15AB lipiodol nanocapsules.

Height image   Phase image

(a)   (b)

(c)   (d)
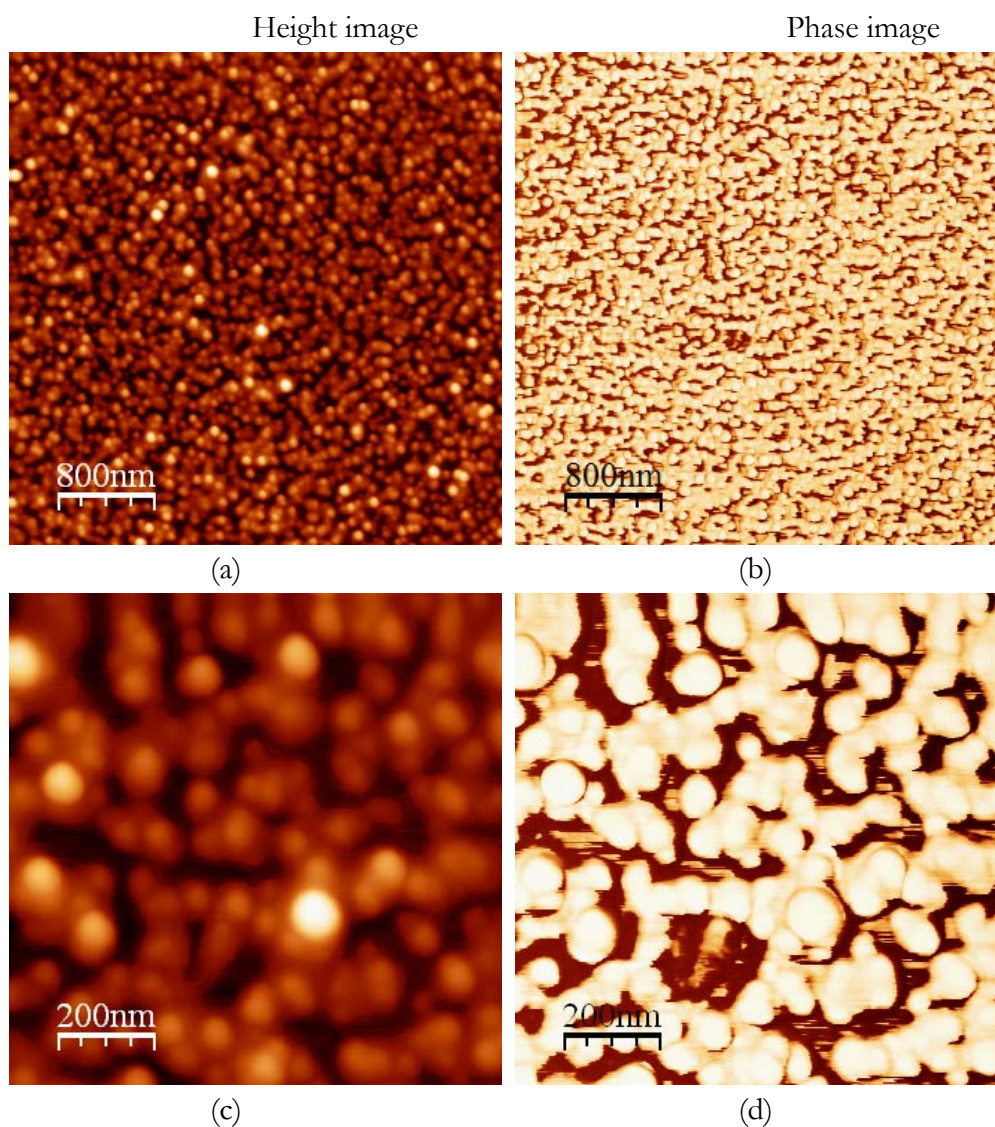
Fig. 3.3-10: AFM tapping mode height images (left side) and phase images (right side) of 15AB nanospheres.

.

The height profiles of AFM images can give information about vertical dimension. Fig. 3.3-11 shows the schematic representation of nanosphere (matrix structure) and nanocapsule (vesicular structure with oily core) on deposition using AFM. The height of one single particle loses partly using tapping mode. For matrix nanospheres, the diameter can be equal to the height or lager than the height with several magnifications. For vesicular nanocapsules, the oily phase surrounded by the polymer shell can be collapsed and the diameter is much larger than the height. Interestingly, the height of particle can be approximate twice of the thickness of the polymer shell. It is thus possible to

determine the shell thickness of nanocapsules by the investigation of height profile in AFM image.
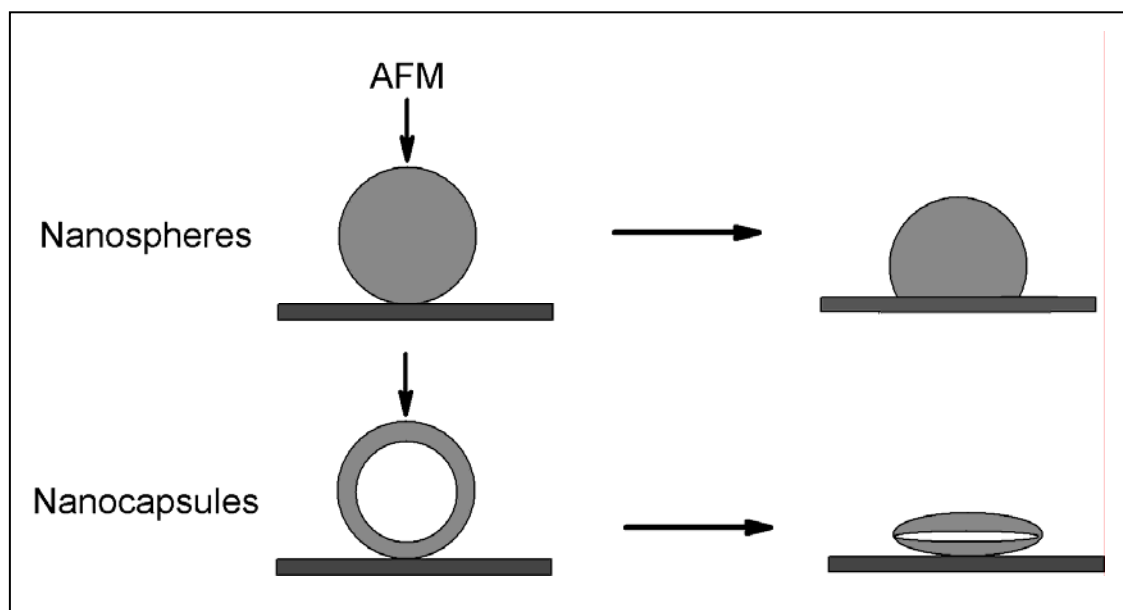
Fig. 3.3-11: Schematic representation of nanosphere (matrix structure) and nanocapsule (vesicular structure with oily core) on deposition using AFM.

Fig. 3.3-12 shows the height profiles of a typical PLGA-PEG nanocapsule (A) and nanosphere (B). From the height profile in Fig. 3.3-12A, the diameter of the nanocapsule was 145 nm, and the height was 23 nm. So, the shell thickness of polymeric nanocapsules ≈height/2=11.5 nm. The wall thickness of nanocapsules determined by AFM is a good agreement with the value of 10 nm from freeze-fractured TEM result in Chapter 3.2. From the height profile in Fig. 3.3-12B, the diameter of the nanosphere with the value of 86 nm was about double value to the height with the size of 44 nm. From the above results, it is possible to investigate the structure of the nanocarriers such as nanospheres and nanocapsules.
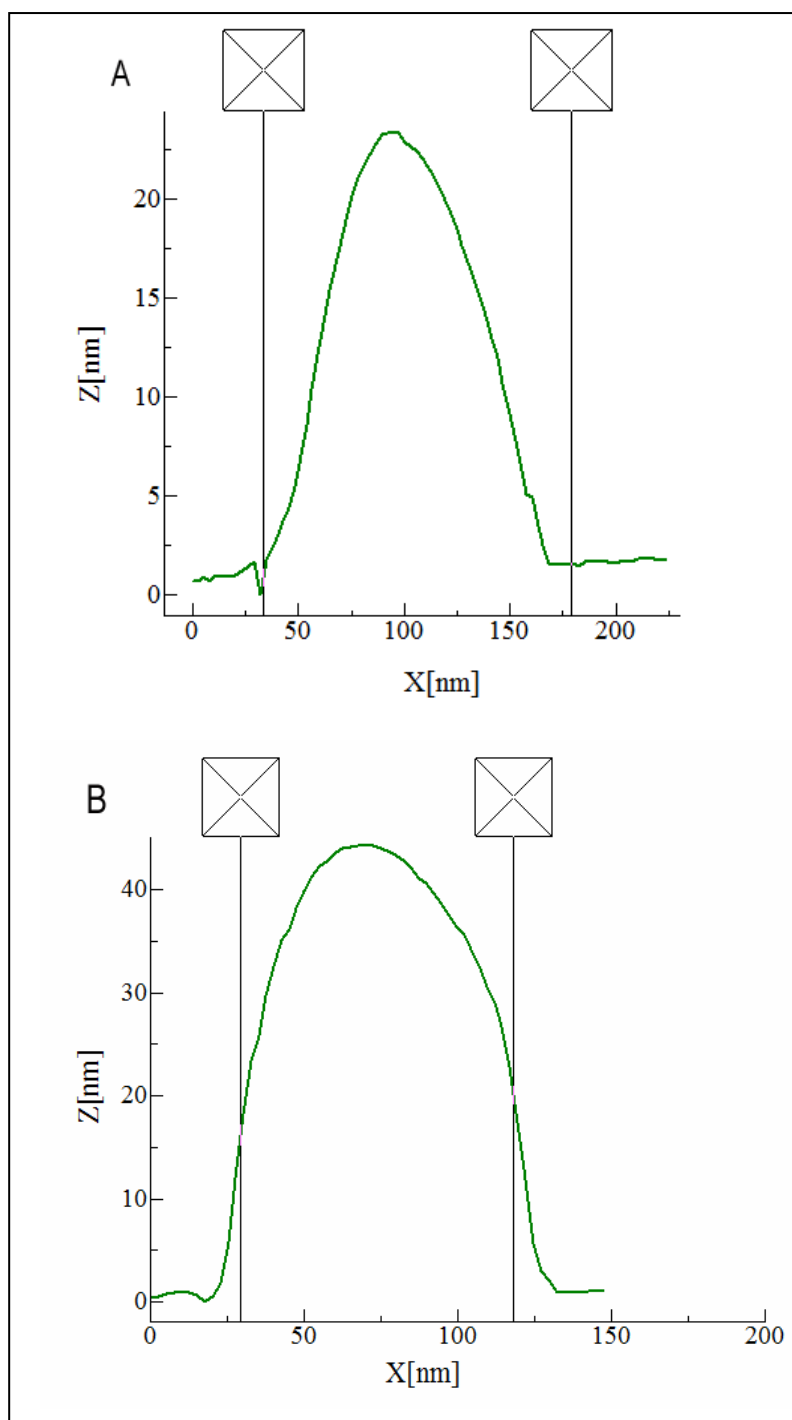
Fig. 3.3-12: Height profiles of typical PLGA-PEG nanocapsule (A) and nanosphere (B).

3.4 Stability and Freeze-drying

3.4.1   Stability of Nanospheres and Nanocapsules

PLGA-PEG nanosphere and nanocapsule suspension prepared by nanoprecipitation method can be stable for several weeks. Fig. 3.4-1 shows the particle size of nanospheres and nanocapsules in 3 weeks. After three-week storage of nanoparticles at 4 $^{\circ}$C in water, no appreciable size change of nanoparticles was detected by PCS and no aggregation of nanospheres and nanocapsule was observed. However, many physical and chemical factors may destabilize the nanoparticles to have a poorly long-term stability (Abdelwahed et al., 2006b), stability upon storage for a long time is thus a concern.
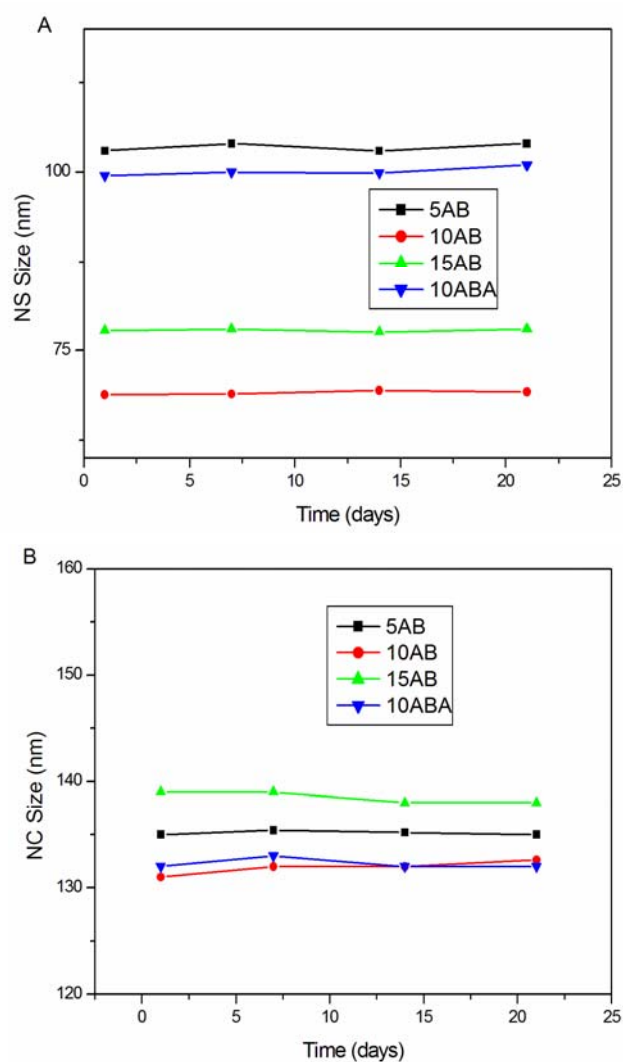
Fig. 3.4-1: Size stability of nanospheres (A) and nanocapsule (B) in 3 weeks, (polymer concentration: 10 mg/ml, polymer: oil=2:5).

3.4.2   Freeze-drying Theory

Freeze drying is an excellent method for the removal of water from frozen material. And, freeze-drying is the widely utilized drying method of nanoparticle suspensions in the pharmaceutical and biomedical application (Schaffazick et al., 2003). Generally, freeze-drying can be divided into three steps: freezing, primary drying (stage of freeze drying involving the sublimation of ice) and secondary drying (prolonged drying stage for continued desorption). During the freeze-drying process, excipients such as sugar must be added to the nanoparticle suspension to protect its fragile system and increase its stability (Hinrichs et al., 2006). Good freeze-drying sample should have a) an elegant cake-like lyophilizate, b) easy and rapid reconstitution, c) smaller or unmodified nanoparticle size, and d) less lose of drug entrapment.

3.4.3   Freeze-thaw Studies

The freeze-thaw studies were considered as pre-tests to avoid too many time consuming freeze-drying processes (Date et al., 2010). If an excipient cannot protect the nanoparticles during the first step of freeze-drying, it is not likely to be an effective cryoprotectant. Therefore, firstly, cryoprotective agents were used to investigate the ability to prevent the agglomeration of PLGA-PEG nanosphere during the freeze-thawing process. The mean particle size and the size distribution of each sample were measured by PCS before and after freeze-thawing procedure. To assess the most suitable concentrations, five excipients (sucrose, glucose, sorbitol, lactose and trehalose) with different concentration (1%, 5%, 10% and 15%) were used in this work.

Table 3.4-1 shows the particle size and size distribution of 15AB nanospheres before frozen and after freeze-thawing. The results indicate that lactose can not been used as an effective cryoprotectant for freezing these nanospheres, and macroscopical particles were

detected with cryoprotectant at low concentration (1%) and without cryoprotective agents after freeze-thaw. Cryoprotectants with different concentration (5%-15% sucrose, 10%-15% glucose, 5%-15% sorbitol, 5-15% trehalose) can be effective for freeze-thaw nanospheres. Almost no appreciable change on the particle size and size distribution of nanospheres can be found before frozen and after freeze-thawing.

Table 3.4-1: Freeze-thaw pre-test of PLGA-PEG-5% nanospheres: Mean particle size (nm) and PDI before frozen and after freeze-thawing of the frozen NPs in the presence of different cryoprotectants (sucrose, glucose, sorbitol, lactose, trehalose) with different concentrations (1%, 5%, 10%, 15%).

Cryoprotectant	Concentration	Z-Ave(nm)[a]	PDI[a]	Z-Ave(nm)[b]	PDI[b]
Sucrose	1%	80.6	0.102	***	***
	5%	81.2	0.118	81.9	0.119
	10%	80.3	0.099	81.0	0.126
	15%	81.5	0.115	80.9	0.111
Glucose	1%	80.3	0.1	***	***
	5%	80.0	0.084	***	***
	10%	80.5	0.106	81.4	0.115
	15%	81.1	0.116	80.8	0.117
Sorbitol	1%	79.7	0.122	***	***
	5%	79.8	0.115	82.9	0.104
	10%	80.4	0.111	86.5	0.155
	15%	81.1	0.106	81.3	0.112
Lactose	1%	79.7	0.106	***	***
	5%	79.7	0.106	***	***
	10%	81.2	0.108	***	***
	15%	83.3	0.121	***	***
Trehalose	1%	79.9	0.112	***	***
	5%	80.2	0.123	83.1	0.129
	10%	80.7	0.106	82.7	0.131
	15%	80.7	0.119	83.8	0.166

a, before frozen; b, after freeze-thaw; ***, redisperison can not be possible.

3.4.4 Freeze-drying of Nanospheres

The PLGA-PEG nanospheres were lyophilised in the presence of increasing concentrations of sucrose, glucose, sorbitol and trehalose, respectively. As to the sorbitol for cryoprotective agent, redisperison can not be possible and macroscopic and irreversible aggregations were observed after dissolved the drying nanoparticle samples with water. Fig. 3.4-2 shows the most suitable concentration (10%-15%) of cryoprotective agents (sucrose, glucose and trehalose) for the freeze-drying process of 5AB nanospheres. All the lyophilised cakes except with glucose were brittle and white, easy and rapid to reconstitute. The freeze-drying nanospheres with the cryoprotectant of glucose were very sticky. For the formulations without cryoprotective agents, redisperison can not be possible and a macroscopic and irreversible aggregation was observed. Sucrose (5-15%) and (10-15%) trehalose were identified as being the most suitable excipients for freeze-drying nanospheres.
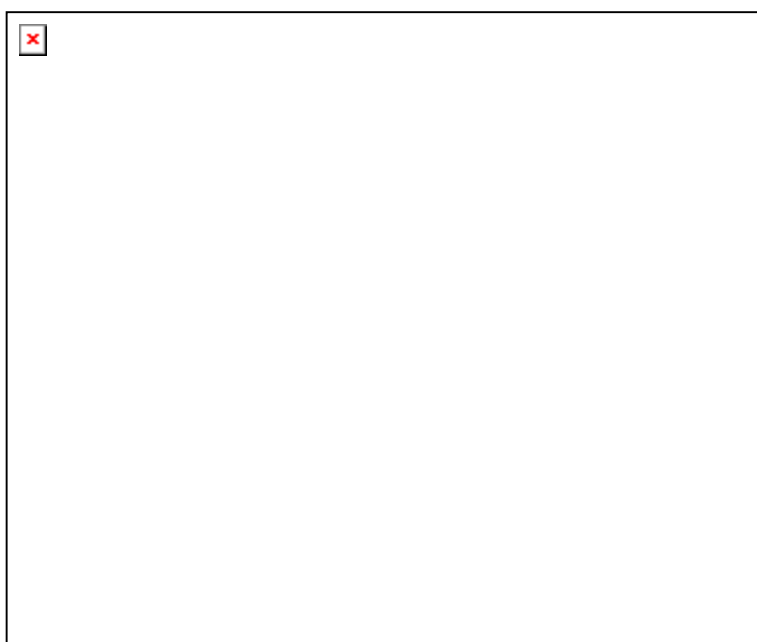
Fig. 3.4-2: Freeze-drying of 5AB nanosphere: mean particle size (nm) and PDI before frozen and after freeze-drying of the nanospheres in the presence of different cryoprotectants (10%-15% sucrose, glucose and trehalose).

Fig 3.4-3 shows the most suitable concentration (5%-10%) of sucrose and trehalose for nanospheres prepared with the different polymer (5AB, 10AB, 15AB and 10ABA). 5% and 10% sucrose can be effective cryoprotectant to freeze-drying the PLGA-PEG and PLGA-PEG-PLGA nanospheres. With increasing cryoprotectant concentration, a

reduced change of particle size between before freeze-drying and after freeze-drying can be found in all the nanospheres. 5% trehalose can not be able to act as an effective cryoprotectant for 10AB and 15AB nanospheres, and a macroscopic and irreversible aggregation was observed. When trehalose concentration increased to 10%, a slight size change can be found between before freeze-drying and after freeze-drying in 10AB nanosphere, while a big size change in 15AB nanospheres. Both 5% and 10% sucrose and trehalose can be effective for freeze-drying of the 10ABA nanospheres, which may be attributed to the different polymer architecture. Therefore, stabilization by sugar became worse with increasing degree of PEGylation of the nanoparticles when PEG content increased from 5% (5AB) to 15% (15AB). The amount of cryoprotectant required an increase when the PEG content of polymer increased.
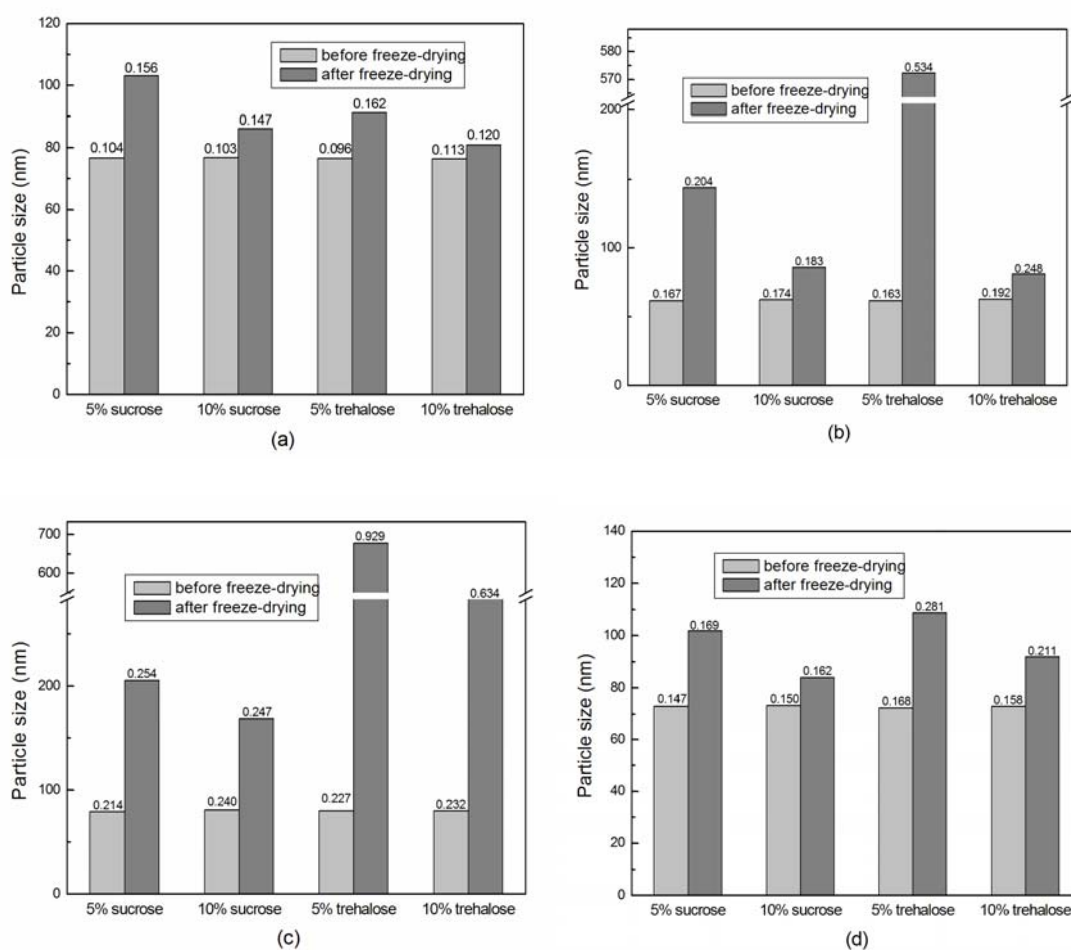
Fig. 3.4-3: Freeze-drying of nanospheres: mean particle size (nm) and PDI before frozen and after freeze-drying in the presence of 5%, 10% sucrose and trehalose, a) 5AB, b) 10AB, c) 15AB, d) 10ABA.

In conclusion, sugars like sucrose and trehalose can act as effective cryoprotectants during the freeze-drying process. Addition of cryoprotectants to an aqueous nanosphere suspension allows the recovery of nanospheres of similar size as originally formulated. The effective ability depends on the type of cryoprotectant, cryoprotectant concentration and polymer nature such as PEG content. In addition, without cryoprotectants, the nanospheres aggregated to a few micrometers in size and were difficult for further *in vivo* investigation.

3.4.5   Freeze-drying of Nanocapsules

Compared with nanospheres, nanocapsules have a thin polymer shell that may not withstand the stresses during freeze-drying process (Abdelwahed et al., 2006a). In general, cryoprotectants have to be added as the protection to the nanocapsule formulation. With the investigations of the ability of cryoprotective agents (CPA) for freeze-drying nanospheres in Chapter 3.4.4, therefore, only two cryoprotective agents (sucrose, and trehalose) were used to prevent the agglomeration of nanocapsules during the freeze-thawing and freeze-drying process. However, trehalose can not act as an effective cryoprotectant during the freeze-drying process of nanocapsules. Redisperison of the freeze-drying nanocapsules can not be possible and a macroscopic and irreversible aggregation was observed.

The mean particle size and the size distribution of each sample were measured by PCS before and after a freeze-thawing procedure. The measurements were used to determine mean particle size of the samples after the freeze-thawing cycle (Sf_1), after freeze-drying (Sf_2) and the initial mean particle size (Si). Table 3.4-2 shows the particle size and PDI before frozen, after freeze-thawing and after freeze-drying of the NPs in the presence of sucrose with different concentrations (5% and 10%). The results indicate that no significant changes in mean particle size were detected with cryoprotective agents. Also,

when the CPA concentration increased from 5% to 10%, a reduced size change can be found after freeze-drying and before freeze-drying. Thus, sucrose (5-10%) was identified as being the suitable excipients for freeze-drying PLGA-PEG and PLGA-PEG-PLGA nanocapsules.

Table 3.4-2: Particle size of nanocapsules after freeze-thaw and after freeze-drying in the presence of sucrose with different concentrations (5%, 10%).

polymer	CPA concentration	Ratio (Sf1/Si)	Ratio (Sf2/Si)
5AB	5% sucrose	1.017±0.010	1.258±0.090
	10% sucrose	0.987±0.008	1.191±0.033
10AB	5% sucrose	1.035±0.009	1.184±0.012
	10% sucrose	1.007±0.003	1.122±0.009
15AB	5% sucrose	0.985±0.006	1.339±0.041
	10% sucrose	0.994±0.005	1.242±0.014
10ABA	5% sucrose	0.993±0.006	1.079±0.022
	10% sucrose	1.004±0.006	1.057±0.018

Sf_1, mean size after freeze-thaw; Sf_2, mean size after freeze-drying; Si, initial mean particle size; n=3; data are shown as mean±SD.

3.5 NMR Studies

3.5.1   Core-Corona Structure of Nanospheres

^{1}H-NMR analysis was made on polymeric nanospheres in attempt to investigate the core-corona structure of PLGA-PEG nanospheres. As seen in Fig. 3.5-1, NMR spectra of all nanospheres in D_2O shows the presence of methylene protons of PEG chains at 3.607 ppm. Signals from PLGA methyl or methylene protons were absent or diminished in intensity. This might indicate that PLGA protons are in solid environment and cannot be detected whereas PEG chains must be in mobile state. Previous work also confirmed their core-corona structure of PLGA-PEG nanospheres (Hrkach et al., 1997). Our

results are in accordance with the above-cited reference suggesting nanospheres made of PLGA core and PEG corona. Thus, ^{1}H-NMR analysis of nanospheres might indicate that hydrophilic polymer parts (PEG) are oriented towards the outer phase (water) during precipitation, while the more lipophilic polyester PLGA parts form the inner core. Signals intensity at 2.136 ppm in the NMR spectra can be attributed to the residual acetone. In addition, an increased intensity of PEG peak can be found when the PEG content increases from 5% to 15%.
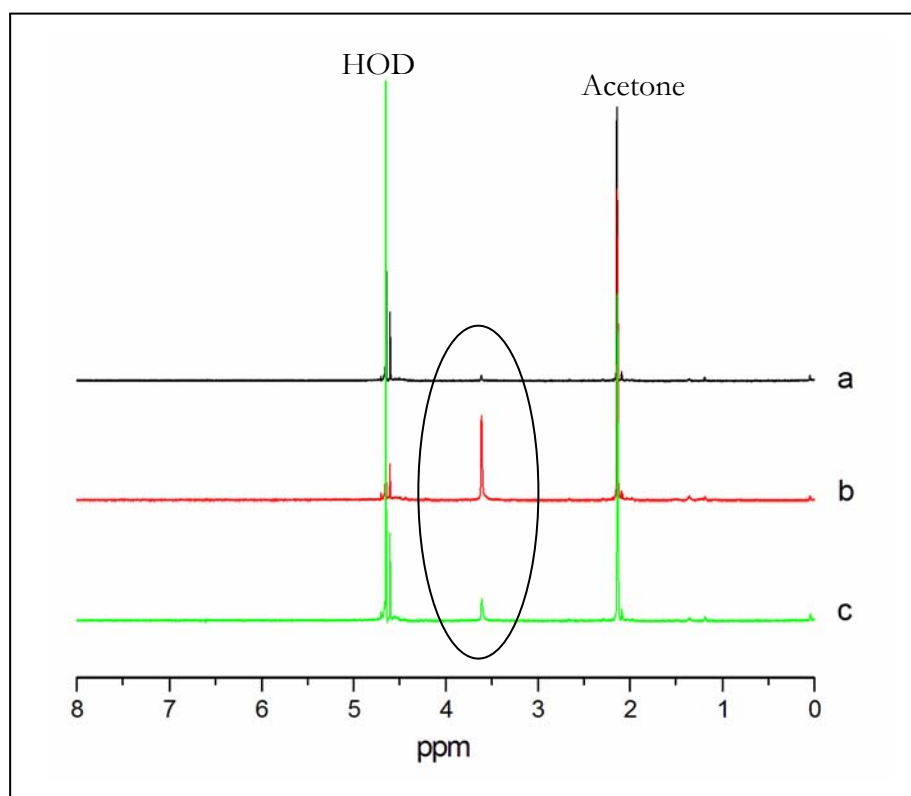
Fig. 3.5-1: ^{1}H-NMR of nanosphere suspension of 5AB (a), 15AB (b) and 10ABA (c) in D_2O. PEG peaks at 3.6 ppm are enricircled.

3.5.2 Structural Analysis of Nanocapsules

The proton NMR spectra of the nanocapsules (Fig 3.5-2a) show typical peaks of water (4.6 ppm) and lipiodol (peaks a–g). Also, the pecks of PEG (3.6 ppm), residual acetone (2.1 ppm) can be found in the spectra. Lipiodol can be regarded as oily phase in the nanocapsules with the same properties, because the relation of the peak integrals is

almost identical (Fig. 3.5-2). The nanocapsule suspension shows signals in the aliphatic region, which is in agreement with the liquid state of its lipiodol oily core because aliphatic groups with highly mobile chains in the liquid state. These results represent that the nanocapsules have a liquid core.
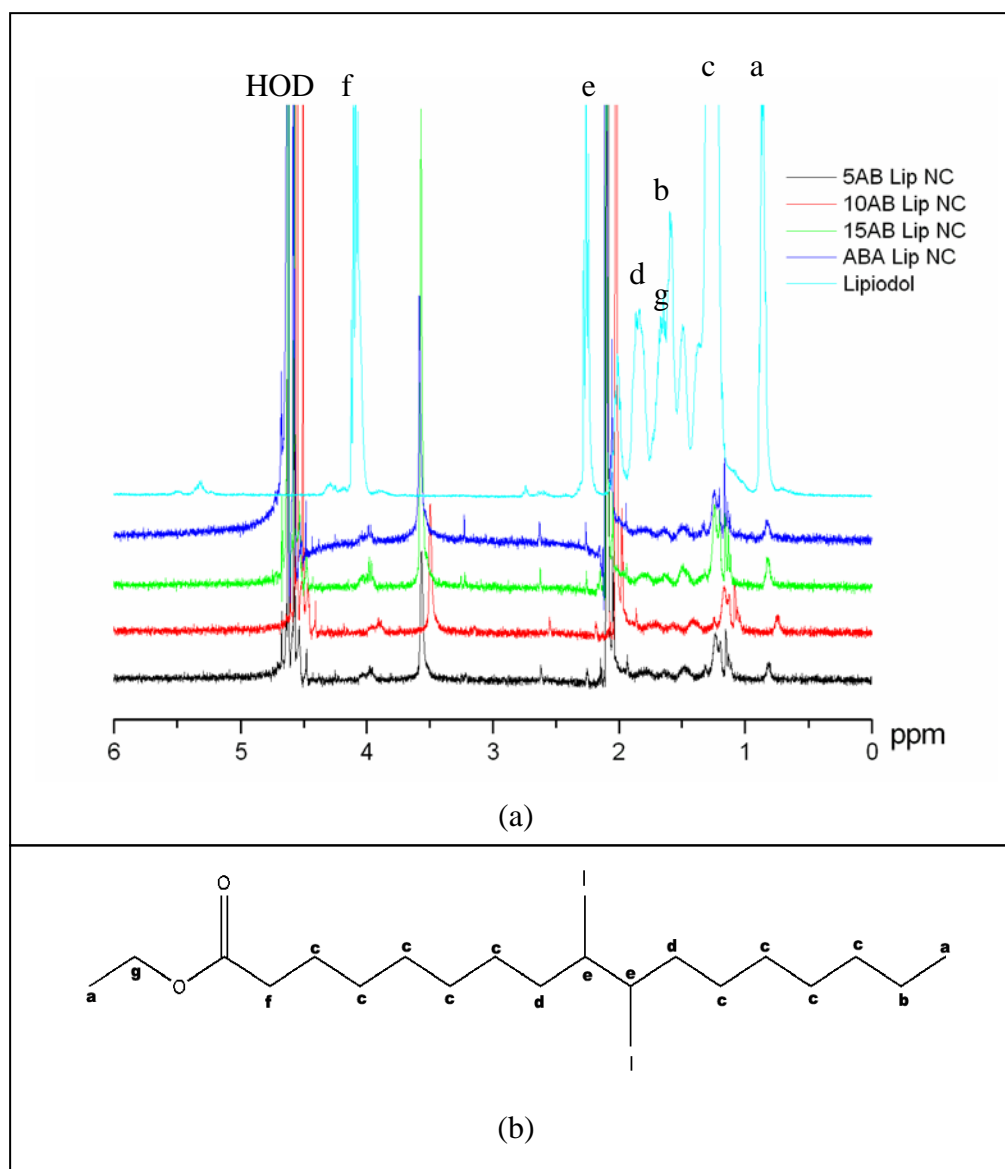
Fig. 3.5-2: ^{1}H-NMR spectra of the lipiodol oil in CDCl$_3$ and 5AB, 10AB, 15AB and 10ABA nanocapsule suspension in D$_2$O (a), structure of lipiodol oil with assignment of the ^{1}HNMR signals (b).

3.6 ESR Studies

3.6.1   ESR in Drug Delivery

Electron spin resonance (ESR), also called electron paramagnetic resonance (EPR), is a magnetic resonance method related, in its basic principles, to the more popular nuclear magnetic resonance (NMR) spectroscopy. It is commonly used to investigate materials containing unpaired electrons, such as free radicals. Due to their short relaxation times (causing severe loss of signal) of the paramagnetic species, ESR gives information which is very difficult from regular NMR. In particular, ESR spectroscopy can be used to investigate polymeric drug delivery system, including a wide range of properties for the successful design and formulation of drug carries (Kempe et al., 2010; Martini and Ciani, 2009). The majority of polymeric drug delivery samples are ESR silent, requiring the addition of paramagnetic molecules or groups for detection. A lot of information about drug delivery system can be obtained by ESR spectroscopy, such as mobility, micropolarity, microviscosity and drug release properties (Lurie and Mäder, 2005).

3.6.2   Characterization of HDPMI-loaded Nanoparticles

Since ESR measurements require the existence of paramagnetic molecules, the ESR spin probe should be incorporated into the nanoparticles as a reporter molecule. HDPMI can be functioned as a poorly water-soluble lipophilic model drug, and its chemical structure represents in Fig. 3.6-1.
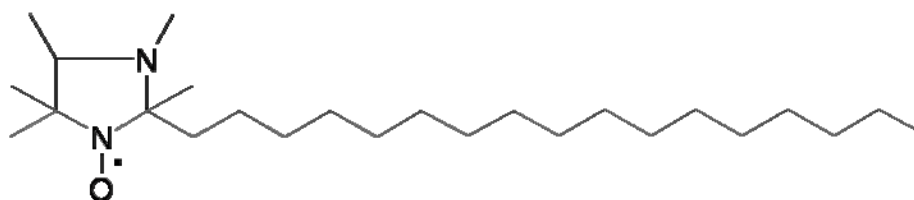
Fig. 3.6-1: Chemical structure of ESR spin probe HDPMI

As seen in Table 3.6-1, HDPMI-loaded nanocapsules and nanospheres showed particle

size below than 150 nm and narrow size distribution (especially for nanospheres). Compared with the blank nanocapsules and nanospheres in Chapter 3.2, no change in particle size could be found.

Table 3.6-1: Particle size and size distribution of NC and NS incorporated with HDPMI.

Sample	Z-Ave (nm)	PDI
15AB Lipiodol NC	144	0.226
15AB NS	66.8	0.108
5AB NS	105	0.101
PLGA NS	120	0.062

3.6.3 ESR Results

ESR spectra can provide more information about the microenvironment of the model drug inside the nanoparticles (Rübe and Mäder, 2005). Fig. 3.6-2 shows the ESR spectra of HDPMI in lipiodol oil and 15AB nanocapsules incorporated with HDPMI. The results represent that the spectra of the nanocapsules (Fig. 3.6-2b) can be simulated with a single species with exactly the same spectral pattern as HDPMI dissolved in lipiodol oil (Fig. 3.6-2a).

Fig. 3.6-3 shows the ESR spectra of HDPMI-loaded nanospheres prepared with different polymer. As compared with Fig. 3.6-2 and Fig. 3.6-3, whereas the ESR spectra of nanocapsules indicate that the majority of the HDPMI molecule is dissolved within the oily core of the nanocapsules, the spectra of nanospheres indicate an immobilization of the spin probe inside these systems. Thus, with the incorporation of a paramagnetic reported molecule (HDPMI) into the produced nanoparticles, this ESR study provides information about the systems of interest that can not be obtained by other methods.
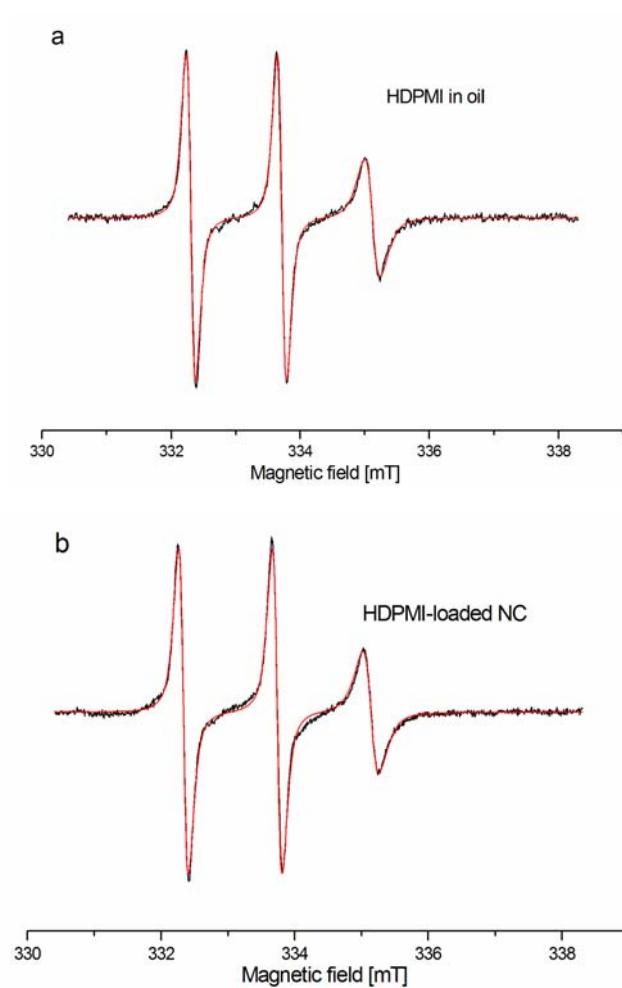
Fig. 3.6-2: ESR spectra of HDPMI in lipiodol oil (a) and nanocapsules incorporated with HDPMI (b).

Magnetic field [mT]
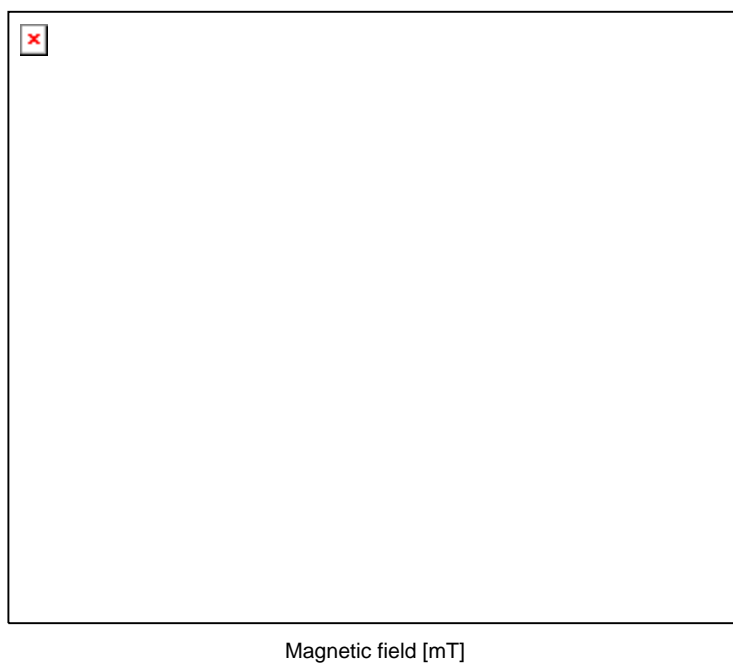
Fig. 3.6-3: ESR spectra of HDPMI-loaded nanospheres prepared with different polymer.

64

3.7 *In Vivo* and *Ex Vivo* Distribution of Nanospheres

3.7.1   Fluorescent Dyes for Imaging

"Seeing is believing". The visualization of nanoparticles in drug delivery system by a non-invasive and radiation-free manner using relatively simple equipment is very important. To obtain efficient biodistribution information, the nanocarriers should be nontoxic with long half-time in blood stream. Many researches have been focused on the factors of *in vivo* distribution of polymeric nanoparticles, such as composition, particle size, core and surface charge (Alexis et al., 2008). However, until now, a large amount of conflicting data of biodistribution represents in the literature (Owens Iii and Peppas, 2006).

Optical imaging, including fluorescence and bioluminescence imaging, represents a very attractive technology by offering an easy, noninvasive, longitudinal and relatively economical method for *in vivo* imaging (Rao et al., 2007). However, the main challenge of optical imaging is the lack of penetration depth, especially only a few millimeters at visible wavelengths. While light in the near infrared (NIR) region (700–900 nm) can penetrate more deeply, to depths of several centimeters. Recently, it has been shown that a wide variety of lipophilic dyes are quite suitable for *in vivo* fluorescence imaging (Tong et al., 2010). Among of them, DiI and DiR are the most common fluorescent dyes for widely investigated because of their low toxicity.

Fluorescence imaging allows the direct visualization of nanoparticles after i.v. injection. Organic dyes and quantum dots are the most common fluorescent labels for fluorescence imaging. Quantum dots (QD), a class of inorganic nanocrystals with their photostability and bright emissions, have attracted a great deal of interest for biomedical imaging application; however, the severe toxicity of QD restricted the application in humans, which is related to the incorporation of heavy metal elements, such as cadmium (Resch-Genger et al., 2008). In contrast to QD, the toxicity of organic dyes has widely

been investigated, which depends on the kind of dyes, from very low to high. Nile Red (NR) is a fluorescent dye used widely to study fat accumulation in many types of cells. And, NR is almost non-fluorescent in pure water but becomes intensely fluorescent in a lipid-rich environment. The chemical structure of NR is shown in Fig. 3.7-1A. Another group of organic dyes that has attracted much interest recently is the carbocyanine dyes. The structure of these dyes consists two positive-charged conjugated rings attached to a long hydrocarbon chain by methine groups. The most widely used carbocyanine dyes now are DiR (1,1'-dioctadecyl-3,3,3',3'-tetramethylindotricarbocyanine iodide) and DiI (1,1-dioctadecyl-3, 3,3,3-tetramethylindocarbocyanine perchlorate), which both have an 18 C hydrocarbon chain. Their basic structure is shown in Fig. 3.7-1B. They have minor alterations in their ring structure and it is the particular ring structure and number of methine groups that determine the fluorescence characteristics of the molecule (O'Brien and Lummis, 2007). In this work, fluorescent dyes NR, DiR and DiI as reported molecule were used to fluorescence imaging and confocal microscopy.
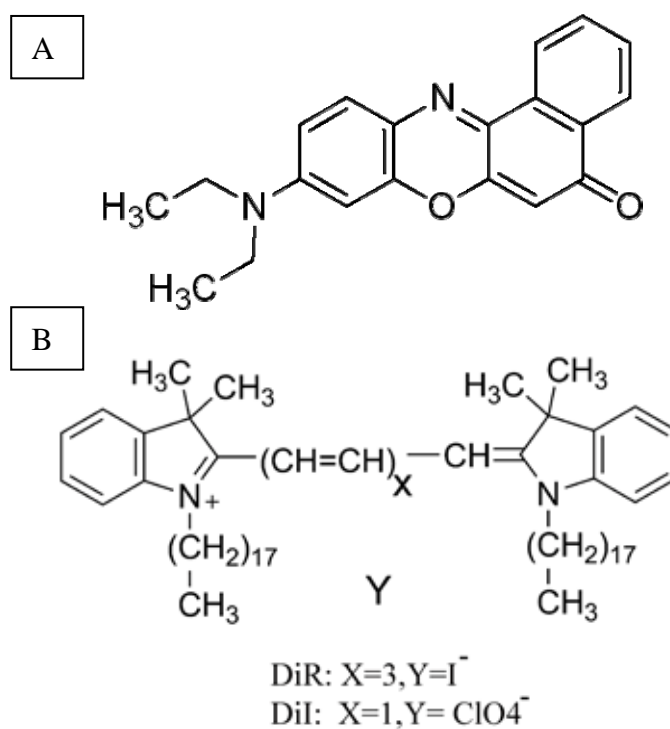
Fig. 3.7-1: Chemical structures of nile red (A) and carbocyanine dyes (B): DiR and DiI.

3.7.2   Characterizations of Dye-loaded Nanospheres

Two fluorescent dyes (NR and DiR) were used to incorporate into PLGA-PEG nanospheres for the *in vivo* investigation. Fig. 3.7-2 shows the schematic representation of DiR-NR-loaded nanospheres. The PEG grafted PLGA nanosphere demonstrated a core-corona structure, in which the dyes were dispersed. Hydrophilic polymer parts (PEG) are oriented towards the outer phase and more lipophilic polyester PLGA remains in the inner core. DiR dye with the log P values about 20 is more lipophilic than NR with the log P values about 5.1 (Greenspan et al., 1985).
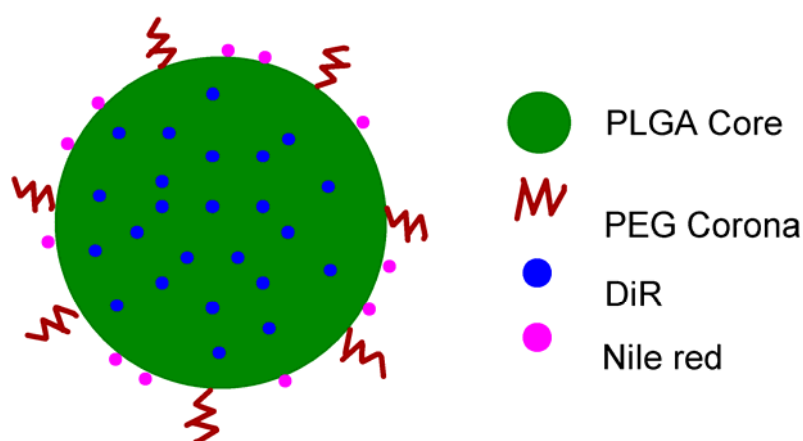
Fig. 3.7-2: Schematic representation of DiR-NR-loaded PLGA-PEG nanospheres.

PLGA-PEG nanospheres (10 mg/ml) incorporated with NR (23.0±1.6 µg/ml) and DiR (45.8±2.7 µg/ml) had a mean particle of 86.3±3.1 nm and narrow size distribution with a PDI value of 0.113±0.006. The dye-loaded nanospheres are more stable without any precipitation for at least three weeks. Fig. 3.7-3 shows the size change of NR and DiR-loaded nanospheres in three weeks. The results show that particle size can remain almost the same, and a very slight decreased PDI value.
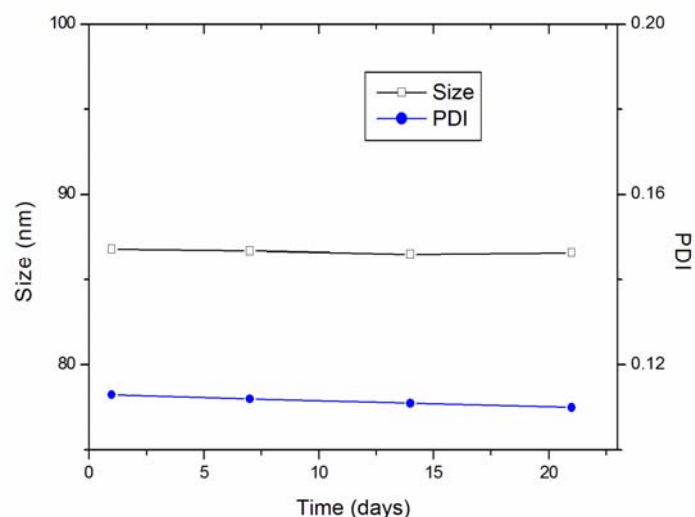
Fig. 3.7-3: Particle size and size distribution of NR-DiR-loaded nanospheres in 3 weeks.

The CRi Maestro *in vivo* imaging system has several Masestro filter set conditions such as blue, green, yellow, red, deep red and NIR depending on the excitation and emission, and the detailed conditions can be shown in Table 3.7-1. In this study, detection of NR was carried out with the green filter set (503 to 555 nm excitation filter, 580 nm long pass emission filter, 550 to 800 nm in 10 nm steps acquisition setting), and DiR was carried out with the NIR filter set (710 to 760 nm excitation filter, 800 nm longpass, 780 to 950 nm in 10 nm steps acquisition setting).

Table 3.7-1: Masestro Filter set condition.

Masestro Filter Set	Excitation Filter	Emission Filter	Acquisition Setting
Blue	445 to 490 nm	515 nm longpass	500 to 720 nm in 10 nm steps
Green	503 to 555 nm	580 nm longpass	550 to 800 nm in 10 nm steps
Yellow	575 to 605 nm	645 nm longpass	630 to 850 nm in 10 nm steps
Red	615 to 665 nm	700 nm longpass	680 to 950 nm in 10 nm steps
Deep Red	671 to 705 nm	750 nm longpass	730 to 950 nm in 10 nm steps
NIR	710 to 760 nm	800 nm longpass	780 to 950 nm in 10 nm steps

Fig. 3.7-4 shows the *in vitro* and *in vivo* fluorescence intensity of DiR-NR-loaded 15AB nanosphere suspension. A shift of NR emission spectra between in *vitro* and *in vivo* can be clearly found, which can be explained by the influence of the local polarity on NR emission maxima. An increased polarity can lead to a shift of the emission maxima to higher wavelengths and a reduced quantum yield. However, almost no change in DiR

spectra between *in vitro* and *in vivo* indicated that the penetration of emitted fluorescence light through living tissue, which presented no influence on the spectra profile with exact detection of nanospheres *in vivo*.
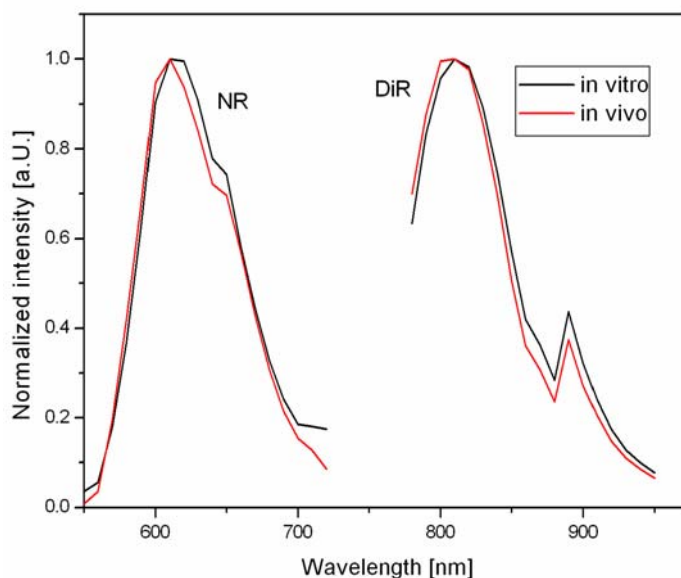
Fig. 3.7-4: Fluorescence (*in vitro* and *in vivo*) intensity of DiR-NR-loaded 15AB nanosphere suspension.

3.7.3   *In Vivo* **Fluorescence Imaging of Nanospheres**

Fig. 3.7-5 shows the fluorescence intensity images (DiR signal) of a mouse 5 min, 30 min, 60 min, 3 h and 24 h after injecting NR-DiR nanospheres. Intensity weighted images were used to illustrate the nanospheres distribution in the mice. From red over orange and yellow up to dark blue regions, the intensity indicated the decreased nanosphere amounts. It was visible that DiR concentration in the nanospheres was sufficient for *in vivo* fluorescence imaging study.
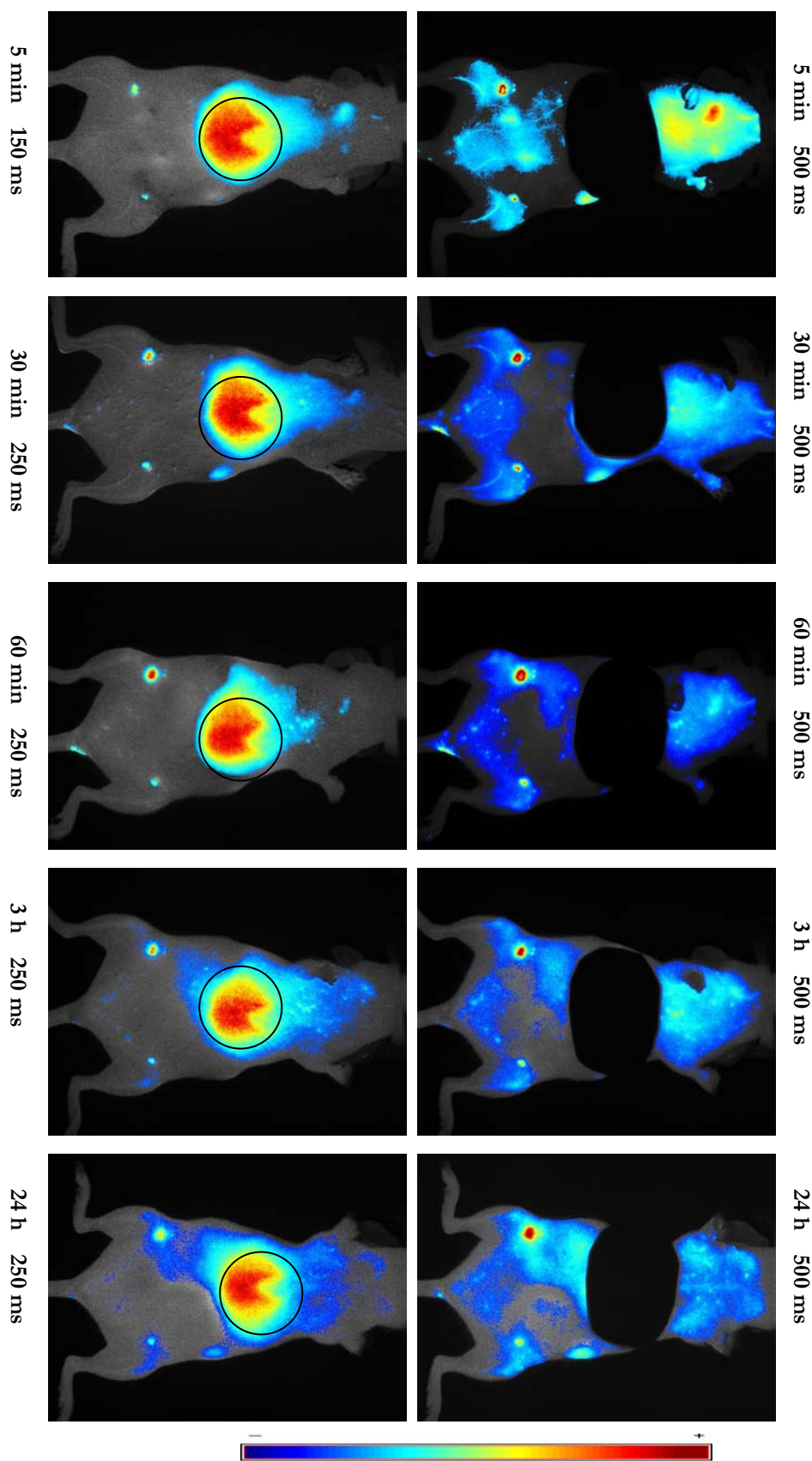
Fig. 3.7-5: Fluorescence intensity images (DiR signal) of a mouse in different time points (5 min, 30 min, 60 min, 3 h and 24 h) after injecting NR-DiR nanospheres (150 ms, 250 ms and 500 ms), The circle points to the accumulation in the liver.

Already in the first 5 min, nanospheres were accumulated by the liver. And, the fluorescence intensity remained almost the same in 24 h. The right part of Fig. 3.7-5 was obtained with masked liver to try to get more detailed distribution of other organs due to the high intensity in liver. The very lipophilic properties of the DiR dye can prevent a release from the nanospheres, which can be explained by the fact that highly lipophilic dye was very slowly released from the nanospheres. The research investigated by Petersen et al (2010) shows that only a few amount of the highly lipophilic DiI dye was transferred after a period of weeks.
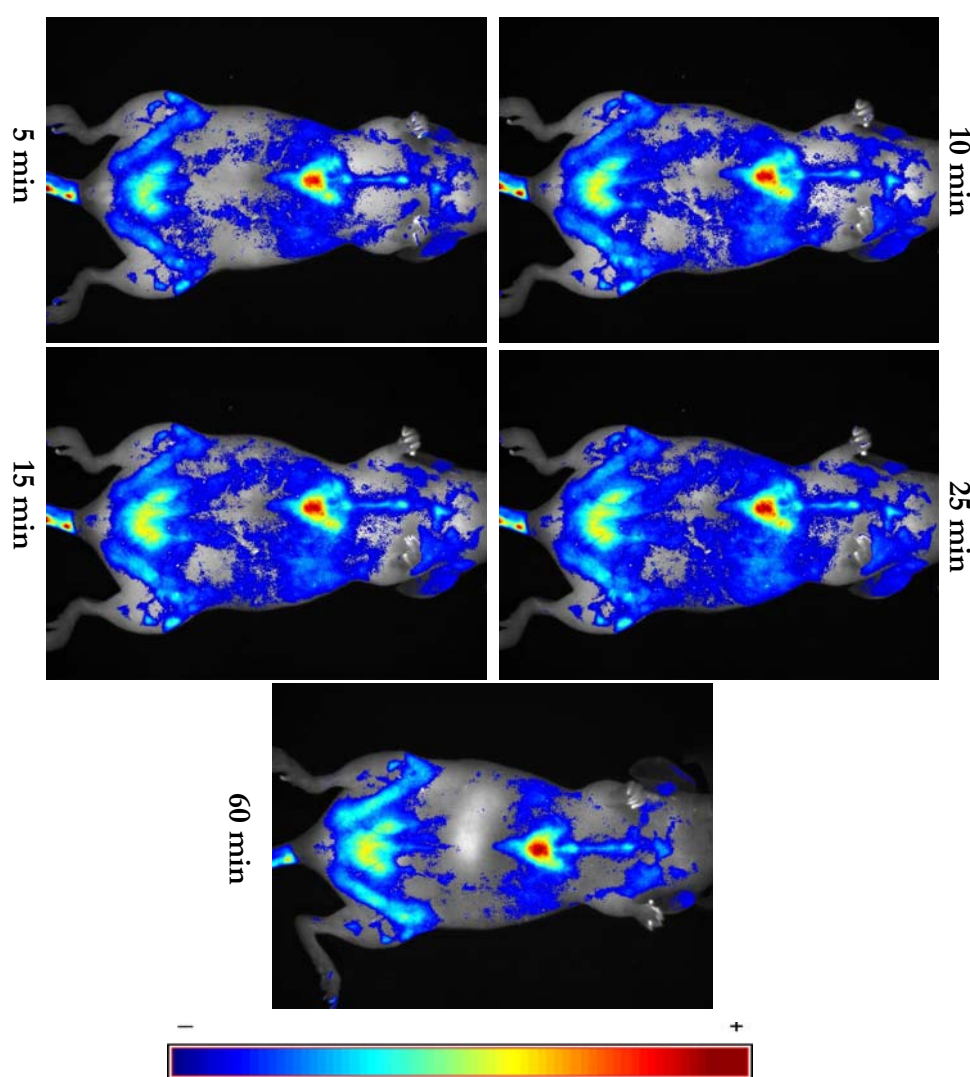
Fig. 3.7-6: Fluorescence intensity images (NR signal) of mice in different time point (5 min, 10 min, 15 min, 25 min and 30 min) after injecting NR-DiR nanospheres.

Fig. 3.7-6 shows the fluorescence intensity images (NR signal) of a mouse 5 min, 10 min, 15 min, 25 min and 30 min after injecting NR-DiR nanospheres. The results indicate that *in vivo* distribution of the nanospheres by fluorescence imaging is also in possible with the NR dye, not only for the NIR dyes. However, nanosphere accumulation in liver could not be detected, which can be explained by that the NR dye has high photon absorbance of biological tissues. Furthermore, the images are in agreement with the previous *in vitro* NR release studies. Petersen et al (2010) investigated a fast release of NR from the particles and elimination of the dye through the urine pathway. Due to its low log P value, NR is fast released from the particles. Although NR does not fluoresce in water, the dye may bind to proteins, which are circulating through the blood stream thus remaining fluorescent. The high fluorescence signal in the urine (Fig. 3.7-6) can be explained by the binding of NR to smaller proteins, which are normally eliminated by the kidneys via the urine.

(a)   (b)

(c)
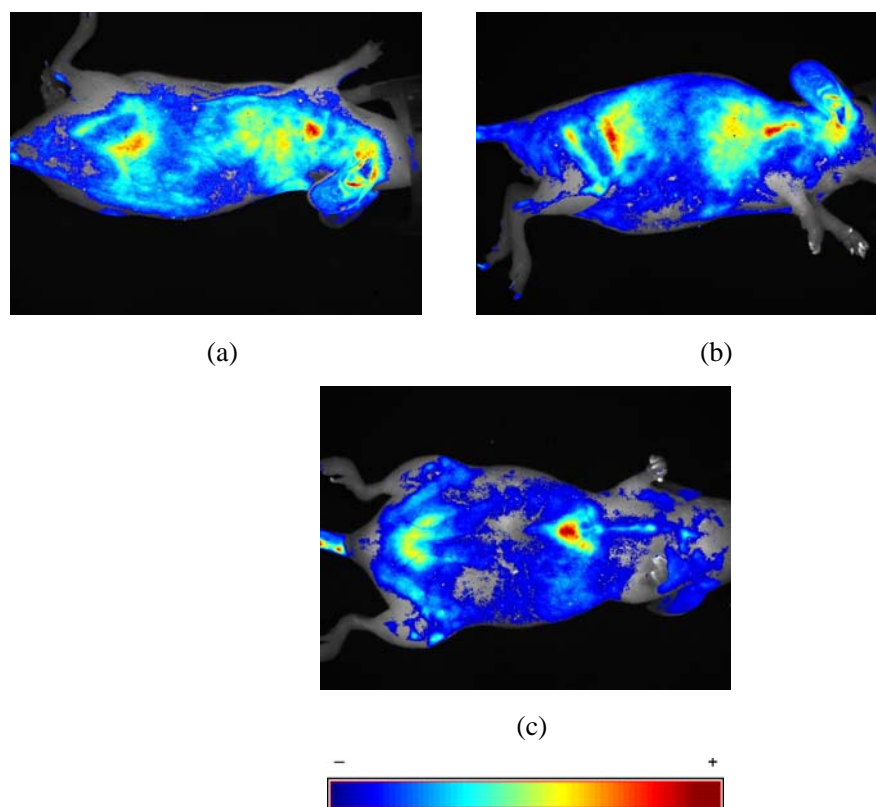
Fig. 3.7-7: Fluorescence intensity images (NR signal) of a mouse 30 min after injecting NR-DiR nanospheres from different side (a, left; b, right; c, abdomen).

In order to get more detailed information about *in vivo* imaging of nanospheres, fluorescence intensity images (NR signal) of a mouse 30 min after injection were obtained from left, right and abdomen side, as seen in Fig. 3.7-7. However, no intensity was also found.
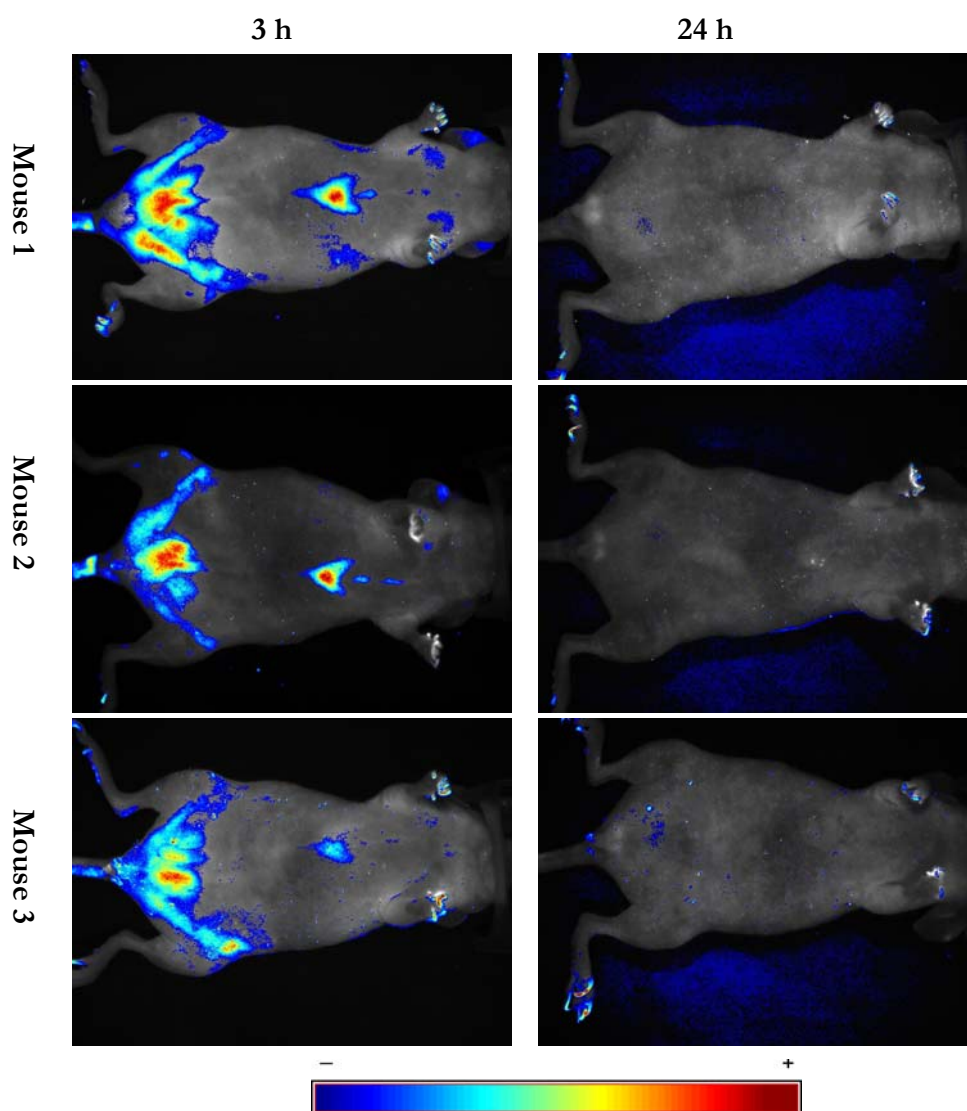
Fig. 3.7-8: Fluorescence intensity images (NR signal) of three mice 3 h and 24 h after injecting NR-DiR nanospheres.

Fluorescence intensity images (NR signal) of three mice 30 h and 24 h after the injection were obtained from abdomen side, as seen in Fig. 3.7-8. The results show the same *in vivo* images of the three different mice. After 24 h, no fluorescence intensity can be found in the mice.

3.7.4   *Ex Vivo* Fluorescence Imaging of Nanospheres

Ex vivo studies were done to measure the fluorescence intensities of different organs. This method can identify the possible excretion pathways by detecting slight accumulations in other organs, such as kidneys and intestine, which can not be visible by *in vivo* imaging.

The mice were autopsied 24 h after the injection of NR-DiR nanospheres. The autopsied viscera were separately located in a separate hole of a 24-hole well plate. Fig. 3.7-9 shows the *ex vivo* results of different organs in a 24-hole well plate 24 h after injecting 15AB NR-DiR NS. For each small figure, from the left side to right side, the organ follows as: intestine, fat, uterus and ovary, liver, gall bladder, lung, spleen, kidneys and heart. And, the *ex vivo* images were taken both from NR signal and DiR signal. The intensity weighted images were used to illustrate the *ex vivo* distribution of nanospheres in the mice.

Ex vivo images based on NR signal in Fig. 3.7-9 show nanospheres were primarily removed by the fat, which can be explained by the property of NR dye. And, no fluorescence intensity in other organs agrees with the *in vivo* images in Fig. 3.7-6. In agreement with the *in vivo* distribution results (Fig. 3.7-5), *ex vivo* imaging based on DiR signal of excised organs in fluorescence intensities showed that nanospheres were accumulated in the liver. Furthermore, a higher intensity in spleen can be found.
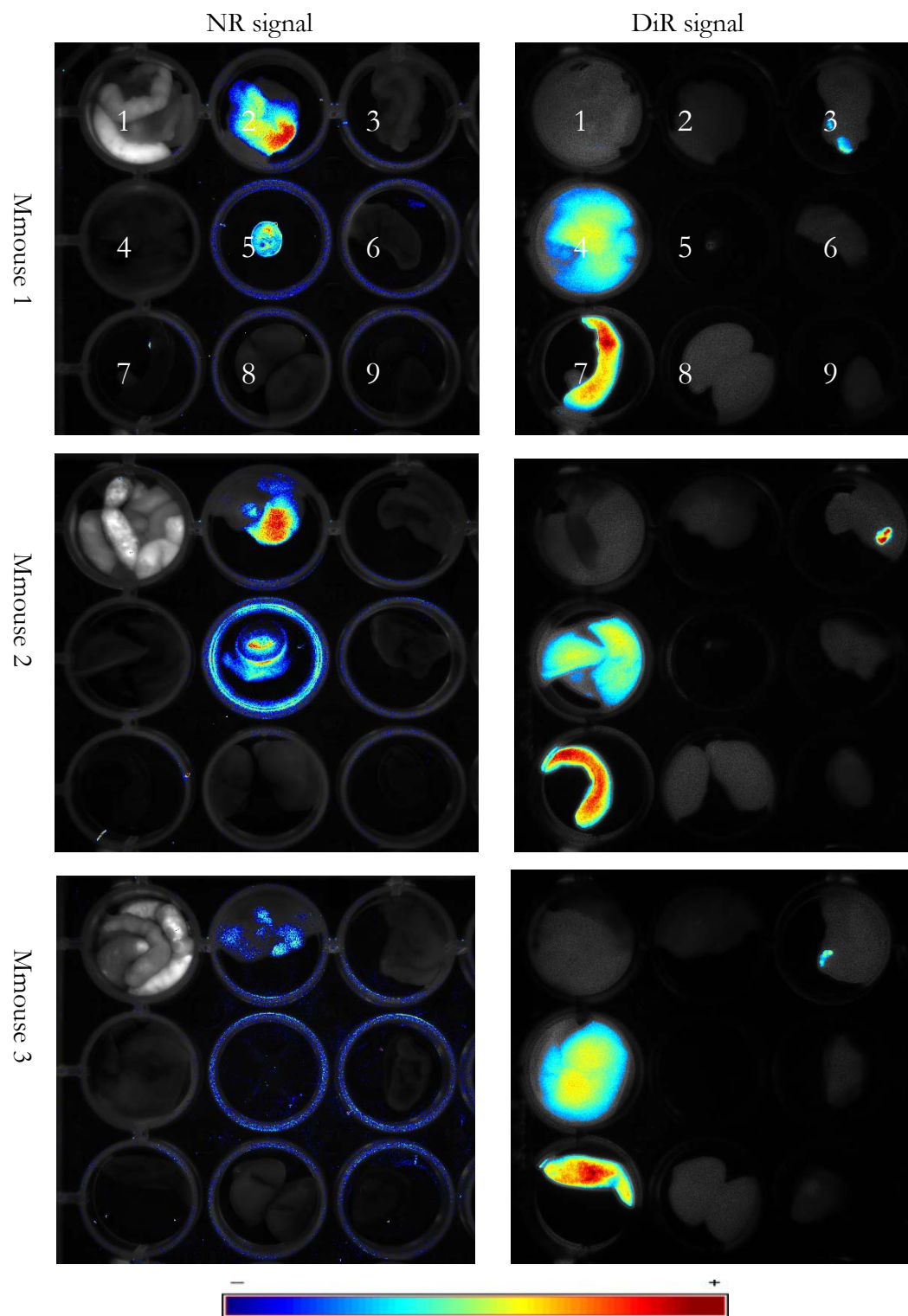
Fig. 3.7-9: *Ex vivo* results (NR signal and DiR signal) of different organs in a 24-hole well plate 24 h after injecting 15AB NR-DiR nanosphere suspension. Order from the organs from left to right, initiating from the top: 1 = intestine, 2 = fat, 3 = ovary, 4 = liver, 5 = gall bladder, 6 = lung, 7 = spleen, 8 = kidneys, 9 = heart, (500 ms exposure time).

3.8 *In Vivo* and *Ex Vivo* Distribution of Nanocapsules

3.8.1   Characterization of Dye-loaded Nanocapsules

In this study, the pegylated PLGA nanocapsules demonstrated a reservoir system composed of core-shell structures with an oily core, in which the dye was dispersed, surrounded by an outer polymer shell with hydrophobic PLGA block and hydrophilic PEG block. Fig. 3.8-1 shows the schematic representation of diblock copolymer PLGA-PEG (AB) and triblock copolymer PLGA-PEG-PLGA (ABA) nanocapsules incorporated with fluorescent dye (DiR or DiI). Since DiR and DiI are very lipophilic with log P values about 20.0 (Rashid and Horobin, 1990), most of these fluorescent dyes are remaining in the oily phase. The hydrophobic core composed of lipiodol oil is thus effective to provide an ideal microenvironment to keep the lipophilic dye more stable and protection after administration (Bae et al., 2007).
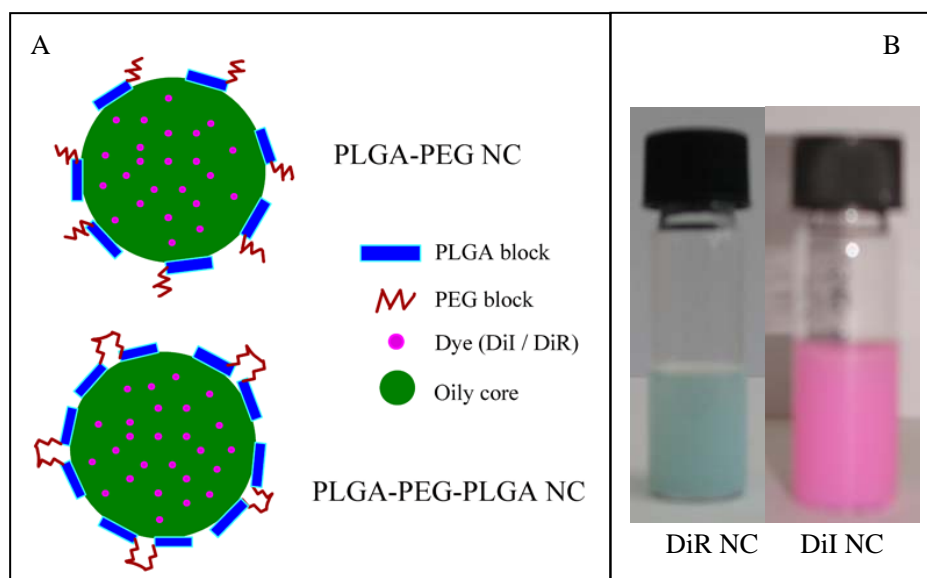
Fig. 3.8-1: Schematic representation of lipophilic dyes (DiR/DiI) incorporated into the oily core of PLGA-PEG and PLGA-PEG-PLGA NC (A) and images of DiR-loaded NC and DiI-loaded NC suspension (B).

Particle size and size distribution of the nanocapsules were measured by PCS and LD in

the different formulations (Table 3.8-1). The DiR-loaded nanocapsules (Batch A-F) had mean diameters between 146 and 156 nm with PDI between 0.102 and 0.163. Size determination of these nanocapsules by LD yielded a D50 diameter (obtained from the volume distribution) around 143-155 nm. Consequently, size results of DiR-loaded nanocapsules obtained by PCS and LD measurements are in good agreement. Similarly, for 15AB DiI-loaded nanocapsules, the particle size determined by PCS was 154 nm with a PDI of 0.129, and the LD result showed the D50 diameter of 149 nm. The small difference of sizes obtained by PCS and LD could be attributed to the different measurement principles. Whereas PCS measures the fluctuation of the intensity of the scattered light which is caused by particle movement (e.g. the hydrodynamic diameter), LD is based on angle dependence scattering of the particles.

Table 3.8-1: Particle size and size distribution of polymeric dye-loaded nanocapsules determined by PCS and LD (n=3; data are shown as mean±SD).

Polymer	Dye	PCS		LD		
		Z-Ave	PDI	D (0.1)	D (0.5)	D (0.9)
		(nm)		(nm)	(nm)	(nm)
5AB	DiR	152±15	0.102±0.016	100±2	154±6	222±14
10AB	DiR	146±11	0.140±0.018	95±7	150±8	234±16
15AB	DiR	149±11	0.124±0.029	96±13	143±16	224±22
10ABA	DiR	156±12	0.163±0.008	94±8	155±12	231±15
15AB	DiI	154±14	0.129±0.026	93±7	149±14	232±25

3.8.2   *In Vivo* Distribution Studies of Nanocapsules

In recent developments of *in vivo* imaging, lipophilic dyes such as DiI and DiR have been widely used for cell-tracking. The carbocyanine dyes have a good stability, a high quantum yield and they are non-toxic to living cells. Due to the non-toxicity and high fluorescence intensity, they are well suited for tracing nanocarriers *in vivo*. Excitation and emission in the NIR region (700–900 nm) are needed for deep-tissue fluorescence imaging (John V, 2003). Hence, NIR fluorescence light offers a unique advantage for the imaging of deep tissue. Therefore, we used a NIR dialkylcarbocyanine dye (DiR,

excitation/emission: 751/780 nm) for our study.

The fluorescence imaging system was monitored to get the emission spectra and images of 15AB Lipiodol DiR nanocapsule, which could be found in Fig. 3.8-2. High intensity of nanocapsules was able to manage the *in vivo* and *ex vivo* study by fluorescence imaging.
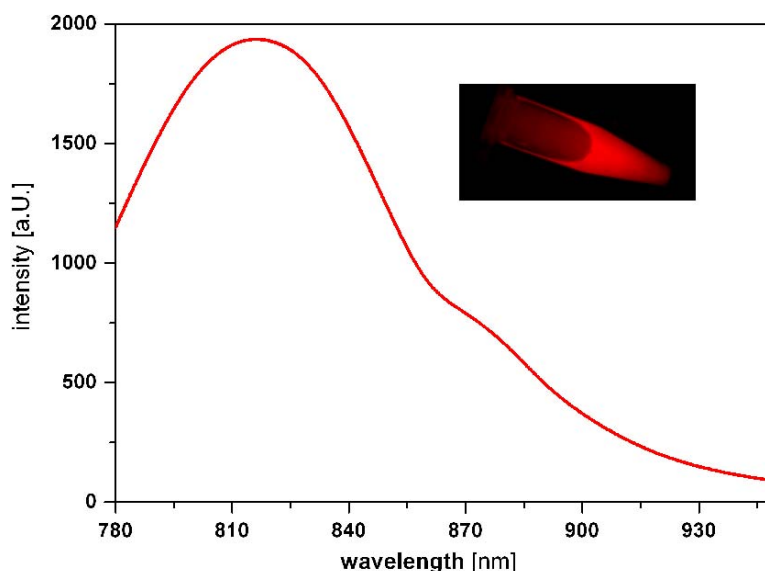
Fig. 3.8-2: Fluorescence emission spectra and image (insert) of DiR-loaded 15AB nanocapsule suspension *in vitro* (20 ms exposure time).

The *in vivo* fate of polymeric nanocapsules following i.v. administration represents the physicochemical and biological properties which have to be considered in the design of colloidal drug delivery systems. In this study, firstly, the *in vivo* fate of 15AB DiR-loaded nanocapsules was examined after i.v. injection in mice. Intensity weighted images were used to illustrate the nanocapsules distribution in the mice (Fig. 3.8-3). From red over orange and yellow up to dark blue regions, the intensity indicated the decreased nanocapsule amounts. In the pictures it was visible that DiR concentration in the nanocapsules was sufficient for *in vivo* fluorescence imaging. Shortly about few minutes after injection, these nanocapsules were distributed through the whole body and an imaging of the nanocapsules in the subcutaneous blood vessels was possible (not shown). Already in the first 15 minutes nanocapsules were accumulated by the MPS organs (liver and spleen). Large amounts of the nanocapsules were still homogeneous distributed

within the blood stream. Due to the fact that the maestro software has a fixed intensity allocation to the jet color profile, these nanocapsules can't be displayed in the images of Fig. 3.8-3.

.
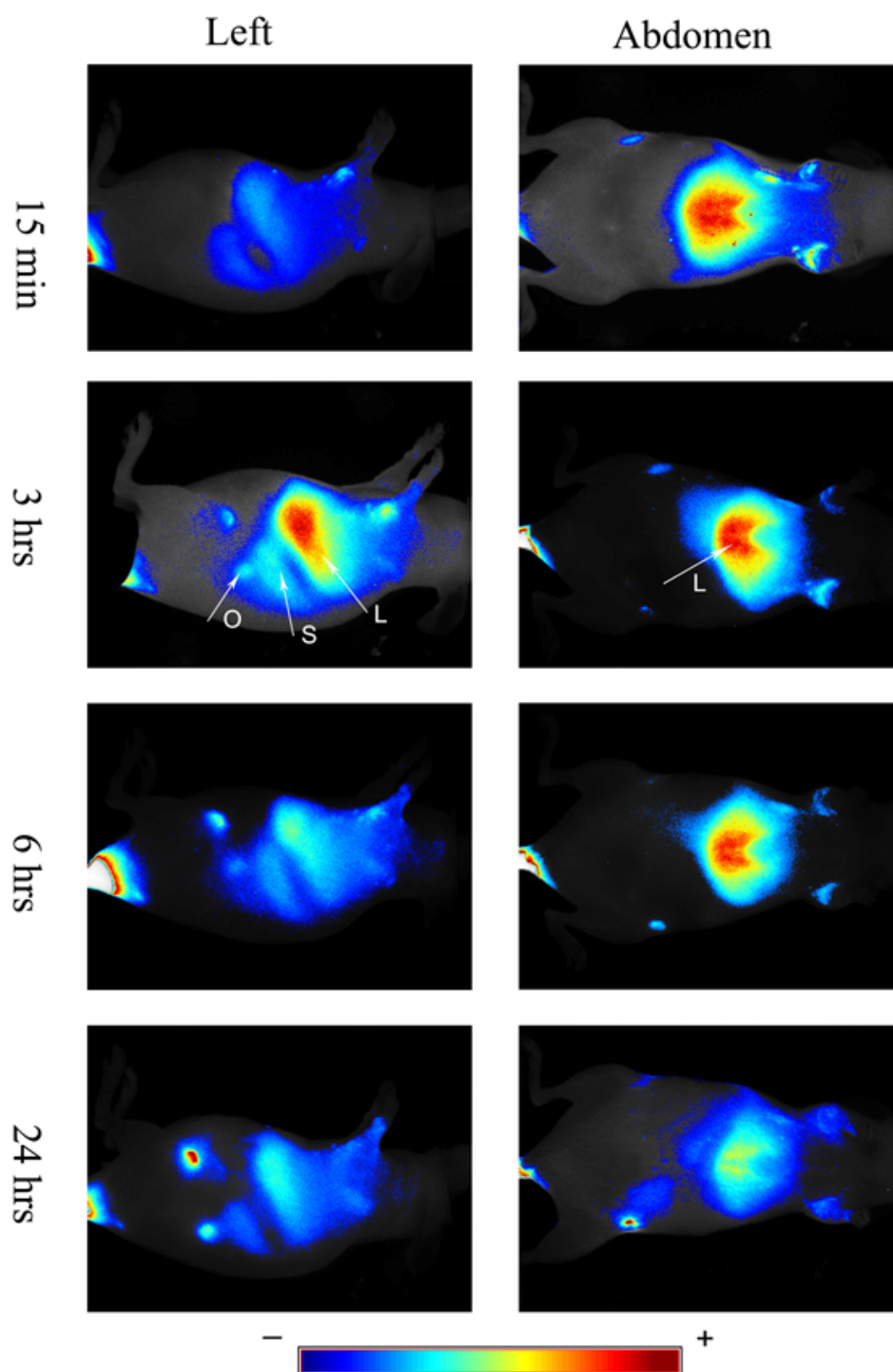
Fig. 3.8-3: Biodistribution and organ accumulation of 15AB DiR-loaded nanocapsules after i.v. injection to the mice. Each image was acquired with an exposure time of 800 ms. The jet color represents the intensity of the detected DiR signal. L: liver; S: spleen; O: ovary.

The *in vivo* images demonstrated that the 15AB DiR nanocapsules circulated in blood stream for 6 h. The visible accumulation in the liver and spleen, as revealed by strong fluorescence from these organs remained more or less constant during the first 6 h. 24 h after injection, a decreased intensity could be observed, which indicated that nanocapsules started to eliminate. In addition to the accumulation in liver, spleen and ovary, comparative high fluorescence values were measured in the area of the foreleg, which may be caused by enrichment of the nanocapsules in the lymphatic system. An accumulation can also be seen in the tail of the mice which was probably a result of the administration procedure where they must be slightly fixed for immobilization to allow to the injection into the vein of the narcotized mice. Interestingly, in the images from the left side of the mouse there was a punctual enrichment in the left of the spleen which could be allocated to the ovary. The intensity in this area increased up to 24 h.

To analyze the accumulation of nanocapsules in organs which are not visible *in vivo* by fluorescence imaging, the mice were autopsied 48 h after the injection (Fig. 3.8-4). After this time all nanocapsules accumulated by respective tissues and should not any more circulating via the blood stream. The autopsied viscera were separately located in a separate hole of a 24 holes well plate shown in Fig. 3.8-4. For each small figure, from the left side to right side, the organ follows as: intestine, fat, uterus and ovary, liver, gall bladder, lung, spleen, kidneys and heart. In agreement with the *in vivo* distribution results (Fig. 3.8-3), *ex vivo* imaging of excised tissues in fluorescence intensities showed that polymeric nanocapsules were primarily removed by the liver.
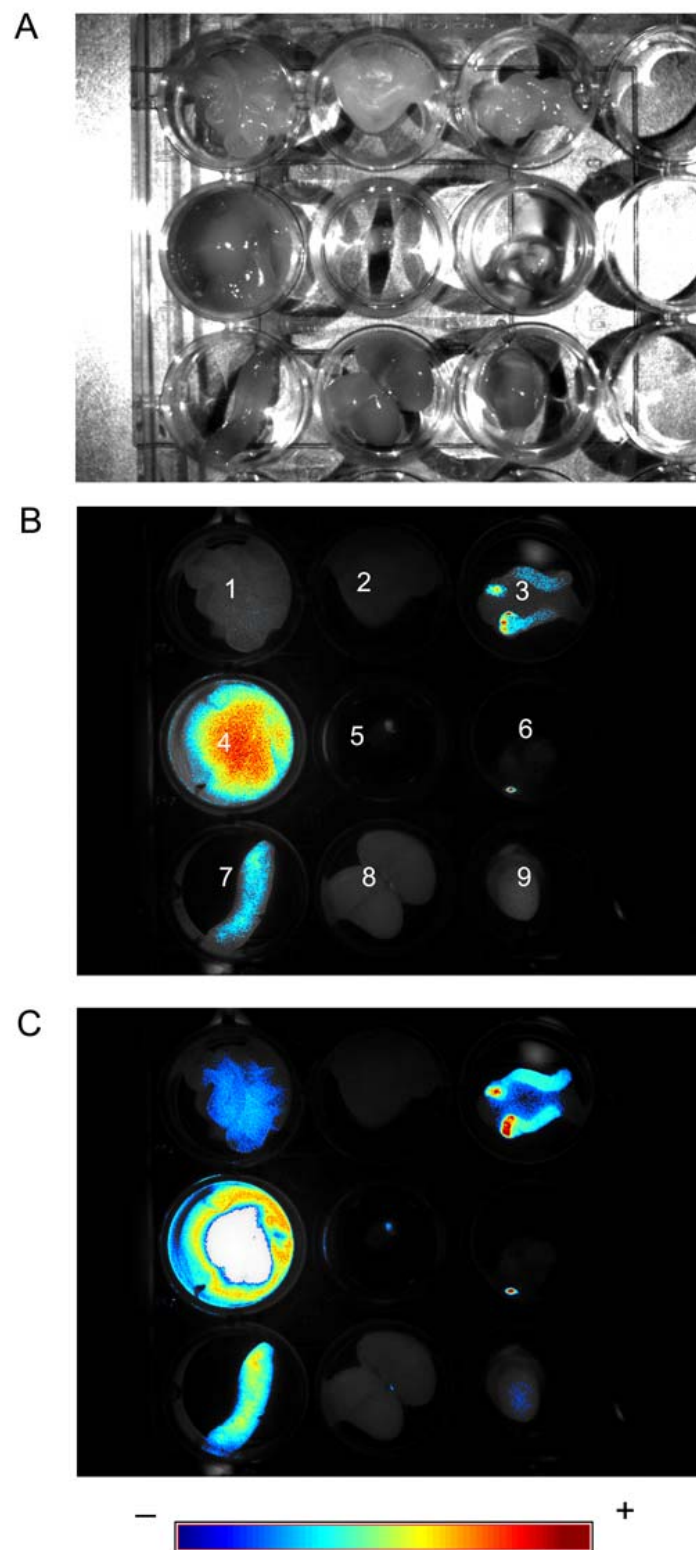
Fig. 3.8-4: Autopsy biodistribution results of different tissues in a 24-hole well plate 48 h after injecting 15AB DiR nanocapsules. Order from the organs from left to right, initiating from the top: 1 = intestine, 2 = fat, 3 = ovary, 4 = liver, 5 = gall bladder, 6 = lung, 7 = spleen, 8 = kidneys, 9 = heart, A = original photograph, B = 400 ms exposure time, C = 1200 ms exposure time.

The intensity in various organ decreased in the order of liver > spleen > ovary > intestine. Almost no fluorescence nanocapsules were found in the fat, lung, kidney and heart. The absence of nanocapsules in the kidneys indicated that they were not excreted with the urine. Comparing different exposure times of 400 ms (Fig. 3.8-4B) and 1200 ms (Fig. 3.8-4C), the biodistribution results of nanocapsules revealed a slight dye signal in the intestine at higher exposure time (Fig. 3.8-4C), which indicated that the nanocapsules were degraded in the liver and the DiR dye was eliminated via the enterohepatic circulation pathway. The white area of the liver in the image measured with 1200 ms exposure time was the result of the quenched fluorescence signal and was necessary to visualize possible low concentrated accumulations in other tissues.

3.8.3   Biodistribution in Dependence of PEG Content

PEG is a hydrophilic, non-immunogenic polymer and has been widely used to increase the surface hydrophilicity of colloidal carriers to act as a shield against MPS uptake. To study the role of PEG content on the biodistribution of polymeric nanocapsules, we investigated diblock copolymer PLGA-PEG (AB) nanocapsules with different PEG contents from 5% to 15% and a triblock copolymer PLGA-PEG-PLGA (ABA) nanocapsule with 10% PEG in this study. Fig. 3.8-5 shows the fluorescence emission spectra of used lipiodol DiR nanocapsule suspensions with different polymers: 5AB, 10AB, 15AB and 10ABA. In contrast to diblock copolymer 5AB and 15AB, DiR nanocapsules prepared with diblock copolymer 10AB and triblock copolymer 10ABA had high intensity of fluorescence emission spectra. This result may be explained by the fact that nanocapsule suspension formulated with different polymer had different DiR concentration (10AB: 32.70 µg/ml, 10ABA: 28.44 µg/ml, 15AB: 27.41 µg/ml and 5AB: 16.62 µg/ml) in the experimental part.
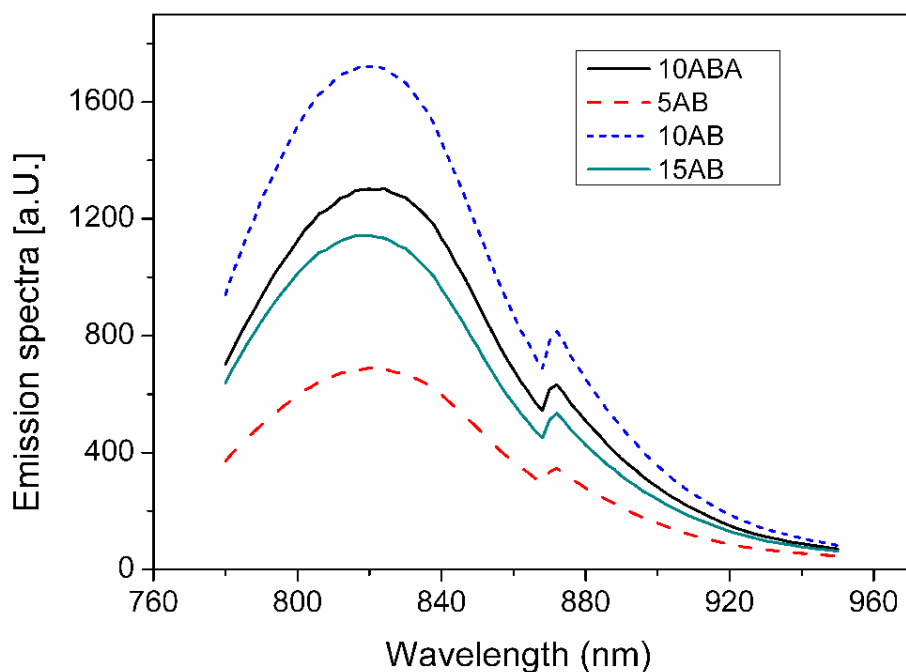
Fig. 3.8-5: Fluorescence emission spectra of DiR-loaded nanocapsules with different polymers: 5AB, 10AB, 15AB, 10ABA. The results were acquired with an exposure time of 15 ms.

The *ex vivo* fluorescence intensity values were divided by the maximal intensity of the *in vitro* emission spectra of the nanocapsule suspensions from Fig. 3.8-5. And, all the *ex vivo* intensities values were normalized to 100% related to the highest fluorescence intensity. The *ex vivo* normalized maximal intensity and total intensity of DiR-loaded 5AB, 10AB, 15AB, 10ABA nanocapsules in spleen and liver 24 h after administration are shown in Fig. 3.8-6. The maximal signal represented the highest pixel value within the ROI, while total signal is the sum of all the pixel values in the ROI. The fluorescence signal ratios of liver and spleen of the maximum and total intensity are shown in Fig. 3.8-6. Both intensities are dependent on the concentration of the fluorescent dye and the fluorescent properties of the tissue (light penetration and emission properties). In contrast to the maximum intensity, the total intensity does also depend on the organ size. The liver has a larger size (pixel) than the spleen.

For maximal intensities, 5AB had a significantly higher intensity in the spleen than other

polymers, for 10AB ($p= 0.00113$) and 15AB ($p= 0.00052$), 10ABA ($p= 0.00578$). And, 15AB had a significantly lower intensity in the spleen than other polymers, for 5AB ($p= 0.00052$) and 10AB ($p= 0.00113$), 10ABA ($p= 0.00157$). In addition, 5AB had a significantly higher intensity in the liver than 10AB ($p= 0.01342$) and 15 AB ($p= 0.00687$). For total intensities, 15AB had a significantly lower intensity in the spleen than 5AB ($p= 0.00095$) and 10AB ($p= 0.00627$), and 10AB had a significantly lower intensity in the spleen than 5AB ($p= 0.01131$). In addition, 15AB had a significantly lower intensity in the liver than 5AB ($p= 0.01442$) and 10 AB ($p= 0.00492$).

In general, a reduced fluorescence intensity of diblock copolymer AB and triblock copolymer ABA nanocapsules in liver and spleen was observed from both the maximum intensity (Fig. 3.8-6A) and the total intensity (Fig. 3.8-6B) when PEG content increased from 5% to 15%. In additional, compared to the diblock copolymer 10AB (PEG: 5 kDa), the triblock copolymer 10ABA with higher PEG molecular weight (6 kDa) had an increased maxima intensity and total intensity in the spleen, but no distinct increased intensity in the liver was found.
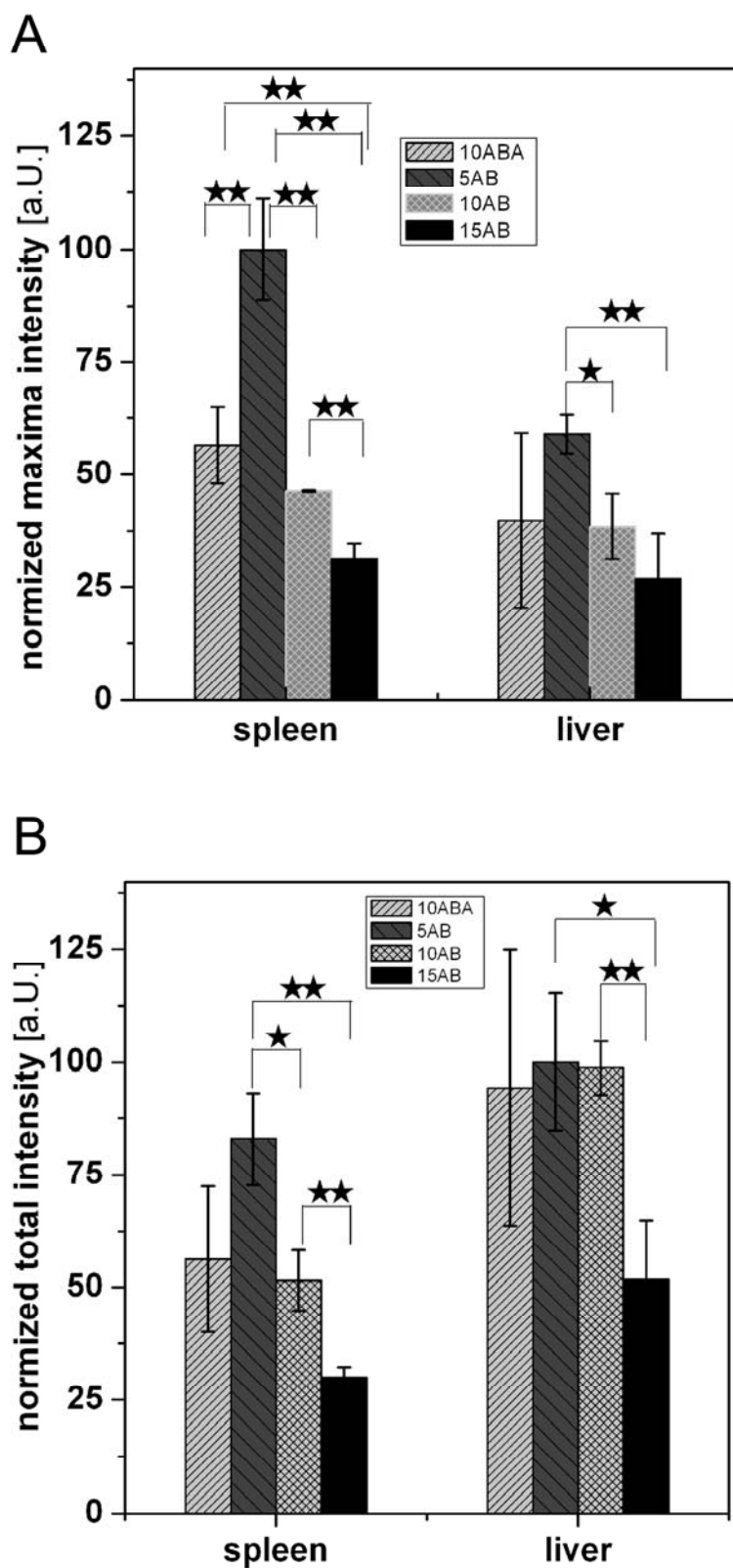
Fig. 3.8-6: Normalized maximal (A) and total *ex vivo* fluorescence intensities (B) of DiR loaded 5AB, 10AB, 15AB, 10ABA nanocapsules in spleen and liver 24 h after administration. All data points show mean±SD for 3 mice (*, $p < 0.05$; **, $p < 0.01$).

Consequently, from the *in vivo* and *ex vivo* studies, we can conclude that the PEG-grafted PLGA nanocapsules loaded with DiR can circulate in blood stream for 6 h, and nanocapsules were mostly accumulated in liver, spleen, ovary and intestine after 24 h. Moreover, the accumulation in the liver and spleen can be reduced by increasing the ratio of PEG and polymer. PEG content is effective in limiting the MPS uptake. Differences in the PEG content (5%, 10% and 15%) of polymer resulted in an altered distribution of DiR nanocapsules in the tissues and organs.

Many researches have been focused on the role of PEG content on the *in vivo* distribution of polymeric nanoparticles (Alexis et al., 2008). However, in most cases, particle size varied with the PEG content of the polymer, especially for nanospheres (Avgoustakis et al., 2003). It is well established that particle size can significantly affect the biodistribution. Thus, it is unclear whether the effect of *in vivo* fate was due to particle size or PEG content. In this study, polymeric nanocapsules with similar particle sizes and narrow size distributions were prepared from different polymers, which included PLGA-PEG copolymers with 5%, 10%, 15% PEG and a triblock PLGA-PEG-PLGA with 10% PEG. The fluorescence intensity of nanocapsules in liver and spleen decreased with increasing PEG content from 5% to 15% (Fig. 3.8-6), which demonstrated the efficiency of PEG to reduce the MPS (liver and spleen) uptake. Thus, the modification of the surface (PEG content) resulted in distinct alterations in the biodistribution of our PEG-grafted PLGA nanocapsules.

3.8.4   *Ex Vivo* Confocal Microscopy Studies

In order to obtain more information about the detailed localization within the organs, further *ex vivo* analyses were preformed by means of confocal microscopy, where DiI-loaded 15AB nanocapsules were investigated 24 h after i.v. injection to the mice.

Fig. 3.8-7 shows confocal microscopic pictures from the nanocapsule suspension (A) dropped on the cover slide and from the sliced ovary (B), liver (C), spleen (D) and kidney (E). The high fluorescent nanocapsules (red spots) were clearly visible in the digital magnification (Fig. 3.8-7A). The nanocapsules were homogenously distributed, and no agglomerates could be found. Fig. 3.8-7C showed the confocal microscopy image from the liver of treated (left part) and untreated (right part) animals. In contrast to the untreated animal, high fluorescent spots were presented in the liver of the treated animal. In addition, uniform allocation of the fluorescent spots was also visible in the Fig. 3.8-7B and Fig. 3.8-7D, which indicated that the nanocapsules could be clearly found in the ovary and spleen tissue. Only very weak signals from fluorescent nanocapsules could be seen in the kidney (Fig. 3.8-7E).
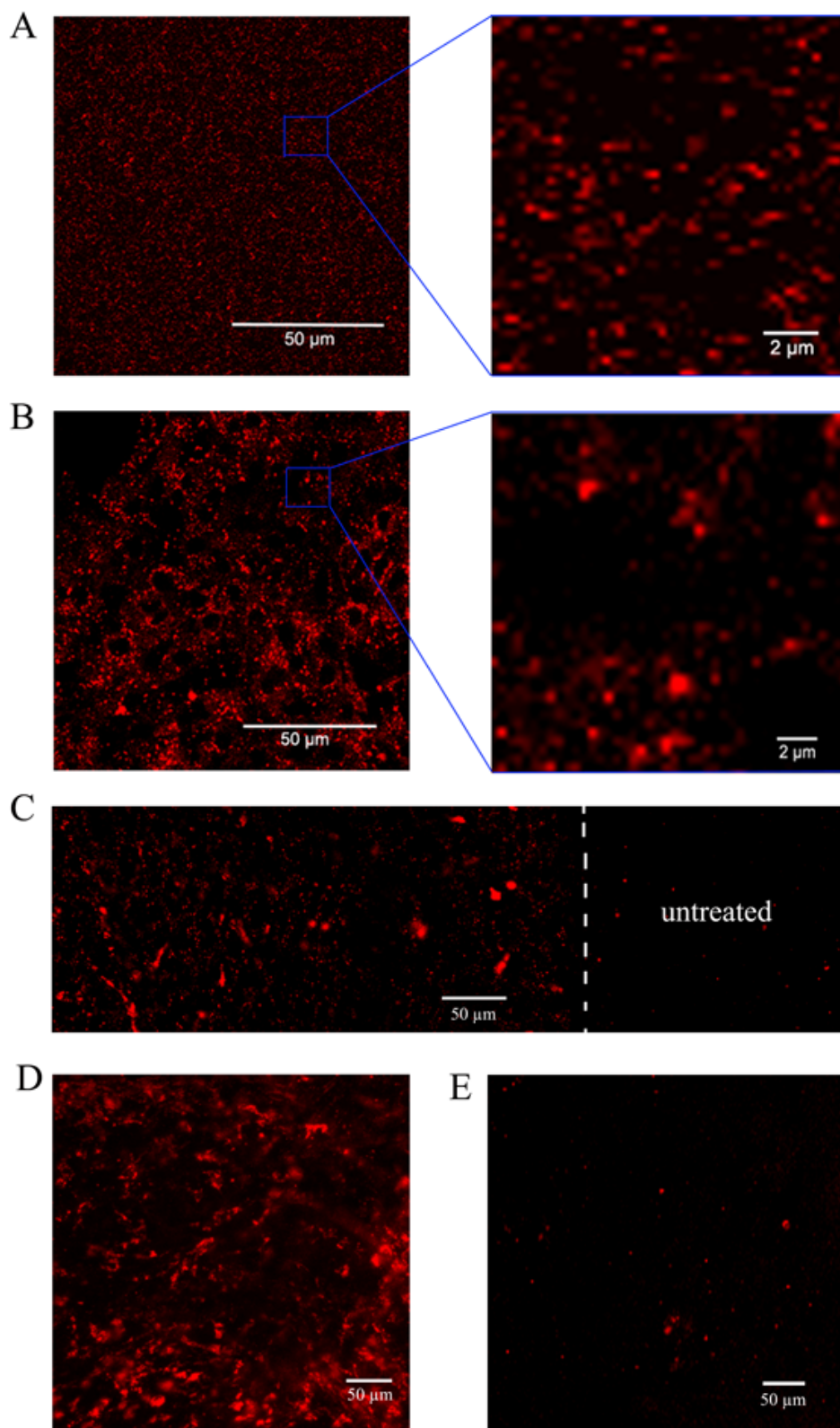
Fig. 3.8-7: Confocal microscopy in vitro images of a DiI nanocapsule suspension (A) and *ex vivo* ovary (B), liver (C), spleen (D) and kidney (E) tissue images 24 h after i.v. injection of DiI-loaded 15AB nanocapsules, red homogeneous spots present the DiI loaded nanocapsules.

3.9 Nanospheres for Betulinic Acid Delivery

3.9.1   Preparation of Betulinic Acid Nanospheres

Betulinic acid (BA) (Fig. 3.9-1) is a triterpene of natural origin isolated from various plants. It can be isolated from the extract of Tryphyllum peltatum, Diospyros leucomelas, Tetracera boliviana, Zizyphus joazeiro and Syzygium formosanum. Betulinic acid has already been shown to exhibit anti-HIV, anticancer, antibacterial, antiviral, anti-inflammatory, and anthelmintic activities although the clinical activity is not established (Yogeeswari and Sriram, 2005).

$C_{30}H_{48}O_3$
MW456.70
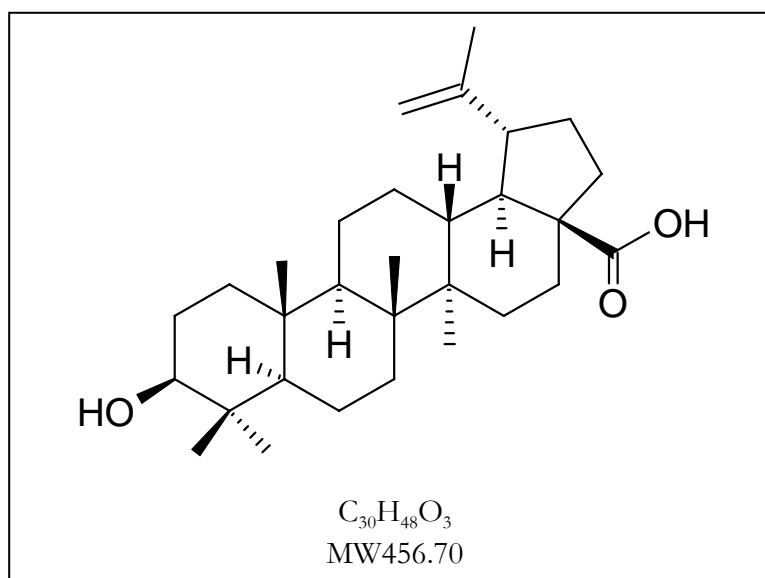
Fig. 3.9-1: Chemical structure, formulae and molecular weight of betulinic acid.

BA has a very poorly water-soluble activity. The solubility of BA in water is only 0.02 µg/ml at 25°C. When administered intravenously, BA has a low bioavailability to limited *in vivo* drug administration, which represents a major limitation of this biological compound. Nano-drug delivery system (NDDS) has gain increasing attention as possible means to obtain a higher therapeutic effect, a lower toxicity and a protection from *in vivo* metabolization of a incorporated drug (Peer et al., 2007). Until now, nanocarriers for BA delivery have focused on the research of liposomes (Csuk et al., 2010); however, its physical stability is always a critical problem. Thus, it is extremely important to develop

novel polymeric nanoparticles for BA delivery.

3.9.2   Characterization of BA-loaded Nanospheres

The nanoprecipitation method is a direct, rapid and easy technique to perform and is mostly applied to prepare polymeric nanospheres. In this study, BA-loaded nanospheres were prepared from PLGA-PEG using nanoprecipitation method. Apparent proof of the introduction of BA molecules in nanospheres came from HPLC analysis (data not shown). Compared with blank nanospheres, BA-loaded nanospheres showed a betulinic acid peak at 13.903 min, which was consistent with the retention time of free BA (13.787 min).

The loading capacity of the nanospheres was assessed using fixed amounts of the polymer and variable quantities of BA. As shown in Fig. 3.9-2, 10AB had a higher loading capacity of BA than other polymers (15 times higher than 15AB and 2 times than 10ABA). And, 5AB had almost no ability to encapsulate the drug, which can be explained that the drug has a very low affinity for 5AB.
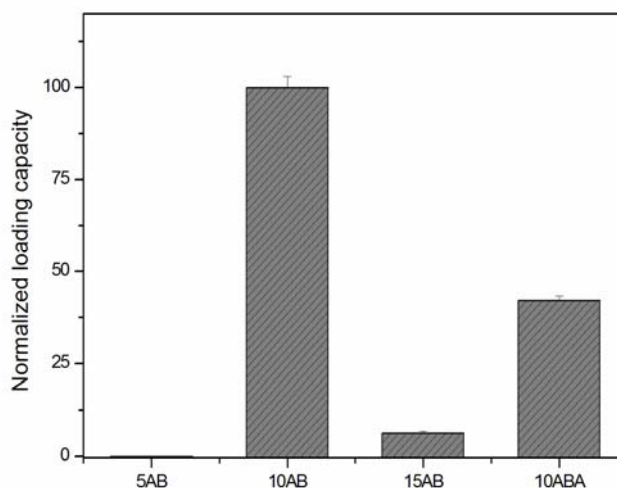
Fig. 3.9-2: Normalized loading capacity of the 5AB, 10AB, 15AB and 10ABA Nanospheres formulated with the same amount of polymer and BA. All data points show mean±SD for 3 measurements.

Table 3.9-1 showed that the 10AB BA-loaded nanospheres had a mean size around 70 nm and narrow size distribution (PDI). When the theoretical concentration of BA was at or above 75 µg/ml, BA precipitated in the form of crystals. The results indicated the maximum loading capacity of the nanospheres was reached. The encapsulation efficiency of BA in the nanospheres was 40.2%, 46.3% and 37.6% according to a theoretical concentration with the value of 30 µg/ml, 40 µg/ml and 50 µg/ml.

Table 3.9-1: Encapsulation parameters and particle size of 10AB BA-loaded nanospheres (acetone: water = 1:2).

Theoretical Concentration (µg/ml)	Final Concentration (µg/ml)	Encapsulation efficiency (%)	Mean Size (nm)	PDI
30	12.6±1.3	40.2±4.3	70.8±1.22	0.122±0.008
40	18.5±1.2	46.3±3.0	70.9±1.31	0.119±0.011
50	18.8±1.6	37.6±3.2	71.6±1.35	0.126±0.014
75	crystals of BA	N.D	71.5±1.12	0.124±0.012
100	crystals of BA	N.D	72.8±1.51	0.129±0.013

Values express the mean±SD values of three batches, ND. Not determined.

The effect of the ratio of acetone to water during the nanosphere formulation was assayed on the encapsulation efficiency and particle size of the nanospheres (Fig. 3.9-3). Particle sizes had almost no change when the ratio of acetone to water was varied from 1:1 to 1:10. The BA concentration in nanospheres changed between 8.5 mg/ml and 23.8 mg/ml, depending on the ratio of acetone to water. The highest BA concentration in nanospheres was obtained with the value of 23.8 mg/ml, when the formulation prepared with the ratio of acetone to water (1: 10).
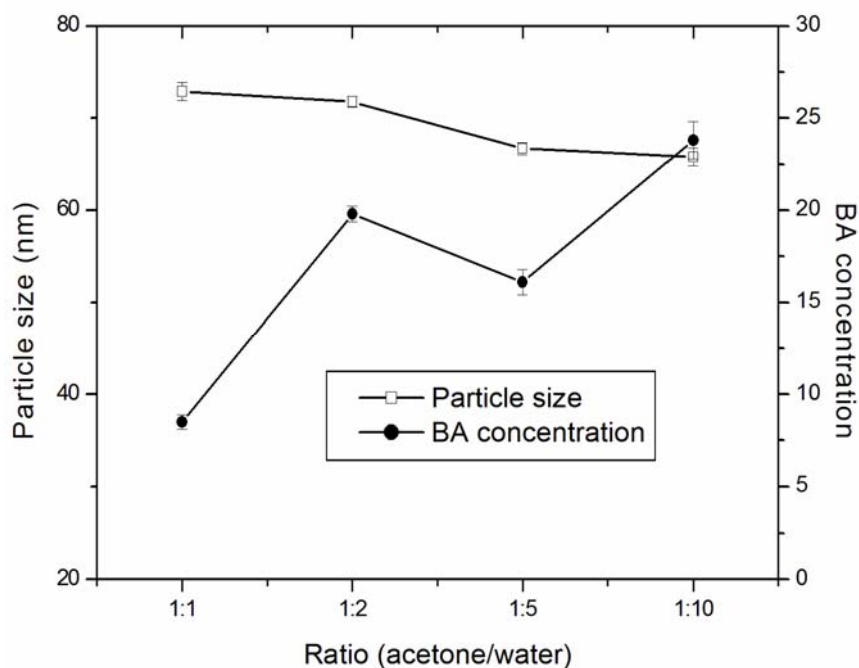
Fig. 3.9-3: Particle size and encapsulation efficiency of 10AB BA-loaded nanospheres prepared with the different volume ratio of acetone to water.

3.9.3   Cell Culture Studies

The cytotoxic activity of PLGA-PEG nanospheres loaded with BA was evaluated on A549 cells using the SRB assay, as control free BA was used. Additionally, cells were treated with PBS in the same way as with nanospheres loaded with BA in order to prove if sufficient quantity of medium was present for normal cell grow (the highest ratio medium/PBS = 100/100 μl). It was found that adequate amount of medium was present during experiment (see influence of the PBS on the cell survival: Fig. 3.9-4). The BA-loaded nanospheres exhibited a dose-dependent cytotoxicity against A549 cell line, and exhibited lower IC_{50} value (3.5 μM) than free BA (4.7 μM). The above results revealed that BA-loaded nanospheres exhibited higher cytotoxicity than free BA on the A549 cell line.
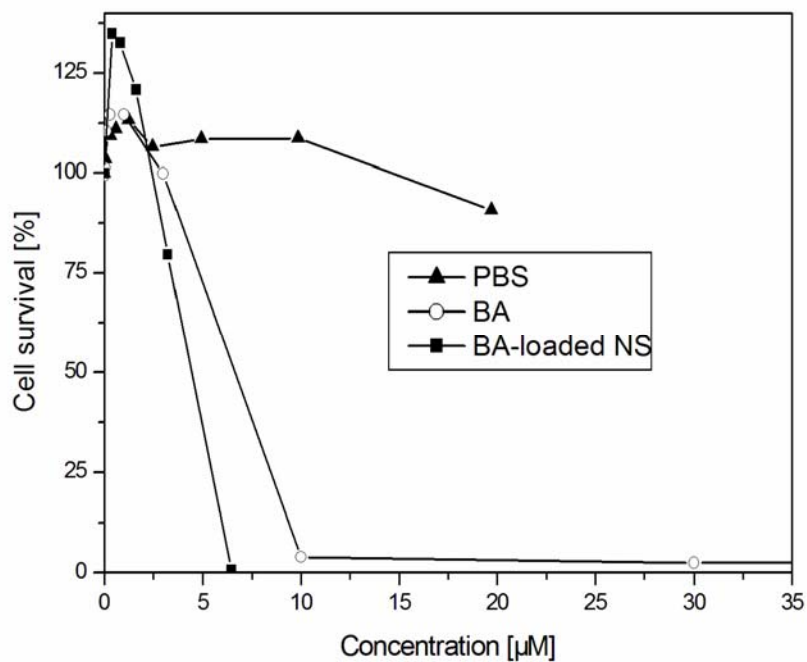
Fig. 3.9-4: Representative graphs showing survival of A549 (human lung carcinoma) cell line treated with PBS, pure BA, and BA-loaded NS, determinated with SRB assay; the values are the mean±standard deviation of three determinations.

4 Summary and Conclusions

Polymeric nanoparticles including nanospheres and nanocapsules have attracted great interest for use as diagnostic and therapeutic agents. Poly-(lactic-co-glycolic acid) (PLGA) is a common choice since its safety and biofate have already been established in the clinic. Di-block PLGA-PEG and tri-block PLGA-PEG-PLGA copolymers are widely investigated for both fundamental research and product development because pegylated polymeric nanoparticles can significantly reduce systemic clearance compared to PEG-free particles. However, a commercial nanosphere or nanocapsule product is still not on the market.

The objective of this study was the development, characterization and *in vivo* evaluation of biodegradable nanospheres and oily core nanocapsules. Nanospheres and oily core nanocapsules were prepared using nanoprecipitation method. The influence of the PEG: PLGA ratio (5:95, 10:90, 15:85) and architecture (PLGA-PEG vs. PLGA-PEG-PLGA) on the *in vitro* and *in vivo* properties of nanoparticles was characterized.

The particle size, size distribution and morphology of nanoparticles were determined by photon correlation spectroscopy, laser diffraction, transmission electron microscopy and atomic force microscopy. Structure and dynamics of nanoparticles were determined by nuclear magnetic resonance and electron spin resonance. The ability of sugars to prevent the aggregation of nanoparticles was investigated during freeze-drying process. The *in vivo* and *ex vivo* fate and organ accumulation of the nanoparticles in nude mice were investigated using the noninvasive method of multispectral optical imaging. In order to obtain more information about the detailed localization within the organs, DiI loaded nanocapsules were also investigated *ex vivo* by means of confocal microscopy. Finally, nanospheres were developed for betulinic acid delivery, and physical characterizations and cytotoxicity on A549 cell lines were evaluated.

Particle sizes of nanospheres increased when the polymer concentration in acetone increased. Using the linear correlation of the particle size and polymer concentration, nanospheres with predefined and desirable sizes could be achieved. Nanocapsules prepared from PLGA-PEG with 5%, 10% and 15% PEG and PLGA-PEG-PLGA with 10% PEG had similar particle size which could be attributed to the same oily phase. It was found that nanoparticles exhibited spherical shape and nanocapsules had a core-shell structure with 10 nm homogeneous polymer shells. AFM results confirmed the spherical shape of nanoparticles, and the height profile was possible to investigate the structure of matrix nanospheres and vesicular nanocapsules.

Addition of sugars to an aqueous nanoparticle suspension was allowed to the recovery of nanoparticles of similar size as originally formulated. 10%, 15% sucrose and trehalose can act as effective cryoprotectants during the freeze-drying process of nanospheres. The amount of cryoprotectant for freeze-drying nanospheres required increase when the PEG content of the polymer increased. For freeze-drying nanocapsules, sucrose (5, 10%) was identified as being the suitable excipients. And, a reduced size change could be found after freeze-drying when the sucrose concentration increased from 5% to 10%.

^{1}H-NMR results of nanospheres indicated that nanospheres were made of PLGA core and PEG corona. And, signals of nanocapsule suspension in the aliphatic region were in agreement with the liquid state of its lipiodol oily core because of aliphatic groups with highly mobile chains in the liquid state. ESR spectra of nanocapsules indicated that the majority of the HDPMI molecule was dissolved within the lipiodol oily core of the nanocapsules, while the spectra of nanospheres showed an immobilization of the spin probe inside these systems.

The *in vivo* fluorescence imaging showed that nanoparticles circulated in the blood stream for several hours. During this time, accumulation of nanoparticles in liver and spleen increased and reached a maximum after 24 hours. A reduced liver and spleen uptake of nanocapsules was observed with increasing PEG content from 5% to 15%. Both *in vivo*

and *ex vivo* fluorescence imaging indicated that nanocapsules accumulated in the liver, spleen and ovary, which were confirmed by *ex vivo* confocal microscopy.

PLGA-PEG nanospheres were effective to encapsulate betulinic acid to improve its bioavailability. The cytotoxicity assay of BA-loaded nanospheres exhibited a lower IC50 value compared to free betulinic acid on A549 cells.

Further work is suggested to focus on the investigation of nanocapsules for CT-imaging. Due to the nanocapsules compose of lipiodol oil containing a heavy atom (iodine), thus they have great potential for CT-imaging. Using the DiR lipiodol nanocapsules as dual contrast agents, a combination of fluorescence imaging and CT-imaging to get 3D images about the distribution and accumulation of nanocapsules might be possible.

5 Abstrakt in deutscher Sprache

Polymere Nanopartikel einschließlich Nanosphärulen und Nanokapseln sind von Interesse im Hinblick auf ihre Übertragung aus der Grundlagenforschung in klinische Studien. Das Ziel dieser Arbeit war die Entwicklung, Charakterisierung und *in vivo* Evaluierung von biologisch abbaubaren Nanosphärulen und ölbeladenen Nanokapseln.

In dieser Studie wurden Nanosphärulen und ölbeladene Nanokapseln auf Diblockcopolymer PLGA-PEG- und Triblockcopolymer PLGA-PEG-PLGA-Basis unter Verwendung der Nanopräzipitations-Methode hergestellt. Der Einfluss des PEG: PLGA-Verhältnisses (5:95, 10:90, 15:85) auf die *in vitro* und *in vivo* Eigenschaften von Nanopartikeln wurde charakterisiert. Die Partikelgröße, Größenverteilung und Morphologie der Nanopartikel wurden mittels Photonen-Korrelations-Spektroskopie, Laser-Beugung, Transmissions-Elektronenmikroskopie und Rasterkraftmikroskopie bestimmt. Struktur und Dynamik der Nanopartikel wurden durch Kernspinresonanz-und Elektronenspinresonanz-Spektroskopie bestimmt. Die Fähigkeit von Zuckern, die Aggregation von Nanopartikeln zu verhindern wurde während des Gefriertrocknungsprozesses untersucht. Das *in vivo* und *ex vivo* Verhalten und die Anreicherung der Partikel in den Organen von Mäusen wurden mittels Fluoreszenz-Imaging und Konfokalmikroskopie untersucht. Schließlich wurden Nanosphärulen als Freigabesystem für Betulinsäure entwickelt und physikalische Charakterisierungen und Zytotoxizitätstests mit A549-Zelllinien wurden durchgeführt.

Die Partikelgrößen der Nanosphärulen waren abhängig von der Polymerkonzentration und dem PEG-Gehalt, während Nanokapseln mit verschiedenenen PEG-Gehalten eine ähnliche Partikelgröße aufwiesen, was auf die gleiche ölige Phase zurückgeführt werden konnte. Es wurde festgestellt, dass die Nanopartikel kugelförmig waren und Nanokapseln eine Kern-Schale-Struktur mit homogener Verteilung des Polymers besaßen . Die Nutzung der Hilfsstoffe, Saccharose und Trehalose, erwies sich als nützlich bei der Gefriertrocknung der Nanopartikel. Das *in vivo* Fluoreszenzimaging zeigte, dass die Nanopartikel über mehrere Stunden im Blutkreislauf verweilten. Während dieser Zeit

akkumulierten die Nanopartikel verstärkt in Leber und Milz mit einer maximalen Konzentration nach 24 Stunden. Eine verminderte Aufnahme der Nanokapseln in Leber und Milz wurde bei einemsteigenden PEG-Gehalt von 5% auf 15% beobachtet. Sowohl das *in vivo* als auch das *ex vivo* Fluoreszenzimaging zeigte, dass die Nanokapseln in der Leber, der Milz und den Eierstöcken akkumulierten, was u.a. durch Konfokalmikroskopie bestätigt wurde. Die Verkapselung der Betulinsäure in Nanosphärulen war erfolgreich und verbesserte deren Bioverfügbarkeit Der Zytotoxizitätsassay mit A549-Zellen zeigte, dass die Betulinsäure-beladenen Nanosphärulen einen kleineren IC50-Wert besaßen als die freie Betulinsäure.

6 References

Abdelwahed, W., Degobert, G., Fessi, H., 2006a. Investigation of nanocapsules stabilization by amorphous excipients during freeze-drying and storage. European Journal of Pharmaceutics and Biopharmaceutics 63, 87-94.

Abdelwahed, W., Degobert, G., Stainmesse, S., Fessi, H., 2006b. Freeze-drying of nanoparticles: Formulation, process and storage considerations. Advanced Drug Delivery Reviews 58, 1688-1713.

Adams, M.L., Lavasanifar, A., Kwon, G.S., 2003. Amphiphilic block copolymers for drug delivery. Journal of Pharmaceutical Sciences 92, 1343-1355.

Ahmed, F., Discher, D.E., 2004. Self-porating polymersomes of PEG–PLA and PEG–PCL: hydrolysis-triggered controlled release vesicles. Journal of Controlled Release 96, 37-53.

Alexis, F., Pridgen, E., Molnar, L.K., Farokhzad, O.C., 2008. Factors Affecting the Clearance and Biodistribution of Polymeric Nanoparticles. Molecular Pharmaceutics 5, 505-515.

Allen, T.M., Cullis, P.R., 2004. Drug Delivery Systems: Entering the Mainstream. Science 303, 1818-1822.

Anton, N., Saulnier, P., Gaillard, C.d., Porcher, E., Vrignaud, S., Benoit, J.-P., 2009. Aqueous-Core Lipid Nanocapsules for Encapsulating Fragile Hydrophilic and/or Lipophilic Molecules. Langmuir 25, 11413-11419.

Augsten, C., Kiselev, M.A., Gehrke, R., Hause, G., Mäder, K., 2008. A detailed analysis of biodegradable nanospheres by different techniques--A combined approach to detect

particle sizes and size distributions. Journal of Pharmaceutical and Biomedical Analysis 47, 95-102.

Avgoustakis, K., 2004. Pegylated poly(lactide) and poly(lactide-co-glycolide) nanoparticles: preparation, properties and possible applications in drug delivery. Current Drug Delivery 1, 321-333.

Avgoustakis, K., Beletsi, A., Panagi, Z., Klepetsanis, P., Karydas, A.G., Ithakissios, D.S., 2002. PLGA-mPEG nanoparticles of cisplatin: in vitro nanoparticle degradation, in vitro drug release and in vivo drug residence in blood properties. Journal of Controlled Release 79, 123-135.

Avgoustakis, K., Beletsi, A., Panagi, Z., Klepetsanis, P., Livaniou, E., Evangelatos, G., Ithakissios, D.S., 2003. Effect of copolymer composition on the physicochemical characteristics, in vitro stability, and biodistribution of PLGA-mPEG nanoparticles. International Journal of Pharmaceutics 259, 115-127.

Bae, K.H., Lee, Y., Park, T.G., 2007. Oil-Encapsulating PEO−PPO−PEO/PEG Shell Cross-Linked Nanocapsules for Target-Specific Delivery of Paclitaxel. Biomacromolecules 8, 650-656.

Bianco, A., Kostarelos, K., Prato, M., 2005. Applications of carbon nanotubes in drug delivery. Current Opinion in Chemical Biology 9, 674-679.

Bilati, U., Allémann, E., Doelker, E., 2005. Development of a nanoprecipitation method intended for the entrapment of hydrophilic drugs into nanoparticles. European Journal of Pharmaceutical Sciences 24, 67-75.

Bittner, B., Witt, C., Mäder, K., Kissel, T., 1999. Degradation and protein release properties of microspheres prepared from biodegradable poly(lactide-co-glycolide) and ABA triblock copolymers: influence of buffer media on polymer erosion and bovine serum albumin release. Journal of Controlled Release 60, 297-309.

Breitenbach, A., Li, Y.X., Kissel, T., 2000. Branched biodegradable polyesters for parenteral drug delivery systems. Journal of Controlled Release 64, 167-178.

Cauchetier, E., Deniau, M., Fessi, H., Astier, A., Paul, M., 2003. Atovaquone-loaded nanocapsules: influence of the nature of the polymer on their in vitro characteristics. International Journal of Pharmaceutics 250, 273-281.

Chawla, J.S., Amiji, M.M., 2002. Biodegradable poly(ε-caprolactone) nanoparticles for tumor-targeted delivery of tamoxifen. International Journal of Pharmaceutics 249, 127-138.

Chen, G., Wang, W., 2007. Role of Freeze Drying in Nanotechnology. Drying Technology 25, 29-35.

Chen, J., Li, S., Shen, Q., He, H., Zhang, Y., Enhanced cellular uptake of folic acid–conjugated PLGA–PEG nanoparticles loaded with vincristine sulfate in human breast cancer. Drug Development and Industrial Pharmacy 0, 1-8.

Chen, S., Pieper, R., Webster, D.C., Singh, J., 2005. Triblock copolymers: synthesis, characterization, and delivery of a model protein. International Journal of Pharmaceutics 288, 207-218.

Cheng, J., Teply, B.A., Sherifi, I., Sung, J., Luther, G., Gu, F.X., Levy-Nissenbaum, E., Radovic-Moreno, A.F., Langer, R., Farokhzad, O.C., 2007. Formulation of functionalized PLGA-PEG nanoparticles for in vivo targeted drug delivery. Biomaterials 28, 869-876.

Chirila, T.V., Rakoczy, P.E., Garrett, K.L., Lou, X., Constable, I.J., 2002. The use of synthetic polymers for delivery of therapeutic antisense oligodeoxynucleotides. Biomaterials 23, 321-342.

Chorny, M., Fishbein, I., Danenberg, H.D., Golomb, G., 2002. Lipophilic drug loaded nanospheres prepared by nanoprecipitation: effect of formulation variables on size, drug

recovery and release kinetics. Journal of Controlled Release 83, 389-400.

Coester, C., Nayyar, P., Samuel, J., 2006. In vitro uptake of gelatin nanoparticles by murine dendritic cells and their intracellular localisation. European Journal of Pharmaceutics and Biopharmaceutics 62, 306-314.

Couvreur, P., Barratt, G., Fattal, E., Legrand, P., Vauthier, C., 2002. Nanocapsule technology: a review. Critical Reviews™ Therapeutic Drug Carrier Systems 19, 99-134.

Couvreur, P., Vauthier, C., 2006. Nanotechnology: Intelligent Design to Treat Complex Disease. Pharmaceutical Research 23, 1417-1450.

Csuk, R., Barthel, A., Kluge, R., Ströhl, D., 2010. Synthesis, cytotoxicity and liposome preparation of 28-acetylenic betulin derivatives. Bioorganic & Medicinal Chemistry 18, 7252-7259.

Dang, J.M., Leong, K.W., 2006. Natural polymers for gene delivery and tissue engineering. Advanced Drug Delivery Reviews 58, 487-499.

Danhier, F., Lecouturier, N., Vroman, B., Jérôme, C., Marchand-Brynaert, J., Feron, O., Préat, V., 2009. Paclitaxel-loaded PEGylated PLGA-based nanoparticles: In vitro and in vivo evaluation. Journal of Controlled Release 133, 11-17.

Date, P., Samad, A., Devarajan, P., 2010. Freeze Thaw: A Simple Approach for Prediction of Optimal Cryoprotectant for Freeze Drying. AAPS PharmSciTech 11, 304-313.

Desai, M.P., Labhasetwar, V., Walter, E., Levy, R.J., Amidon, G.L., 1997. The Mechanism of Uptake of Biodegradable Microparticles in Caco-2 Cells Is Size Dependent. Pharmaceutical Research 14, 1568-1573.

Desgouilles, S., Vauthier, C., Bazile, D., Vacus, J., Grossiord, J.-L., Veillard, M., Couvreur, P., 2003. The Design of Nanoparticles Obtained by Solvent Evaporation: A Comprehensive Study. Langmuir 19, 9504-9510.

Dunne, M., Corrigan, O.I., Ramtoola, Z., 2000. Influence of particle size and dissolution conditions on the degradation properties of polylactide-co-glycolide particles. Biomaterials 21, 1659-1668.

Farokhzad, O.C., Langer, R., 2009. Impact of Nanotechnology on Drug Delivery. ACS Nano 3, 16-20.

Fessi, H., Puisieux, F., Devissaguet, J.P., Ammoury, N., Benita, S., 1989. Nanocapsule formation by interfacial polymer deposition following solvent displacement. International Journal of Pharmaceutics 55, R1-R4.

Fraunhofer, W., Winter, G., 2004. The use of asymmetrical flow field-flow fractionation in pharmaceutics and biopharmaceutics. European Journal of Pharmaceutics and Biopharmaceutics 58, 369-383.

Ganachaud, F., Katz, J.L., 2005. Nanoparticles and Nanocapsules Created Using the Ouzo Effect: Spontaneous Emulsification as an Alternative to Ultrasonic and High-Shear Devices. ChemPhysChem 6, 209-216.

Gao, K., Jiang, X., 2006. Influence of particle size on transport of methotrexate across blood brain barrier by polysorbate 80-coated polybutylcyanoacrylate nanoparticles. International Journal of Pharmaceutics 310, 213-219.

Gaucher, G., Dufresne, M.-H., Sant, V.P., Kang, N., Maysinger, D., Leroux, J.-C., 2005. Block copolymer micelles: preparation, characterization and application in drug delivery. Journal of Controlled Release 109, 169-188.

Gaumet, M., Vargas, A., Gurny, R., Delie, F., 2008. Nanoparticles for drug delivery: The need for precision in reporting particle size parameters. European Journal of Pharmaceutics and Biopharmaceutics 69, 1-9.

Ghosh, P., Han, G., De, M., Kim, C.K., Rotello, V.M., 2008. Gold nanoparticles in

delivery applications. Advanced Drug Delivery Reviews 60, 1307-1315.

Govender, T., Stolnik, S., Garnett, M.C., Illum, L., Davis, S.S., 1999. PLGA nanoparticles prepared by nanoprecipitation: drug loading and release studies of a water soluble drug. Journal of Controlled Release 57, 171-185.

Greenspan, P., Mayer, E.P., Fowler, S.D., 1985. Nile red: a selective fluorescent stain for intracellular lipid droplets. The Journal of Cell Biology 100, 965-973.

Gref, R., Lück, M., Quellec, P., Marchand, M., Dellacherie, E., Harnisch, S., Blunk, T., Müller, R.H., 2000. 'Stealth' corona-core nanoparticles surface modified by polyethylene glycol (PEG): influences of the corona (PEG chain length and surface density) and of the core composition on phagocytic uptake and plasma protein adsorption. Colloids and Surfaces B: Biointerfaces 18, 301-313.

Gref, R., Minamitake, Y., Peracchia, M.T., Trubetskoy, V., Torchilin, V., Langer, R., 1994. Biodegradable long-circulating polymeric nanospheres. Science 263, 1600-1603.

Guan, Y.-S., Hu, Y., Liu, Y., 2006. Multidetector-row computed tomography in the management of hepatocellular carcinoma with transcatheter arterial chemoembolization. Journal of Gastroenterology and Hepatology 21, 941-946.

Hans, M.L., Lowman, A.M., 2002. Biodegradable nanoparticles for drug delivery and targeting. Current Opinion in Solid State and Materials Science 6, 319-327.

Hinrichs, W.L.J., Manceñido, F.A., Sanders, N.N., Braeckmans, K., De Smedt, S.C., Demeester, J., Frijlink, H.W., 2006. The choice of a suitable oligosaccharide to prevent aggregation of PEGylated nanoparticles during freeze thawing and freeze drying. International Journal of Pharmaceutics 311, 237-244.

Hombreiro Pérez, M., Zinutti, C., Lamprecht, A., Ubrich, N., Astier, A., Hoffman, M., Bodmeier, R., Maincent, P., 2000. The preparation and evaluation of

poly(-caprolactone) microparticles containing both a lipophilic and a hydrophilic drug. Journal of Controlled Release 65, 429-438.

Horcas, I., Fernandez, R., Gomez-Rodriguez, J.M., Colchero, J., Gomez-Herrero, J., Baro, A.M., 2007. WSXM: A software for scanning probe microscopy and a tool for nanotechnology Review of Scientific Instruments 78, 013705.

Hrkach, J.S., Peracchia, M.T., Bomb, A., Lotan, n., Langer, R., 1997. Nanotechnology for biomaterials engineering: structural characterization of amphiphilic polymeric nanoparticles by 1H NMR spectroscopy. Biomaterials 18, 27-30.

Jain, J.P., Kumar, N., 2010. Self assembly of amphiphilic (PEG)$_3$-PLA copolymer as polymersomes: preparation, characterization, and their evaluation as drug carrier. Biomacromolecules 11, 1027-1035.

Janib, S.M., Moses, A.S., MacKay, J.A., 2010. Imaging and drug delivery using theranostic nanoparticles. Advanced Drug Delivery Reviews 62, 1052-1063.

Jeffrey A, H., 1998. Synthetic biodegradable polymers for tissue engineering and drug delivery. Current Opinion in Solid State and Materials Science 3, 246-251.

John V, F., 2003. In vivo near-infrared fluorescence imaging. Current Opinion in Chemical Biology 7, 626-634.

Kabanov, A.V., Vinogradov, S.V., 2009. Nanogels as Pharmaceutical Carriers: Finite Networks of Infinite Capabilities. Angewandte Chemie International Edition 48, 5418-5429.

Kempe, S., Metz, H., Mäder, K., 2010. Application of Electron Paramagnetic Resonance (EPR) spectroscopy and imaging in drug delivery research - Chances and challenges. European Journal of Pharmaceutics and Biopharmaceutics 74, 55-66.

Khemtong, C., Kessinger, C.W., Gao, J., 2009. Polymeric nanomedicine for cancer MR

imaging and drug delivery. Chemical Communications, 3497-3510.

Kim, D.-H., Martin, D.C., 2006. Sustained release of dexamethasone from hydrophilic matrices using PLGA nanoparticles for neural drug delivery. Biomaterials 27, 3031-3037.

Kimura, S., Egashira, K., Nakano, K., Iwata, E., Miyagawa, M., Tsujimoto, H., Hara, K., Kawashima, Y., Tominaga, R., Sunagawa, K., 2008. Local Delivery of Imatinib Mesylate (STI571)-Incorporated Nanoparticle Ex Vivo Suppresses Vein Graft Neointima Formation. Circulation 118, S65-S70.

Kratz, F., 2008. Albumin as a drug carrier: Design of prodrugs, drug conjugates and nanoparticles. Journal of Controlled Release 132, 171-183.

Kumar, N., Ravikumar, M.N.V., Domb, A.J., 2001. Biodegradable block copolymers. Advanced Drug Delivery Reviews 53, 23-44.

Kumari, A., Yadav, S.K., Yadav, S.C., 2010. Biodegradable polymeric nanoparticles based drug delivery systems. Colloids and Surfaces B: Biointerfaces 75, 1-18.

Kuntsche, J., Klaus, K., Steiniger, F., 2009. Size determinations of colloidal fat emulsions: a comparative study. Journal of Biomedical Nanotechnology 5, 384-395.

Lambert, G., Fattal, E., Pinto-Alphandary, H., Gulik, A., Couvreur, P., 2000. Polyisobutylcyanoacrylate Nanocapsules Containing an Aqueous Core as a Novel Colloidal Carrier for the Delivery of Oligonucleotides. Pharmaceutical Research 17, 707-714.

Lassalle, V., Ferreira, M.L., 2007. PLA Nano- and Microparticles for Drug Delivery: An Overview of the Methods of Preparation. Macromolecular Bioscience 7, 767-783.

Le Corre, D.b., Bras, J., Dufresne, A., 2010. Starch Nanoparticles: A Review. Biomacromolecules 11, 1139-1153.

Leo, E., Brina, B., Forni, F., Vandelli, M.A., 2004. In vitro evaluation of PLA nanoparticles containing a lipophilic drug in water-soluble or insoluble form. International Journal of Pharmaceutics 278, 133-141.

Li, R., Li, X., Xie, L., Ding, D., Hu, Y., Qian, X., Yu, L., Ding, Y., Jiang, X., Liu, B., 2009. Preparation and evaluation of PEG-PCL nanoparticles for local tetradrine delivery. International Journal of Pharmaceutics 379, 158-166.

Li, Y.-P., Pei, Y.-Y., Zhang, X.-Y., Gu, Z.-H., Zhou, Z.-H., Yuan, W.-F., Zhou, J.-J., Zhu, J.-H., Gao, X.-J., 2001. PEGylated PLGA nanoparticles as protein carriers: synthesis, preparation and biodistribution in rats. Journal of Controlled Release 71, 203-211.

Liang, M., Liu, X., Cheng, D., Liu, G., Dou, S., Wang, Y., Rusckowski, M., Hnatowich, D.J., 2010. Multimodality Nuclear and Fluorescence Tumor Imaging in Mice Using a Streptavidin Nanoparticle. Bioconjugate Chemistry 21, 1385-1388.

Lockman, P.R., Mumper, R.J., Khan, M.A., Allen, D.D., 2002. Nanoparticle Technology for Drug Delivery Across the Blood-Brain Barrier. Drug Development and Industrial Pharmacy 28, 1-13.

Lurie, D.J., Mäder, K., 2005. Monitoring drug delivery processes by EPR and related techniques--principles and applications. Advanced Drug Delivery Reviews 57, 1171-1190.

Müller, R.H., Mäder, K., Gohla, S., 2000. Solid lipid nanoparticles (SLN) for controlled drug delivery – a review of the state of the art. European Journal of Pharmaceutics and Biopharmaceutics 50, 161-177.

Martini, G., Ciani, L., 2009. Electron spin resonance spectroscopy in drug delivery. Physical Chemistry Chemical Physics 11, 211-254.

McCarron, P.A., Donnelly, R.F., Marouf, W., 2006. Celecoxib-loaded poly(D,L-lactide-co-glycolide) nanoparticles prepared using a novel and controllable

combination of diffusion and emulsification steps as part of the salting-out procedure. Journal of Microencapsulation 23, 480-498.

Mehnert, W., Mäder, K., 2001. Solid lipid nanoparticles: Production, characterization and applications. Advanced Drug Delivery Reviews 47, 165-196.

Moghimi, S.M., Hunter, A.C., Murray, J.C., 2001. Long-Circulating and Target-Specific Nanoparticles: Theory to Practice. Pharmacological Reviews 53, 283-318.

Moinard-Chécot, D., Chevalier, Y., Briançon, S., Beney, L., Fessi, H., 2008. Mechanism of nanocapsules formation by the emulsion-diffusion process. Journal of Colloid and Interface Science 317, 458-468.

Mora-Huertas, C.E., Fessi, H., Elaissari, A., 2010. Polymer-based nanocapsules for drug delivery. International Journal of Pharmaceutics 385, 113-142.

Mosqueira, V.C.F., Legrand, P., Gulik, A., Bourdon, O., Gref, R., Labarre, D., Barratt, G., 2001. Relationship between complement activation, cellular uptake and surface physicochemical aspects of novel PEG-modified nanocapsules. Biomaterials 22, 2967-2979.

Mu, L., Feng, S.S., 2003. A novel controlled release formulation for the anticancer drug paclitaxel (Taxol®): PLGA nanoparticles containing vitamin E TPGS. Journal of Controlled Release 86, 33-48.

O'Brien, J.A., Lummis, S.C.R., 2007. Diolistics: incorporating fluorescent dyes into biological samples using a gene gun. Trends in Biotechnology 25, 530-534.

Owens Iii, D.E., Peppas, N.A., 2006. Opsonization, biodistribution, and pharmacokinetics of polymeric nanoparticles. International Journal of Pharmaceutics 307, 93-102.

Patil, Y., Panyam, J., 2009. Polymeric nanoparticles for siRNA delivery and gene silencing.

International Journal of Pharmaceutics 367, 195-203.

Peer, D., Karp, J.M., Hong, S., Farokhzad, O.C., Margalit, R., Langer, R., 2007. Nanocarriers as an emerging platform for cancer therapy. Nature Nanotechnology 2, 751-760.

Peracchia, M.T., Gref, R., Minamitake, Y., Domb, A., Lotan, N., Langer, R., 1997. PEG-coated nanospheres from amphiphilic diblock and multiblock copolymers: Investigation of their drug encapsulation and release characteristics. Journal of Controlled Release 46, 223-231.

Pereira, M.A., Mosqueira, V.C.F., Vilela, J.M.C., Andrade, M.S., Ramaldes, G.A., Cardoso, V.N., 2008. PLA-PEG nanocapsules radiolabeled with 99mTechnetium-HMPAO: Release properties and physicochemical characterization by atomic force microscopy and photon correlation spectroscopy. European Journal of Pharmaceutical Sciences 33, 42-51.

Petersen, S., Fahr, A., Bunjes, H., 2010. Flow Cytometry as a New Approach To Investigate Drug Transfer between Lipid Particles. Molecular Pharmaceutics 7, 350-363.

Pinto Reis, C., Neufeld, R.J., Ribeiro, A.J., Veiga, F., 2006. Nanoencapsulation I. Methods for preparation of drug-loaded polymeric nanoparticles. Nanomedicine : nanotechnology, biology, and medicine 2, 8-21.

Pisani, E., Tsapis, N., Galaz, B., Santin, M., Berti, R., Taulier, N., Kurtisovski, E., Lucidarme, O., Ourevitch, M., Doan, B.T., Beloeil, J.C., Gillet, B., Urbach, W., Bridal, S.L., Fattal, E., 2008. Perfluorooctyl Bromide Polymeric Capsules as Dual Contrast Agents for Ultrasonography and Magnetic Resonance Imaging. Advanced Functional Materials 18, 2963-2971.

Popovtzer, R., Agrawal, A., Kotov, N.A., Popovtzer, A., Balter, J., Carey, T.E., Kopelman, R., 2008. Targeted Gold Nanoparticles Enable Molecular CT Imaging of Cancer. Nano Letters 8, 4593-4596.

Pourcelle, V., Devouge, S., Garinot, M., Préat, V., Marchand-Brynaert, J., 2007. PCL−PEG-Based Nanoparticles Grafted with GRGDS Peptide: Preparation and Surface Analysis by XPS. Biomacromolecules 8, 3977-3983.

Prabaharan, M., Mano, J.F., 2004. Chitosan-Based Particles as Controlled Drug Delivery Systems. Drug Delivery 12, 41-57.

Qiu, L., Bae, Y., 2006. Polymer Architecture and Drug Delivery. Pharmaceutical Research 23, 1-30.

Rübe, A., Hause, G., Mäder, K., Kohlbrecher, J., 2005. Core-shell structure of Miglyol/poly(d,l-lactide)/Poloxamer nanocapsules studied by small-angle neutron scattering. Journal of Controlled Release 107, 244-252.

Rübe, A., Mäder, K., 2005. Electron Spin Resonance Study on the Dynamics of Polymeric Nanocapsules. Journal of Biomedical Nanotechnology 1, 208-213.

Rao, J., Dragulescu-Andrasi, A., Yao, H., 2007. Fluorescence imaging in vivo: recent advances. Current Opinion in Biotechnology 18, 17-25.

Rashid, F., Horobin, R.W., 1990. Interaction of molecular probes with living cells and tissues. Part 2. Histochemistry and Cell Biology 94, 303-308.

Ren, Y., Wang, G., Huang, J., 2007. Preparation of Liquid-Core Nanocapsules from Poly[(ethylene oxide)-co-glycidol] with Multiple Hydrophobic Linoleates at an Oil−Water Interface and Its Encapsulation of Pyrene. Biomacromolecules 8, 1873-1880.

Resch-Genger, U., Grabolle, M., Cavaliere-Jaricot, S., Nitschke, R., Nann, T., 2008. Quantum dots versus organic dyes as fluorescent labels. Nature Methods 5, 763-775.

Sánchez, A., Tobío, M., González, L., Fabra, A., Alonso, M.J., 2003. Biodegradable micro- and nanoparticles as long-term delivery vehicles for interferon-alpha. European

Journal of Pharmaceutical Sciences 18, 221-229.

Santos-Magalhães, N.S., Pontes, A., Pereira, V.M.W., Caetano, M.N.P., 2000. Colloidal carriers for benzathine penicillin G: Nanoemulsions and nanocapsules. International Journal of Pharmaceutics 208, 71-80.

Schaffazick, S.R., Pohlmann, A.R., Dalla-Costa, T., Guterres, S.S., 2003. Freeze-drying polymeric colloidal suspensions: nanocapsules, nanospheres and nanodispersion. A comparative study. European Journal of Pharmaceutics and Biopharmaceutics 56, 501-505.

Severs, N.J., 2007. Freeze-fracture electron microscopy. Nature Protocols 2, 547-576.

Skehan, P., Storeng, R., Scudiero, D., Monks, A., McMahon, J., Vistica, D., Warren, J.T., Bokesch, H., Kenney, S., Boyd, M.R., 1990. New Colorimetric Cytotoxicity Assay for Anticancer-Drug Screening. Journal of the National Cancer Institute 82, 1107-1112.

Sonke, S., 2009. Dendrimers as versatile platform in drug delivery applications. European Journal of Pharmaceutics and Biopharmaceutics 71, 445-462.

Soppimath, K.S., Aminabhavi, T.M., Kulkarni, A.R., Rudzinski, W.E., 2001. Biodegradable polymeric nanoparticles as drug delivery devices. Journal of Controlled Release 70, 1-20.

Stolnik, S., Davies, M.C., Illum, L., Davis, S.S., Boustta, M., Vert, M., 1994. The preparation of sub-200 nm biodegradable colloidal particles from poly(β-malic acid-co-benzyl malate) copolymers and their surface modification with Poloxamer and Poloxamine surfactants. Journal of Controlled Release 30, 57-67.

Stolnik, S., Illum, L., Davis, S.S., 1995. Long circulating microparticulate drug carriers. Advanced Drug Delivery Reviews 16, 195-214.

Tønnesen, H.H., Karlsen, J., 2002. Alginate in Drug Delivery Systems. Drug

Development and Industrial Pharmacy 28, 621-630.

Tan, W., Wang, K., He, X., Zhao, X.J., Drake, T., Wang, L., Bagwe, R.P., 2004. Bionanotechnology based on silica nanoparticles. Medicinal Research Reviews 24, 621-638.

Tong, R., Coyle, V.J., Tang, L., Barger, A.M., Fan, T.M., Cheng, J., 2010. Polylactide nanoparticles containing stably incorporated cyanine dyes for in vitro and in vivo imaging applications. Microscopy Research and Technique 73, 901-909.

Torchilin, V., 2007. Micellar Nanocarriers: Pharmaceutical Perspectives. Pharmaceutical Research 24, 1-16.

Tros de Ilarduya, C., Sun, Y., Düzgüneş, N., 2010. Gene delivery by lipoplexes and polyplexes. European Journal of Pharmaceutical Sciences 40, 159-170.

Uhrich, K.E., Cannizzaro, S.M., Langer, R.S., Shakesheff, K.M., 1999. Polymeric Systems for Controlled Drug Release. Chemical Reviews 99, 3181-3198.

Vauthier, C., Bouchemal, K., 2009. Methods for the preparation and manufacture of polymeric nanoparticles. Pharmaceutical Research 26, 1025-1058.

Veronese, F.M., Pasut, G., 2005. PEGylation, successful approach to drug delivery. Drug Discovery Today 10, 1451-1458.

Vitale, S.A., Katz, J.L., 2003. Liquid Droplet Dispersions Formed by Homogeneous Liquid−Liquid Nucleation: "The Ouzo Effect". Langmuir 19, 4105-4110.

Win, K.Y., Feng, S.-S., 2006. In vitro and in vivo studies on vitamin E TPGS-emulsified poly(d,l-lactic-co-glycolic acid) nanoparticles for paclitaxel formulation. Biomaterials 27, 2285-2291.

Winzenburg, G., Schmidt, C., Fuchs, S., Kissel, T., 2004. Biodegradable polymers and

their potential use in parenteral veterinary drug delivery systems. Advanced Drug Delivery Reviews 56, 1453-1466.

Yang, J., Park, S.B., Yoon, H.-G., Huh, Y.M., Haam, S., 2006. Preparation of poly [var epsilon]-caprolactone nanoparticles containing magnetite for magnetic drug carrier. International Journal of Pharmaceutics 324, 185-190.

Yogeeswari, P., Sriram, D., 2005. Betulinic acid and its derivatives: a review on their biological properties. Current Medicinal Chemistry 12, 657- 666.

Zhou, W., Meng, F., Engbers, G.H.M., Feijen, J., 2006. Biodegradable polymersomes for targeted ultrasound imaging. Journal of Controlled Release 116, 62-64.

Acknowledgments

First of all, I have to express my deep gratitude and heartily appreciation to my supervisor, Prof. Karsten Mäder for giving me this opportunity to work on this interesting study in his group. I am forever indebted to Prof. Mäder, not only for his considerable mentoring, invaluable suggestions and fruitful discussions, but also for his kindness whatever I need.

I am very grateful to Dr. Judith Kuntsche for many valuable discussions and the assistance with field flow fractionation, and to Dr. Hendrik Metz for the useful discussions and instructions regarding ESR simulation.

I have to express my gratitude to Dr. Gerd Hause of the Biocenter for the transmission electron microscopy measurement, Dr. Xiaoli Lu of MPI Microstructure Physics for the atomic force microscopy measurement, and to Dr. Thomas Müller of medical department for the intravenous injection to the mice.

I have to express my gratitude to PD Dr. Reinhard Paschke of the Biocenter for supplying betulinic acid and valuable suggestion. And, I also thank Dr. Jutta Kalbitz and Dr. Goran Kaluderovic, BioSolutions Halle GmbH for HPLC measurements and cell culture study, respectively.

I would like to thank Prof. Dr. Thomas Groth to allow me to use the confocal laser scanning microscopy in his group, particularly thanks to Dr. Jürgen Vogel for his help with the measurements.

In particular, my gratitude also goes to the China Scholarship Council for the financial support during my Ph.D. study.

I also have to thank all the members and technical assistants in the groups of Prof. Dr. Karsten Mäder, Prof. Dr. Reinhard Neubert and Prof. Dr. Andreas Langner for providing a quite friendly working environment. I specially thank Andreas Schädlich for his valuable help with the *in vivo* experiments, and Claudia Preetz, Alexander Lochmann, Anteneh Belete Shibeshi, Hagen Nitzsche, Andreas Nock, Martin Hahn, Johannes Oidtmann and Tamer Hassan for their valuable suggestion, support and friendship throughout my study.

Special thanks to all my friends in China, Germany and elsewhere, who are keep encouraging me during my study.

Last but not least, I would like to thank my parents for their support and understanding to carry out my studies.

Curriculum Vitae

Personal Data

Name: Jun Li

Date of birth: November 3, 1982,

Place of birth: Taizhou, Jiangsu province, China

Material status: Single

Nationality: Chinese

Address: Institute of Pharmacy,

Martin Luther University Halle-Wittenberg,

Wolfgang-Langenbeck-Str. 4, 06120 Halle/Saale, Germany

E-mail: jun.li@pharmazie.uni-halle.de

Professional and Academic Training

Since 09/2008 Ph. D. student in the research group of Prof. Karsten Mäder, Department of Pharmaceutical Technology and Biopharmaceutics, Institute of Pharmacy, Martin Luther University Halle Wittenberg, Halle (Saale), Germany

09/2005–07/2008 College of Bioengineering, Chongqing University, Chongqing, China   (M.Sc. in Biomedical Engineering)

Thesis Topic: Study on Novel Thermo-Sensitive Nanoparticles for Targeted

Drug Delivery

(Outstanding Master's Thesis in Municipality of Chongqing)

09/2001–07/2005 College of Life Science, Chongqing Normal University, China

(B.Sc. in Biology)

Publications

Jun Li, Andreas Schädlich, Gerd Hause, Jürgen Vogel, Judith Kuntsche, Thomas Groth, Karsten Mäder. Preparation and in vitro/in vivo Evaluation of PLGA-PEG Oily Core Nanocapsules, International Journal of pharmaceutics (under review)

Andreas Schädlich, Stefan Hoffmann, Thomas Mueller, Henrike Caysa, Cornelia Rose, Jun Li, Achim Göpferich, Judith Kuntsche, Karsten Mäder. Accumulation of nano-carriers in the ovary: a neglected toxicity risk? Nano Letters (under review)

Jun Li, Andreas Schädlich, Gerd Hause, Judith Kuntsche, Karsten Mäder. In vivo and ex vivo evaluation of novel pegylated PLGA nanocapsules. Controlled Release Society Germany Annual Meeting 2011, March 15-16, 2011, Jena, Germany (Abstract)

Jun Li, Jutta Kalbitz, Goran Kaluderovic, Reinhard Paschke, Karsten Mäder. Development and evaluation of nanospheres for betulinic acid delivery (in preparation)

Jun Li, Judith Kuntsche, Karsten Mäder. Preparation and characteristics of PLGA-PEG nanospheres and oily core nanocapsules (in preparation)

Bochu Wang, Pengyu Shao, Yazhou Wang, Jun Li, Yiqiong Zhang. The application of thermosensitive nanocarriers in controlled drug delivery. Journal of Nanomaterials, 2011, doi:10.1155/2011/389640.

Peng Liu, Bochu Wang, Weili Qiao, Jun Li. Novel thermosensitive nano-micelles from triblock copolymer for drug delivery. Journal of Biomedical Nanotechnology, 2009, 5(3):310-313.

Peng Liu, Bochu Wang, Jun Li, Weili Qiao. Multi-anticancer drugs encapsulated in the micelles: a novel chemotherapy to cancer. Medical Hypotheses, 2008, 71(3): 379-381.

Jun Li, Bochu Wang, Yazhou Wang, Peng Liu, Weili Qiao. Preparation and characterization of thermosensitive nanoparticles for targeted drug delivery. Journal of Macromolecular Science, Part A Pure and Applied Chemistry, 2008, 45(10):833-838.

Jun Li, Bochu Wang, Peng Liu. Possibility of active targeting to tumor by local hyperthermia with temperature-sensitive nanoparticles. Medical Hypotheses, 2008, 71(2): 249-251.

Conference Activities

Controlled Release Society Germany Annual Meeting 2011 & International Symposium of the Thuringian ProExcellence Initiative NanoConSens, March 15-16, 2011, Jena, Germany (Oral Presentation)

2nd European Science Foundation Summer School in Nanomedicine, June 12-16, 2009, Lisbon, Portugal

Controlled Release Society Germany Annual Meeting, March 19-20, 2009, Halle, Germany

Selbständigkeitserklärung

Hiermit erkläre ich, dass ich mich mit der vorliegenden Arbeit erstmals um die Erlangung eines Doktorgrades bewerbe.

Ferner erkläre ich, dass ich die vorliegende Arbeit selbstsändig und ohne fremde Hilfe angefertigt, andere als die von mir angegebenen Quellen und Hilfsmittel nicht benutzt und die den verwendeten Werken wörtlich oder inhaltlich entnommenen Stellen als solche kenntlich gemacht habe.

Halle (Saale), November 2011

Jun Li